The Pennsylvania State University

The Graduate School

PRESSURE DISTRIBUTION EVALUATION OF DIFFERENT FILLING METHODS FOR DEPOSITION OF POWDERS IN DIES: MEASUREMENT AND MODELING

A Thesis in

Agricultural and Biological Engineering

by

Saed Sayyar Roudsari

Submitted in Partial Fulfillment
of the Requirements
for the Degree of

Doctor of Philosophy

December 2007

The thesis of Saed Sayyar Roudsari was reviewed and approved* by the following:

Virendra M. Puri
Professor of Agricultural Engineering
Thesis Advisor
Chair of Committee

Paul Heinemann
Professor of Agricultural Engineering

Ali Demirci
Associate Professor of Agricultural Engineering

Ali Borhan
Professor of Chemical Engineering

Roy E. Young
Professor of Agricultural Engineering
Head of the Department of Agricultural and
Biological Engineering

*Signatures are on file in the Graduate School

ABSTRACT

The aim of this research was to measure, analyze, and model the pressure distribution characteristics of powder deposition into rectangular and circular shallow dies using four filling methods. The feed shoe, the rotational rainy, the point feed, and the pneumatic filling methods were used to investigate the deposition characteristics into shallow dies. In order to evaluate the pressure distribution during filling of shallow dies, factors influencing powder deposition were studied. The factors included particle size and shape, particle size distribution, feed shoe speed, and tube cross-section (in case of feed shoe filling) and deposition rates (in case of rotational rainy, point feed, and pneumatic filling). A battery powder mixture (BPM) and microcrystalline cellulose (Avicel PH102) with median size of 84 and 600 μm, respectively, were used to fill a shallow rectangular die 32×30 mm and 6.5 mm deep and a shallow circular die 35 mm in diameter and 6.5 mm deep.

The second generation of pressure deposition tester (PDT-II) with circular and square feed shoe tube cross-sections was used to measure the two powders' pressure distribution characteristics. An innovative rotational rainy filling device was designed and fabricated. This versatile device can be used to measure filling characteristics at different rotational speeds (1-10 rpm) for various powders. The point feed (funnel fill) method with a funnel of 30 mm inlet diameter and 4.2 mm outlet diameter opening was used to fill the rectangular and circular shallow dies. The pneumatic filling method was designed and fabricated to fill the die using air as the conveying medium in a rectangular cross-section tube. The pneumatic filling device was limited to using only the BPM

powder, since the Avicel powder generated substantial quantity of airborne dust during the test. Symmetry analysis, variance metrics, and uniformity analysis were used to quantify the deposition characteristics.

The results showed that: 1) filled contour plot analysis was the most reliable method for measuring deposition characteristics; 2) for all filling methods, the circular die generated higher uniformity compared to rectangular die; 3) the rainy filling method generated the best uniformity of pressure distribution compared with the other three filling methods (average of 77% uniformity); 4) the point feed method and feed shoe filling method were the second and third best filling methods with the average uniformity of 64% and 55%, respectively; 5) the pneumatic filling method was not a suitable method to fill the die (21% uniformity of pressure distribution); 6) the average filling period for feed shoe, rotational rainy, and point feed were 8 second, 15 second, and 40 second, respectively; 7) higher stress was generated inside the rectangular die than in the circular die; 8) for rotational rainy fill and the point feed, deposition rates did not substantially influence the uniformity of pressure distribution inside the die; 9) feed shoe speed highly influenced the uniformity of pressure distribution inside the die; 10) the feed shoe tube cross-section did not influence the pressure distribution; 11) for feed shoe filling method, the areas of high pressure values (> 60 dm, where dm=decimeter equivalent of pressure) were less than 5% of the total area for both rectangular and circular dies; 12) most particle accumulation was observed in forward region of the die due to leveling process; 13) die geometry highly influenced the uniformity of pressure distribution; 14) the leveling procedure (removing surcharge powder) markedly increased non-uniformity within the die (approximately 20%); 15) the overall rate equation for all three filling

methods was: $dh/dt = \alpha h\, F(t) + \beta$, where *h* is equivalent height, *F(t)* is a function of time, α and β are coefficients ; 16) the root mean square error (RMSE) for feed shoe, rotational rainy, and point feed were 0.16 dm, 0.44 dm, and 0.32 dm; respectively; whereas the average relative difference (ARD) values were 7%, 16%, and 11%, respectively.

TABLE OF CONTENTS

LIST OF FIGURES

LIST OF TABLES

ACKNOWLEDGEMENTS

This thesis has greatly benefited from the efforts and support of many people whom I truly thank. Thanks to my principal academic advisor, Dr. Virendra Puri for his invaluable and unparalleled guidance throughout the course of my Ph.D. study over the last three years. I would like to gratefully acknowledge members of my advising committee Dr. Paul Heinemann and Dr. Ali Demirci for their great support and guidance. It is impossible to exaggerate the importance of Dr. Ali Borhan's contribution to this thesis. He has been a great friend and advisor throughout this work for which I am truly thankful.

I am thankful to Dr. Roy E. Young, Head of the Department of Agricultural and Biological Engineering, for providing me the resources. Thanks to Randall G. Bock and Roderick S. Thomas for their technical support in design and fabrication of research devices.

I owe immeasurable amount of gratitude to my wife, Sahar, for her support throughout the numerous ups and downs that I have experienced. Finally, I am thankful to my parents, my brother and sisters and all my friends that have positively influenced my life.

Chapter 1

Introduction

Powders are processed in numerous industries, such as agriculture, ceramic, chemical, food, pharmaceutical, powder metallurgy, mineral, and mining. Many complex processes, for example, conveying, mixing, and pelletizing, are employed in the particulate industries. Most of these industries are migrating toward the use of materials in particulate form as major products. For instance, more than one-half of Imperial Chemical Industries (ICI) and four-fifth of DuPont's products are made in particulate form. In 1988, $7.5 billion value of products in UK (Geldart, 1990) went through a particulate enlargement process. Each operation requires accurate knowledge to enhance the overall efficiency. Furthermore, the efficiency of subsequent processing steps in the particulate industry is dependent on preceding steps. In order to enhance the quality of products, each process needs to be optimized. In pharmaceutical industry, a number of technical problems can occur during the tabletting such as, high weight and dose variation of the tablet, low mechanical strength of the tablets, capping and lamination of the tablets, adhesion or sticking of powder material to punch tips, and high friction during tablets' ejection. Such problems are related to anisotropy or non-uniform distribution of powder and stresses inside the die. Anisotropy is a major problem in numerous powder compaction processes. The anisotropism is ascribed, in part, to the deposition process. Anisotropy can occur during the filling process, because of non-uniform bulk and pressure distribution into the die. Uniform bulk density and pressure distribution in a die,

are important first steps to avoid undesirable quality for pellets, tablets, and compacts. Deposition uniformity is correlated to filling process parameters, such as, filling rate, filling method, and filling direction, die geometric characteristics, powder characteristics, such as size distribution, shape, bulk density, and also environmental conditions (Dhanoa and Puri, 1997; Mittal and Puri, 2001). Within the past few years, a number of researchers in the rapidly growing powder mechanics field have turned their attention to filling methods in dies and load (i.e., pressure) distributions in large storage structures. By contrast, very little research has systematically studied the filling process into small dies.

Xie (2006) has studied the powder deposition in multiple dies. They used the pressure deposition tester (PDT-II) with the feed shoe filling method to study powder uniformity as characterized by pressure distribution in multiple dies. Though there are other filling methods that are used in industry (such as, rainy, pneumatic, and funnel); to date, there are no systematic investigations for measurement, comparison, evaluation, and modeling of powder deposition in dies using different filling methods. Therefore, four types of filling methods, namely, feed shoe, rotational (to create rainy fill), pneumatic, and point feed were used in order to investigate the pressure distribution uniformity of deposition of various powders in a single shallow die (aspect ratio, height/hydraulic diameter <0.5) in this research.

1.1 References

1- Dhanoa, P. S. and V. M. Puri. 1997. Experimental analysis of deposition of particulate materials into confined spaces. ASAE Paper No. 974106. ASAE, St Joseph, MI.

2- Geldart, D. 1990. Powder processing-the overall view. *In Principles of Powder Technology* (ed. M. Rhodes). pp. 1-7. John Wiley & Sons, England.

3- Mittal, B. and V. M. Puri. 2001. A real-time mass deposition tester for bulk solids deposition profiles in non-simple shape storage containers. ASAE Paper No. 014023. ASAE, St. Joseph, MI.

4- Xie, X. 2006. Uniformity of Simultaneous Powder Deposition in Multiple Dies; Measurement and Modeling. Ph.D. diss., University Park. PA. Pennsylvania State Univ: Agricultural and Biological Engineering Dept.

Chapter 2

Literature review

2.1 Introduction

2.1.1 Powder definition

Particulate materials are defined as a particle system comprised of individual solid entities (i.e., particles) surrounded by fluid and/or gas phases (Puri, 2001). Bulk solids, powders, granular materials, grains, and particulate materials are assumed to be synonymous in this study. Tang (2004) summarized the following characteristics for powders: (1) powders are not solids, but can maintain shape and withstand some deformation (e.g., a conical heap is formed while filling a powder); (2) powders are not liquids, but can be made to flow (e.g., pouring of laundry detergent); (3) powders are not gases, but can be compressed (e.g., making a snow ball).

2.1.2 Powder behavior

Powders often show remarkably different behaviors, compared with liquids, gases, and solid materials. It has been suggested that powders constitute a fourth aggregation state. Two main mechanisms control the behavior of powder comprising fine particles (Rietema, 1991):

1- The particle-particle interaction (such as friction and cohesion are the result of close contact between particles).
2- The solid-gas interaction has two groups:
    a) a hydrodynamic interaction by viscous force,
    b) a physico-chemical interaction via gas adsorption to the solid state.

Bruff and Jenike (1967) mentioned the importance of solid-gas interactions in solids discharged from hoppers. A powder can be made to flow when a certain minimum amount of critical yield stress is applied to the powder. In packed state, if powder can expand, the mobility of particles increases causing the powder mass to flow.

2.1.3 Powder in industry

Powders are widely use in numerous industries. In the food industry, powders are used to produce many type of products, for example, potato starches, corn starches, milk powder, and many other spray-dried products. In the pharmaceutical industry, powders are converted to various shapes to form tablets by compression. In the ceramic industry, many household products are produced via sintering after compression in molds. In the electronics industry, the fluorescent and magnetic powders are widely used to form into parts by pressing. Many industries use powdered coal on a large scale. In the chemical industry, powders are used to form catalysts, while many of the final chemical products, notably plastics and other polymers are delivered as powders.

2.1.4 Powder operations

There are various operations that are carried out with powders. For instance, powders can be:

1- Stored in hoppers and bins,

2- Ground and milled for advanced processing,

3- Mixed to produce products of high quality,

4- Compressed to attain a solid product,

5- Granulated to obtain large grain,

6- Classified with different average particle size and density, and

7- Fluidized to improve the contact between powder particle and fluidization gas.

2.1.5 Powder compaction

Tablets are prepared by forcing particles into close proximity to each other by powder compression, which enable the particles to cohere into a porous, solid specimen of defined geometry. The compression takes place in the die by action of two punches, the lower and the upper, by which the compressive force is applied (Figure **2.1**). Powder compression is defined as the reduction in volume of the powder owing to the application of a force. Because of the increased proximity of particle surface accomplished during compression, bonds are formed between particles which provides coherency to the powder, i.e., a compact is formed. Compaction is defined as the formation of a porous specimen of defined geometry by powder compression.

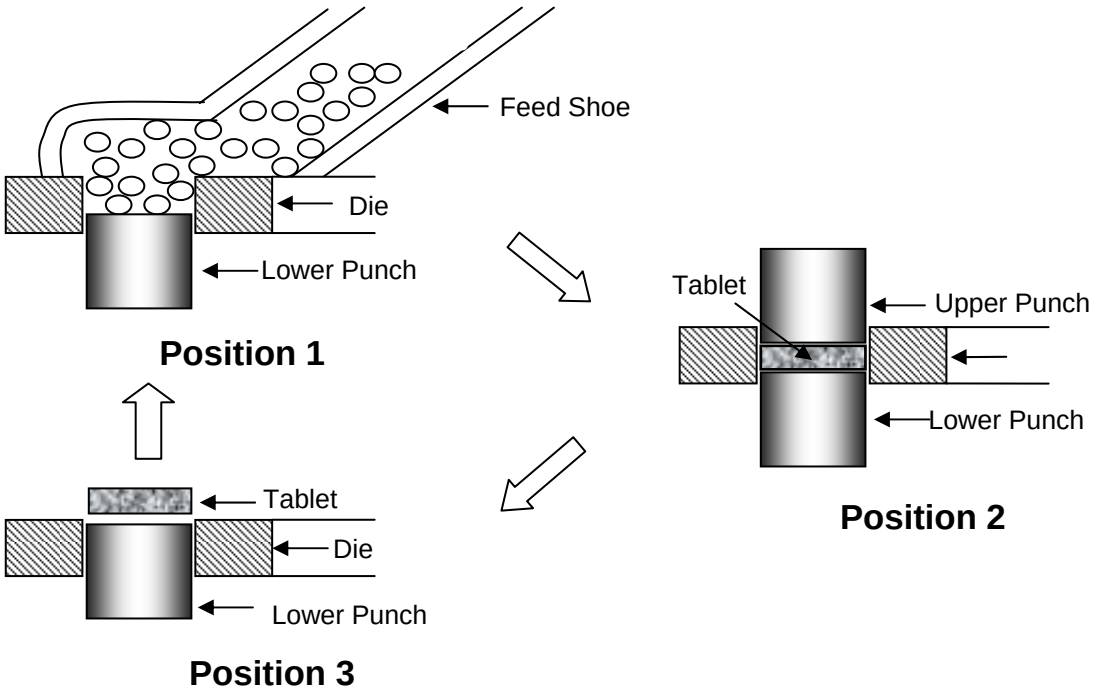

Figure **2.1**: Powder compaction process showing the main steps (Fayed and Otten, 1997)

2.1.6 Mechanism of compaction

The production of powder compact, tablet, or briquet can be done by many ways, the purpose of which is to form the powder into a more or less well-defined shape. When the particulate solid is placed into the cavity or die and pressure is applied, a reduction in volume occurs due to following mechanisms (Figure **2.2**).

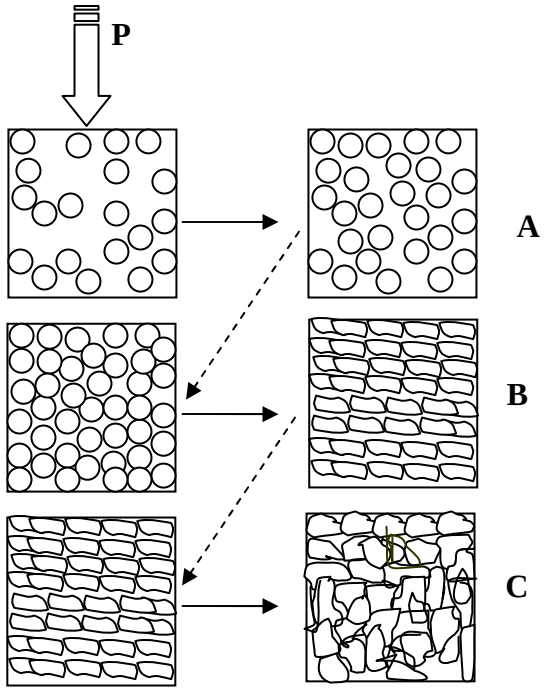

Figure **2.2**: Mechanism of compaction (Fayed and Otten, 1997)

1- If the pressure is low, rearrangement of the particles occurs, resulting in tighter packing (A). In this stage, energy is dissipated in overcoming friction among particles inside the die, and the amount of the friction is highly dependent on the coefficient of interparticle friction. In the case of fine particles, cohesive arches may collapse at this stage (Fayed and Otten, 1997).

2- If the pressure is high, elastic and plastic deformation of the particles may take place, leading particles to flow into void spaces and increasing the area of interparticle contact (B). Interlocking of particles may occur. For material of low melting point and low thermal conductivity, the heat generated at points of contact may be sufficient to raise the local temperature which can increase plasticity and melting that facilitate

particle deformation. In the case of brittle materials, the stress applied at interparticle contacts may lead to particle fracture followed by rearrangement of the fragment to give reduced volume (B).

3- Stages B and C carry on until the tablet density reaches the target density value of the material. Elastic compression of the particle and entrapped air will be present at all stages of the compaction process (Fayed and Otten. 1997).

2.1.7 Tablet process

In pharmaceutical industry, generally, there are two types of tablet presses used in production: the single-punch press and the rotary press (Aulton, 2002). Besides, in research and development work hydraulic presses are utilized as advanced tools for measuring the tabletting properties of powders.

2.1.7.1 Single-punch press

A single-punch press possesses one die and one pair of punches (Figure **2.3**). The powder is held in a hopper, which is connected to a hopper shoe located at the die table. The hopper shoe moves to and over die, by either a translational or a rotational movement. When the hopper shoe is located over the die, the powder is filled into the die by gravity. The amount of powder deposited into the die is controlled by the position of the lower punch. When the hopper shoe is located beside the die, the upper punch moves down and the powder inside the die is compressed. During the compression process, the

lower punch is stationary and the pressure is thus applied by the upper punch and controlled by the upper punch displacement. After ejection, the tablet from the die is pushed away by the hopper shoe as it moves back to the die for the next tablet. The output of single-punch press is about 200 tablets per minute.

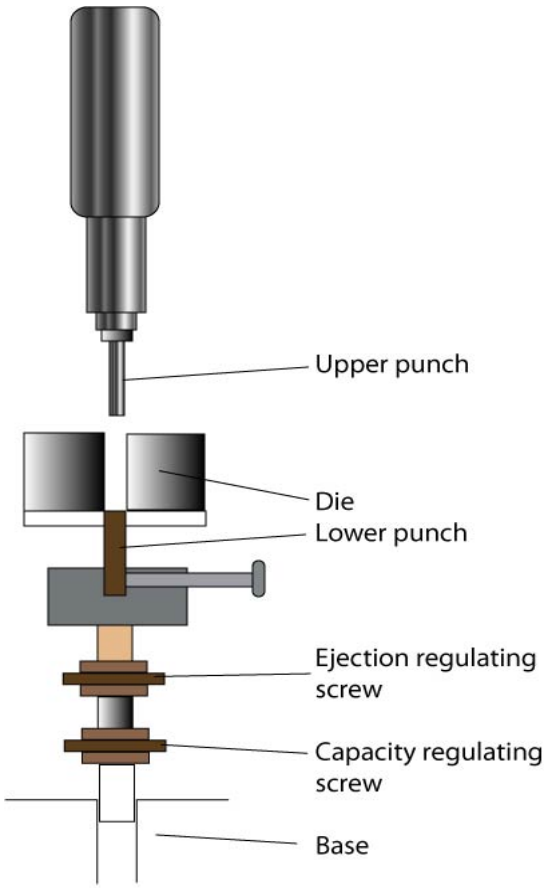

Figure **2.3**: A single-punch press (Aulton, 2002)

2.1.7.2 Rotary press

The rotary press was developed to increase the output of tablets. Outputs of over 10,000 tablets per minute can be obtained by rotary presses (Aulton, 2002). A rotary

press works with a number of dies and sets of punches, which can vary from three for small rotary presses up to 60 or more for large presses. The dies are located in a circle in the die table and both the die table and the punches rotate during operation of the machine, so that one die is always associated with one pair of punches (Figure **2.4**). The vertical movement of the punches is controlled by tracks that pass over cams and rolls used to control the volume of powder fed into the die and the pressure applied during compression. The powder is held in a hopper whose lower opening is located just above the die table. The powder flows by gravity on to the die table and is fed into the die by a feed frame. The reproducibility of the die feeding can be improved by a rotating device, referred to as force feeding

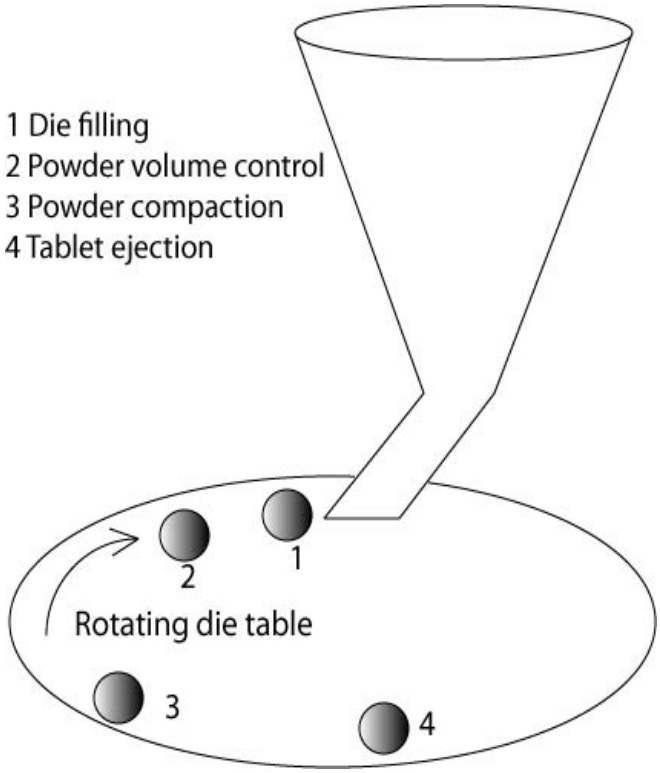

Figure **2.4**: Schematic illustration of the event involved in the formation of tablets with a rotary press (Aulton, 2002)

2.2 Filling methods

Molenda et al. (1993) have studied the influence of filling methods on the static wall load to total grain load ratio (SWL/TGL) and the dynamic-to-static wall load ratio (DSR) in grain bins. Four filling methods, at center and eccentric locations, sprinkle filling, and uniform filling through an annular ring near the bin wall, were evaluated. Three types of bin walls were tested for each filling method: smooth galvanized steel, corrugated galvanized steel, and smooth steel covered with abrasive cloth. Soft and hard winter wheats were used in the experiments. In all, six methods of bin filling (i.e. A, B, C, D, E, and F) were used in the experiments as shown schematically in Figure **2.5**.

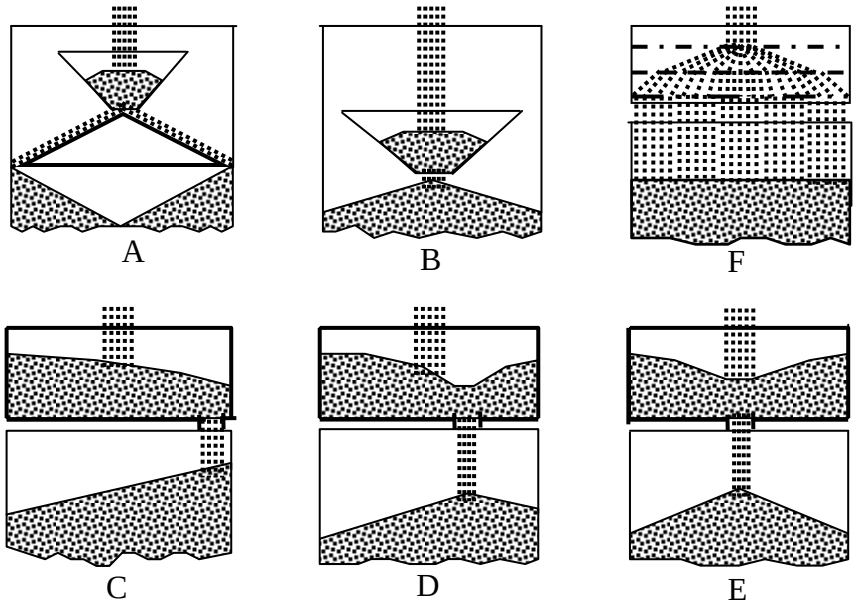

Figure **2.5**: Schematic of bin filling methods (Molenda et al., 1993)

For methods A and B, the bins were filled with a special device inserted into the bin and lifted during filling at a constant rate of 4 mm/s to obtain the desired grain orientation. For method A, the filling device had the shape of a cone with the vertex

directed upward. For method B, the filling device had the shape of a cone with the vertex directed downward and aligned with the center axis of the bin. Grain was deposited on the pile through an orifice at the vertex of the cone. As a result, the grain formed a conical sloping surface with the vertex directed upward and the grain tending to rest with their long axis along a line of the formed cone. For methods C, D, and E, the filling device was a flat-bottom basket having the same diameter as the bin that was fixed 2 cm above the upper edge of the bin wall. Grain was directed into the basket and then fell down through one of the three orifices which were 50 mm in diameter. Method F was used to fill the bin so that no sloping surfaces were formed. This was achieved by placing three layers of wire mesh with 12 mm aperture 15 cm apart in the tube of the same diameter as the test bin. Molenda et al.'s results showed a higher SWL/TGL resulted in a lower dynamic-to-static wall load ratio (DSR). Sprinkle filling produced lower SWL/TGL values on the smooth wall and higher values on the rough and corrugated walls. The filling method and type of wheat significantly influenced the negative friction force on the smooth wall bin. Friction force values were highest for the top filling methods.

In the follow up study, Molenda et al. (1996) continued to study the effect of filling method on load distribution in model grain bins. They studied the spatial arrangement of wheat in bulk on the angle of internal friction determined in triaxial tests and on the load shift in a model bin. A schematic diagram of the experimental apparatus is shown in Figure **2.6.** The three methods of bin filling used in the experiments are shown schematically in Figure **2.7**.

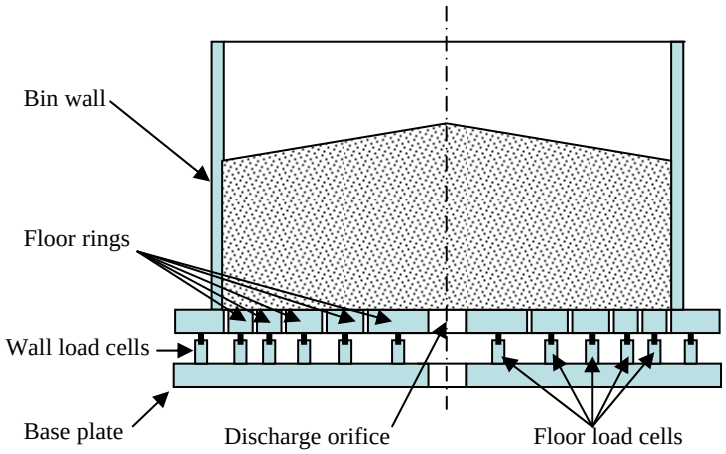

Figure **2.6**: Schematic diagram of stress measurement system (Molenda et al., 1996)

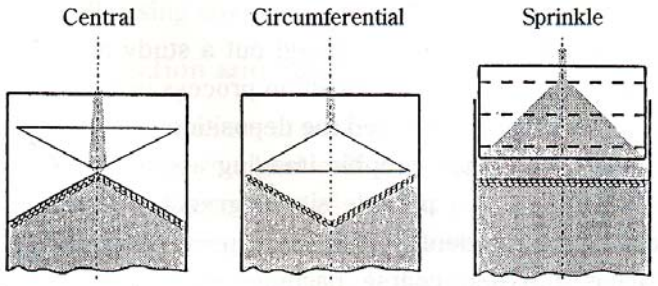

Figure **2.7**: Schematic of bin filling methods (Molenda et al., 1996)

For central filling, the device had a shape of a cone with the vertex directed downward and aligned with the center axis of the bin. For circumferential filling, the filling device had the shape of a cone with the vertex directed upwards. The radius of the cone was 15 mm less than the radius of the bin. As a result, the stream of grain was directed towards the bins wall. The sprinkle filling method used a device to fill the bin so that no sloping surfaces were formed. For each filling method, the bin was filled to the same level at the wall to simplify the calculation of in-bin grain bulk density. The results showed the influence of the bedding structure generated by three filling methods in the

radial distribution of vertical pressure on the bottom of a cylindrical flat-floor bin and the resultant lateral to vertical pressure ratio (k). The filling method significantly influenced the radial distribution of vertical pressure on the floor of the bin.

Rice and Tengzelius (1986) have studied the die filling characteristic of a metal powder. They used a filling shoe technique with different filling test apparatuses, such as, the morganite flow meter, Oakley flow meter, and Swedish filling plate. They investigated the effect of direction of motion of filling shoe, speed of motion, the number of passes, and also the effect of vibration on filling density on dies. The conclusion was that none of the procedures examined were suitable for standardization. The morganite apparatus and the counting of the number of passes of the shoe required to fill the die were good for fine powders. Moreover, this method failed completely to differentiate between powders which were free flowing and not free flowing in a flow meter.

Smid et al. (1993) have studied the effect of filling method on the packing distribution of a catalyst bed. They measured the bulk density of a catalyst bed in a 2-dimensional reactor model by using the radiogauging method. Three ways of introducing the catalyst into the two-dimensional plane model of reactor were investigated (Figure **2.8)**.

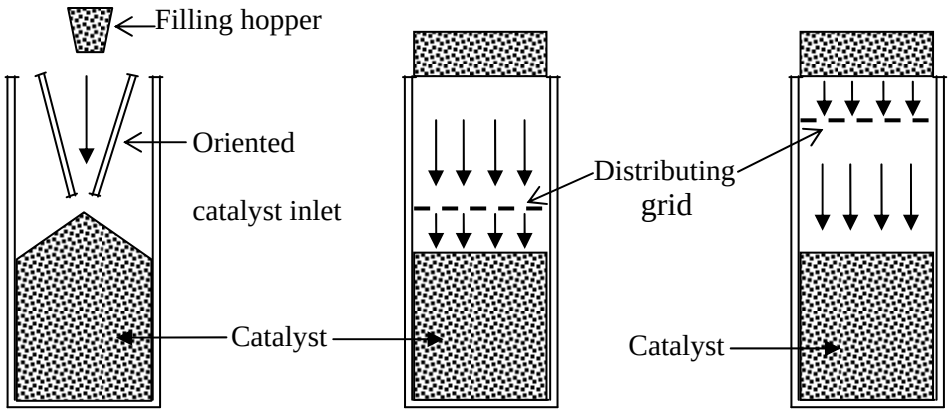

Figure **2.8**: Filling methods: a) free pouring; b) "rainy" filling with distributor in low position; c) "rainy" filling with distributor in high position (Smid et al., 1993)

Free pouring, rainy filling with distributing grid in a low position, and rainy filling with the distributing grid in a high position were employed. Attention was paid to bulk density near the wall and the bottom of the model. Differences in the bulk densities in the center of the reactor were obtained for free pouring method. The results showed that the bulk density of a layer of cylindrical catalyst particles (particle size 3 mm) revealed a central region of increased density over entire height of the layer. The region of higher bulk density was narrower in the direction of the free surface of the catalyst layer. The reactor model was filled with freely poured particles so that a layer with a characteristic slope corresponding to the angle of repose was formed.

Bocchini (1987) studied the influence of a small die width on filling and compacting densities. A special apparatus consisting of rectangular dies of various widths was utilized with copper and mixed elemental bronze powder. The results showed that filling densities decreased with decreasing die opening. The angle between the direction of motion during filling and the main die axis also influenced the filling density. Bocchini

also concluded that the decrease in filling density caused by decrease in wall thickness can be explained by introducing the concept of boundary layer existing at the die wall.

Dhanoa and Puri (1997) designed and built a mass deposition tester (MDT) to evaluate the effect of filling method, rate of fill, die cross-section and die size (aspect ratio, the ratio of die width to depth) on the spatial fill density distribution (Figure **2.9**). A funnel filling method and sieve filling method were used by Dhanoa and Puri (1998) to study the uniformity of particle material on small dies. They invented the real time spatial particulate mass deposition tester to determine the in-situ pre-compaction particulate density distribution.

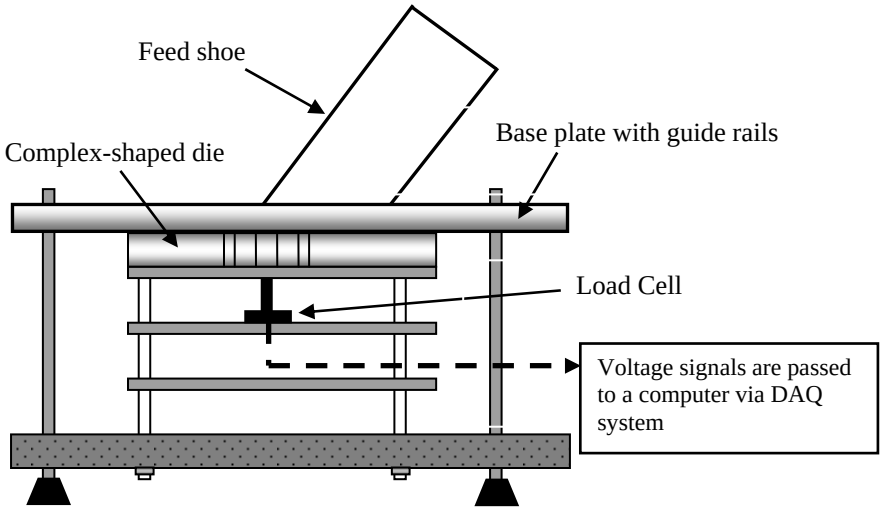

Figure **2.9**: Schematic of MDT along with feed shoe deposition method (Dhanoa and Puri, 1997)

The effect of three different deposition methods (feed shoe, funnel, and rainy) as shown in Figure **2.10** on the compaction response were studied by Mittal and Puri (1999).

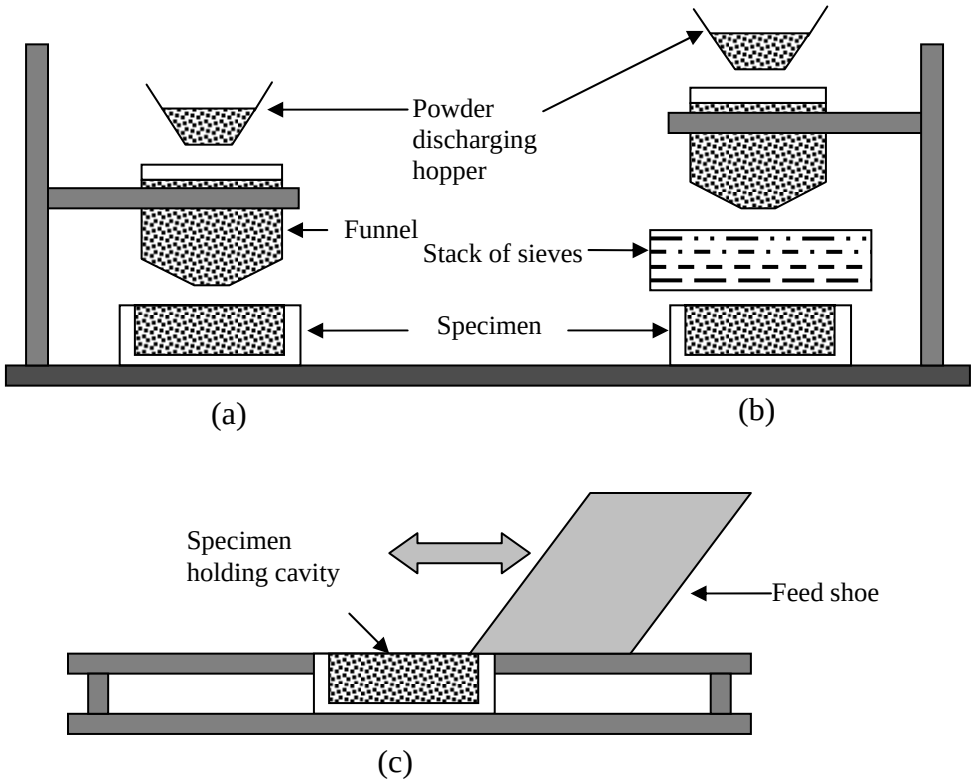

Figure **2.10**: Schematic of the three powder deposition methods (Mittal and Puri, 1999)

A silicon nitride-based ceramic powder (KY 3500) and a microcrystalline cellulose (MCC)-based pharmaceutical powder were used to test the stress-strain response using a medium pressure (<35 MPa) flexible boundary cubical triaxial tester (CTT). Bulk modulus, shear modulus, compression index, and swelling index were evaluated for each of the three deposition methods at different isotropic pressure values.

The results showed that deposition methods have a significant influence on certain constitutive parameters (elastic and plastic) of tested powders. For KY 3500 powder, it was concluded that the shear modulus and compression index values were sensitive to deposition methods. For the MCC powder, it was determined that all of the four constitutive parameters were sensitive to all three deposition methods.

A real time cumulative mass deposition tester (MDT) was used by Mittal et al. (2001) to study the deposition behavior of a free-flowing manganese zinc ferrite or MZF powder (Figure **2.11**). The feed shoe deposition method was used to fill the powder in toroid and E-shape containers. Two different feed shoe approach directions were used for the E-container and one direction for the toroid container. The results showed powder deposition was affected by both fill direction and container shape for the E-container. Each filling direction had unique characteristics (Figure **2.12**).

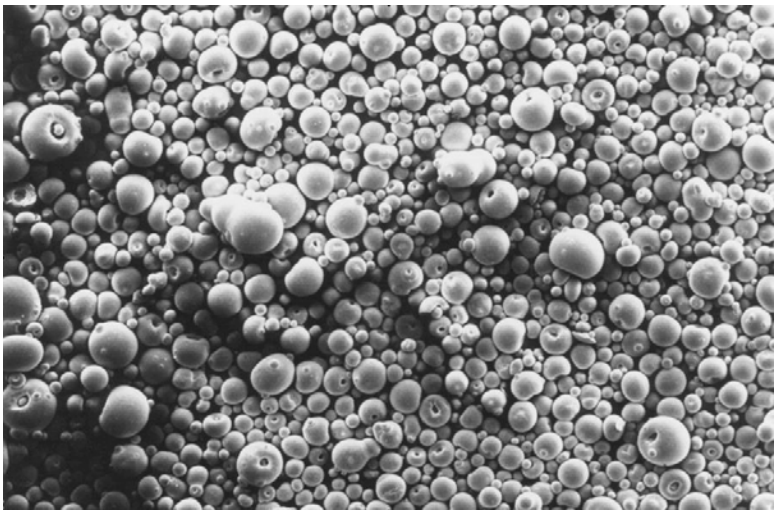

Figure **2.11**: Scanning electron microscope photograph of MZF powder (Photo courtesy of Spang and Co., Butler, PA)

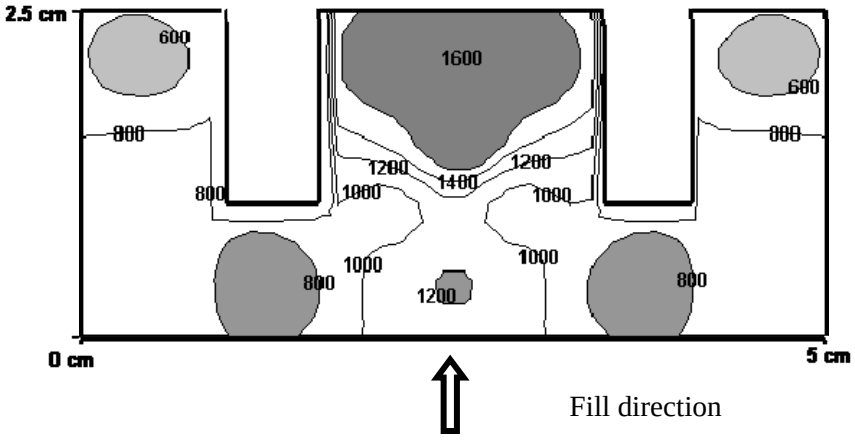

Figure **2.12**: Powder's spatial mass distribution at the end of fill process for shown fill direction for E-Shaped die (Mittal et al., 2001)

The results also illustrated that the powder mass was highly concentrated in the middle leg of the toroid-container and the powder experienced noticeably less influence from container walls during deposition in the middle leg (Figure **2.12**). In addition, powder mass distribution of a toroid die is shown in Figure **2.13**. The mass distribution is symmetric with concentration in the forward end of process.

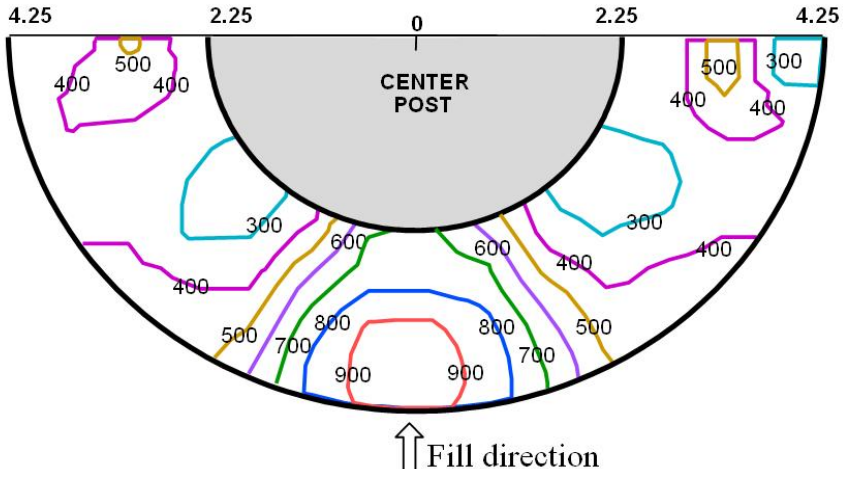

Figure **2.13**: Powder's spatial mass distribution for toroid die (Mittal et.al., 2001)

A feed shoe filling model was developed by Cocks et al. (2001) and Wu et al. (2003) to simulate the commercial die filling process. The feed shoe initial acceleration was varied over the range of 0.1–100 m/s^2 and the steady state velocity of the feed shoe was varied over the range of 0.05–1 m/s. They observed that during the forward stroke of feed shoe movement, the granular material was caused to move to the back of the feed shoe due to inertia when the feed shoe accelerated from rest. In the case of a short height of powder in the feed shoe, a space was created at the front of the feed shoe, and the powder adopted a nose shaped profile, as shown in Figure **2.14**.

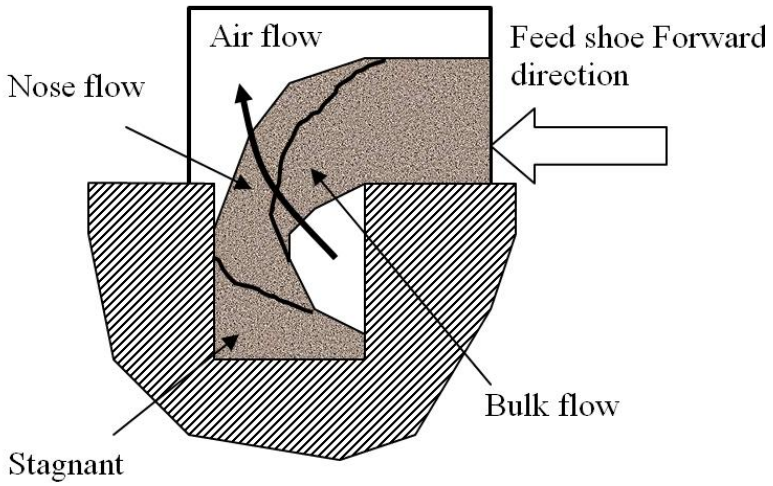

Figure **2.14**: General features of die filling process with the feed shoe method (Wu et al., 2003)

The influence of the filling shoe movement on the powder density in a filled, ring shaped cavity was investigated by Hjortsberg (2000). The outer and inner diameters of the cavity were 29 cm and 26.2 cm, respectively, and the approximate weight of powder in a filled cavity was 650 g. The density variations between different parts of the ring and different types of filling operations were measured. It was determined that the movement

of the filling shoe causes density variations in the filled powder and that these density variations are identified for rings filled under the same conditions. Conventional filling, where the filling shoe only performs one filling cycle resulted in density variations from 0.354 to 0.363 in relative density. Hjortsberg and Bergquist (2002) listed various factors that are expected to influence die filling in feed shoe method as shown in Table **2.1**. These factors were prioritized based on their possible effect on filling powder density, as shown by the numbers in the table. The larger the number, the greater is the effect.

Table **2.1**: Factors expected to influence die filling in feed shoe method

Property	**Expected importance**
Feed shoe speed	9
Feed shoe acceleration	9
Feed shoe vibration	9
Number of additional filling cycles over a filled cavity	9
Cavity geometry	9
Cavity vibrations	9
Apparent density of powder	9
Powder flow	9
Powder level of feed shoe	3
The time the shoe spends stationary in the filling position	3
Suction or gravity filling	3
Particle size distribution	3
Powder tap density	3
Fill table levelness	3
Powder and machine temperature	1
Component density in powder mix	1
Method to fill feed shoe	1

A funnel filling method was used by Tukiendorf (2003) to evaluate grain distribution in the chosen cross sections of the cylindrical shape bins. Mustard granules

were chosen and characteristic distribution was observed and using photography that showed seeds were mixing with steel particles. Steel particles were placed in the middle of the input bin while the mustard particles were put in the upper and lower as tracers. Tukiendorf used digital picture analysis to evaluate the tracer color distribution and its volume participation in the sample. The results showed that the character of these changes is different for various mixing ways. Figure **2.15** shows a distribution of steel particles in the mid-height section generated during mixing of granular materials.

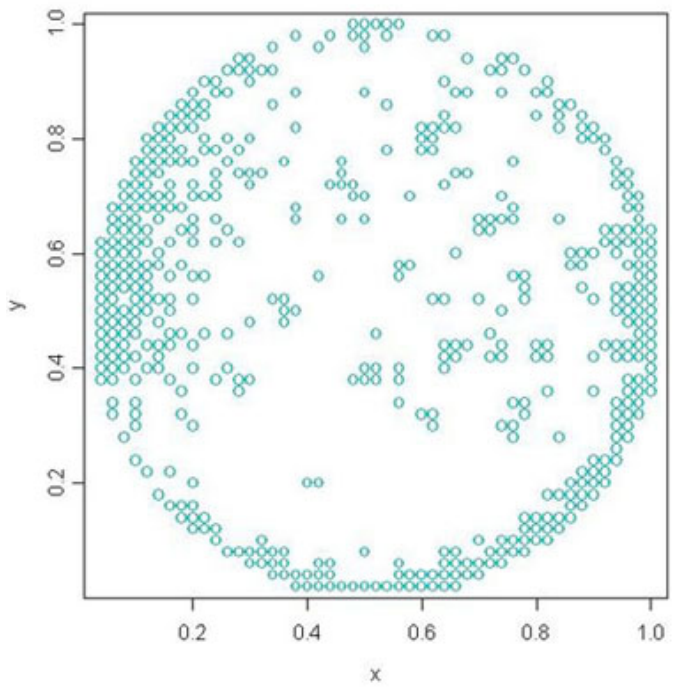

Figure **2.15**: Scatterplot of the tracer's locations for the mixing data (Tukiendorf, 2003)

Xie and Puri (2006) conducted research with second generation of mass deposition tester (MDT-II). They used three parallel cylindrical containers and three parallel toroidal dies containers (Figure **2.16**). To investigate the effect of die locations, die shape, and feed shoe speed. The results revealed that the right die had higher mean

final mass value than center die. Feed shoe speed, 100 vs. 500 mm/s for toroidal die, showed that the mean final mass values were similar at these two speeds except for 0^0 and 180^0 orientations. For cylindrical dies, 500 mm/s feed shoe speed had higher mean final mass value that 100 mm/s feed shoe speed for most locations. Between cylindrical and toroidal dies, toroidal dies had lower measured mean final mass values.

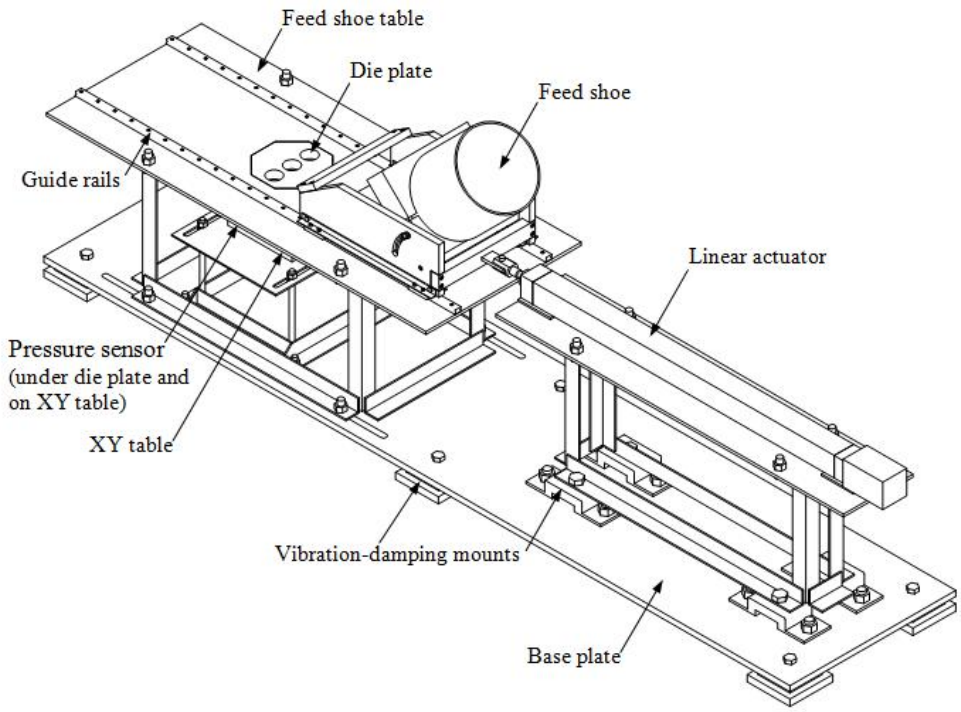

Figure **2.16**: A design schematic of the new MDT (Xie, 2006)

Xie et al. (2003) also investigated the parameters that influenced the uniformity of powder deposition in multiple dies. Three cylindrical dies were filled simultaneously at two different speeds, 20 mm/s and 100 mm/s. Experimental results showed that for the center die, most locations within the half radius had higher pressure than locations close to the wall. The results showed MDT was an effective and efficient device for

investigation of powder uniformity in multiple dies and most of the pressures at different locations of the right die were higher than those of the center die. In addition, a faster shoe speed was observed to favor most of the half radius locations for higher pressures.

Zahrah et al. (2001) developed a fluidized fill shoe to increase powder flow rates and improved the uniformity of fill for complex-shaped die cavities (Figure **2.17**). Zahrah used gas to 'lubricate' powder particle to eliminate inter-particle friction and to improve powder flow rates. A fluidized fill shoe with a custom designed delivery chute enabled the delivery of powder in a fluidized state to the die cavity. Their results demonstrated that the fluidized fill shoe added flexibility to the conventional powdered metal process by providing additional control to the user and improving production rates, while reducing the standard deviation on weight and dimensions of the products. This fluidized fill shoe could typically increase fill density for parts with a thin wall and for powders with poor flow characteristics.

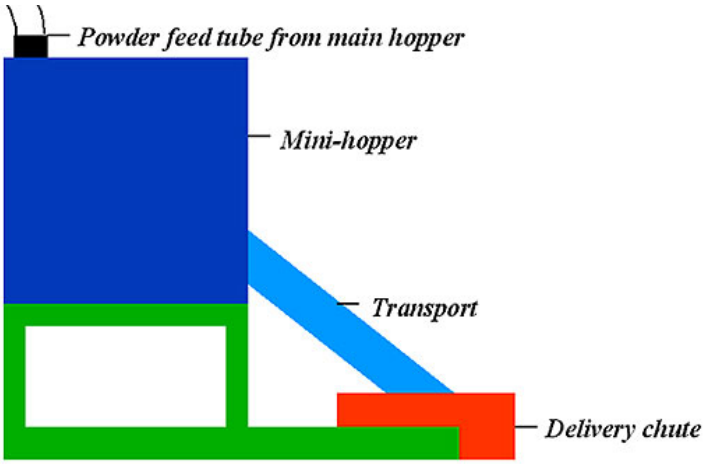

Figure **2.17**: Schematic of fluidized fill shoe system (Zahrah et al., 2001)

Solid deposition in the horizontal pipeline of a pneumatic filling system was studied both mathematically and experimentally by Li et al. (2004). Mathematically modeled results using the coupled discrete element method (DEM) and computational fluid dynamics (CFD) approaches have demonstrated an intensive exchange of particles between the stationary layer (deposited particles) and the moving slug and a variation of solids concentration and pressure and velocity distribution across the slug. Li et al. showed a tendency of more solids deposition with lower gas mass flow rate in slug flows except that, below a certain amount of solids mass flow rate, the deposition becomes independent of gas flow rate.

Pecora and Goldstein (1993) developed a new solids feed valve based on the destruction of the repose cone resulting from the deposition of bulk solids over a horizontal surface by fluidization of its base, followed by pneumatic transport of the fallen particles. Tests were carried out to determine the mass flow rate of bulk solids.

2.3 Discharge rate from hopper

There are two basic modes of flow, namely mass flow and funnel flow. Funnel flow or core flow occurs in bins with the flat bottom or with a hopper with shallow slope. Solids flow to the outlet orifice within the channel. The channel is usually conical in shape, and the diameter of this channel is approximately equal to the largest dimension of the active area of the outlet. A storage bin having a funnel flow pattern usually is designed to supply maximum volume for storage without considering that the actual discharge capacity may be much less due to accumulation of stagnant material.

The mass flow occurs in bins with sufficiently steep and smooth hoppers and where material discharges from the entire area of the outlet. All material is in motion including sliding against the wall of the vertical section and conveying hoppers (Figure **2.18**).

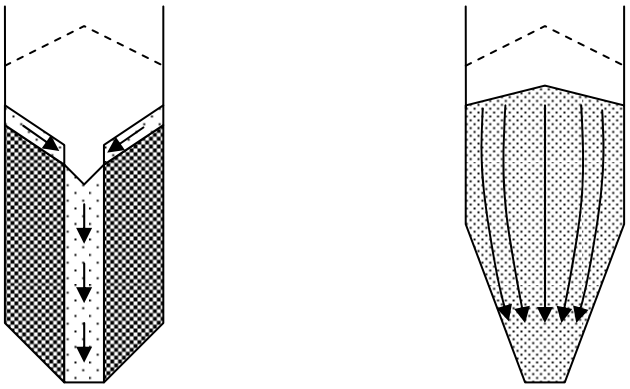

(a) Funnel flow (b) Mass flow

Figure **2.18**: Bin flow characteristics (Fayed and Otten,1997)

Particle in the vertical part moves uniformly downward where the level is above some critical distance above the hopper-cylinder transition. If the level drops below that point, the material in the center of the channel will flow faster than the material at the walls.

Mass flow has the following advantages over the funnel flow:

a. Erratic flow, channeling, and flooding of powder are avoided.
b. Stagnant regimes within the silo are eliminated.
c. Particle segregation is significantly reduced.
d. Material in the silo acts as a gas seal.

Expanded flow is the combination of funnel flow and mass flow. The mass flow section is used to expand the active flowing volume, to minimize stagnant areas, and to provide reliable discharge without bridging that could lead to a smaller discharge opening.

2.3.1 Correlation for discharge rate through orifice

The discharge of granular material through outlet orifice is shown in Figure **2.19**. The stress analysis of Shaxby and Evans (1923) showed that the weight of the material is borne substantially by the walls, and there is no dependence of the mass flow rate W on height H. Brown and Richards (1965) reported that the W is constant provided $D>2.5D_0$ and the latter gave correction factor for smaller value of hopper diameter D. Franklin and Johanson (1955) suggested that $D-D_0>30d$, where d is the particle diameter.

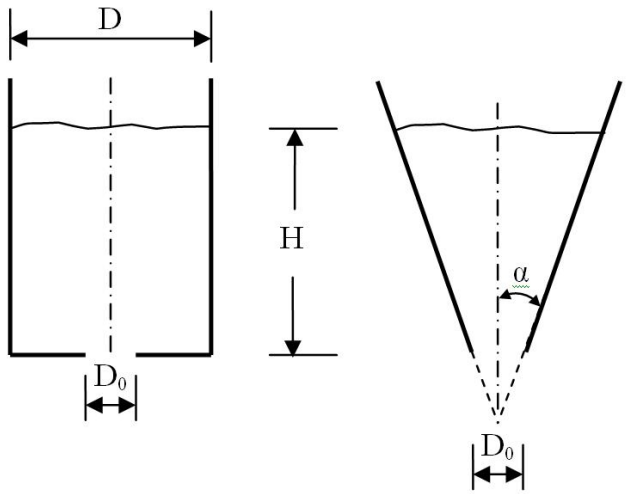

Figure **2.19**: Schematic diagram defining the notation in cylindrical and conical hoppers

Ignoring the possible effect of the particle diameter, d, dimensional analysis suggests that $W \propto \rho g^{\frac{1}{2}} D_0^{\frac{5}{2}}$. However, many early researchers suggested that $W \propto D_0^n$ where n is considerably greater than 2.5. Under this condition, the correlation must contain dimensional empirical constants or $d^{2.5-n}$. Beverloo et al. (1961) plotted $W^{\frac{2}{5}}$ against D_0 and obtained a linear relationship shown in Figure **2.20** . Their flow rate equation is given in Equation **2.1** .

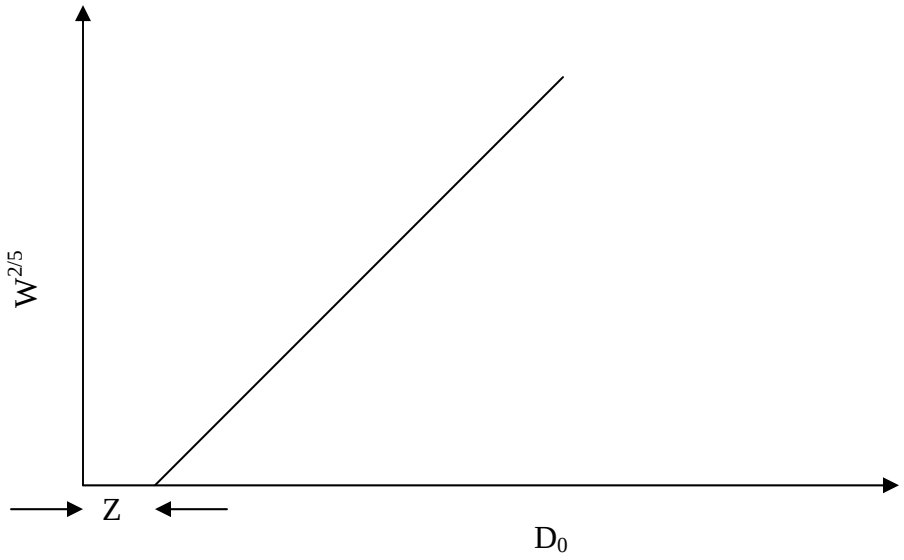

Figure **2.20**: Graphical representation of Beverloo et al. (1961) discharge rate equation

$$W = C\rho g^{\frac{1}{2}} (D_0 - Kd)^{\frac{5}{2}} \qquad \text{Equation } \mathbf{2.1}$$

where

W=mass discharge rate

C=Beverloo coefficient

ρ = bulk density

g =acceleration due to gravity

D_0= orifice diameter

K= dimensionless constant

d= particle diameter

The Z value (the space needed by a particle at the orifice to exit) was correlated linearly with the particle diameter Z=Kd. For spherical particles, *K* approximately is 1.5, and somewhat larger values were found for angular particles. Beverloo et al. also found the value of K depends significantly on the choice of typical dimension of the particle. The constant K was found to be a function only of the particle shape with no dependence on properties. The Beverloo equation is valid for funnel flow and coarse particles (particles>500 μm in diameter). This correlation is not recommended outside this range.

Although Myers and Sellers (1978) found that K depends on wall slope; Huntington and Rooney (1971) found that their results could be correlated equally well by correlations of the Beverloo et al. type equation. They presented Equation **2.2** :

$$W = A\rho D_0^{2.96} \qquad \text{Equation } \mathbf{2.2}$$

where

A= orifice area

D_0= orifice diameter

ρ = particulate density

However, while *C* and *K* were found to be the same for all the materials studied, no simple correlation could be found between A and the nature of the particles. Fowler

and Glastonbury (1959) have presented an alternative formulation for the effect of particle and outlet diameters as shown in Equation **2.3**.

$$W \propto AD_h^{\frac{1}{2}}\left(\frac{D_h}{d}\right)^{0.185} \qquad \text{Equation } \mathbf{2.3}$$

where D_h is hydraulic mean diameter and d is particle diameter

Rose and Tanaka (1959) presented Equation **2.4**

$$W \propto D_0^{\frac{5}{2}}\left\{\frac{D_0}{d}-3\right\}^{0.3} \qquad \text{Equation } \mathbf{2.4}$$

and Harmens (1963) presented Equation **2.5**

$$W \propto D_0^{\frac{5}{2}}\left\{f(\phi)-\frac{0.35\left(\frac{d}{D_0}\right)^{1.5}}{0.45+\left(\frac{d}{D_0}\right)^{1.5}}\right\} \qquad \text{Equation } \mathbf{2.5}$$

where $f(\phi)$ is a function of the angle of repose, ϕ

Though in many circumstances these different equations give equally good correlations, the physical arguments behind them are less satisfying than those leading to the Beverloo et al. correlation. All these correlations break down for fine materials, d<500 μm, due to the effects of interstitial pressure gradients. Clearly, the Beverloo et al. correlation requires a density for dimensional consistency but there is dispute as to the appropriate value to use since the density within a hopper varies with respect to both time and position.

Johanson (1965) presents an Equation **2.6** for mass flow discharge for coarse particles (particle>500 μm in diameter)

$$W = \rho A\sqrt{\frac{Bg}{2(1+m)\tan(\theta)}} \qquad \text{Equation } \mathbf{2.6}$$

where θ = hopper angle

W=discharge rate

ρ =bulk density

g=gravity acceleration

Depending on whether it is a conical or a symmetric slot opening hopper, the remaining parameters in the equation are given in Table **2.2** .

Table **2.2**: Johanson equation parameters

Parameter	Conical hopper	Symmetric slot hopper
B	D, diameter of outlet	W
A	$\frac{\pi}{4}D^2$	WL
m	1	0

Fine particles (d_p<500 μm) tend to flow slower by factor of 100 to 1000 than that predicted by the Johanson equation. The reason for this is the effect of air drag on the motion of the particles is much greater for fine particles. Particle beds need to dilate (increase distance between particles) before the powder can flow. This means air must penetrate into the bed through the bottom surface of the hopper as the powder moves through the constriction formed by the conical walls. For fine particles, the pore diameters in the powder bed are small and there is a significant amount of air drag that resists the powder motion.

Carleton (1972) gives an expression for predicting the velocity of the solids shown in Equation **2.7**.

$$\frac{4V_0^2 \sin\theta}{B} + 15\frac{\rho^{\frac{1}{3}}\mu^{\frac{2}{3}}V^{\frac{4}{3}}}{\rho_p d^{\frac{5}{3}}} = g \qquad \text{Equation } \mathbf{2.7}$$

where V_0 =average velocity of solids discharging

B= given in Table 2.2

ρ, μ = air density and viscosity

ρ_p = particle density

θ = hopper angle

d_p = particle diameter

Verghese and Nedderman (1995) studied the flow rates of coarse materials through conical hoppers conforming to the models of Beverloo et al. (1961) and Rose and Tanaka (1959); with the mass flow rate being proportional to $D^{5/2}$, where D is the orifice diameter. The results showed that for fine materials in the wider cones, i.e. cones of half-angle greater than 45 degree, the flow was not steady. Regular oscillations in the flow rate were seen and these were accompanied by a pulsing of the top surface. The results for the coarsest sand and the kale seed were analyzed according to the Beverloo et al. model by plotting $W^{5/2}$ vs. D. In both cases, excellent agreement was obtained with correlation coefficients in excess of 0.98. They also concluded that the pressure gradient values were, however, found to be independent of orifice diameter and inversely proportional to the square of the particle diameter. A correlation was proposed in which the mass flow rate was proportional to $D^{5/2}$ multiplied by a factor which has a linear

function of particle diameter squared. Larid and Roberts (1979) studied non-constant slope hopper walls. For a hopper as shown in Figure **2.21**, the mass flow rate was found to depend only on α_1 and not α_2 provided the length of the lower section was greater than $3r_0$, where r_0 is radial distance to the orifice plane from the virtual apex.

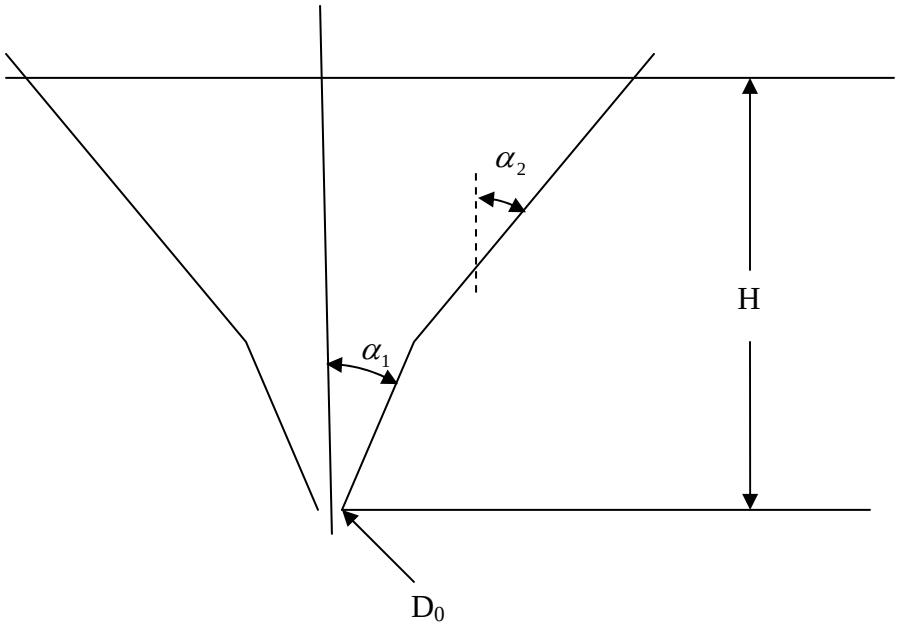

Figure **2.21**: Schematic diagram of a hopper with changing wall slope

Some work has been done on mixture of powders of different sizes by Danish and Parrot (1971). This work was mainly concerned with powders of interest to the pharmaceutical industry. They found that for commonly used particle size distributions the effect of interstitial pressure could not be neglected.

2.4 Theories of mass flow rate

The minimum energy theorem of Brown and Richards (1965) is dependent on the details of the free-fall arch as shows in Figure **2.22**.

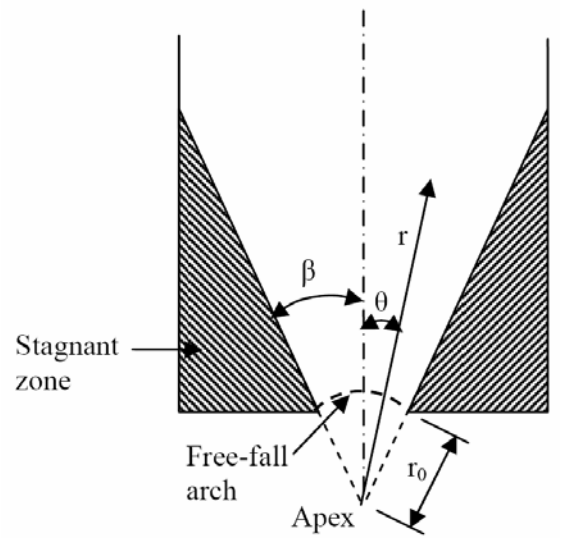

Figure **2.22**: Minimum energy theorem of Brown and Richards (1965)

They considered an equation of the Bernoulli type for the total energy content, T, of unit mass of material as it flows radially toward a point sink somewhat below the orifice as sown in Equation **2.8**

$$T = gr\cos\theta + \frac{V^2}{2} + \frac{\sigma}{\rho} \qquad \text{Equation } \mathbf{2.8}$$

where T= total energy content

g =acceleration due to gravity

r= radial coordinate

θ = angular coordinate

V= velocity

σ = normal stress

ρ = density

They argued that the energy content must decrease with time and hence that (dT/dr) must be positive. They further assumed that the contribution of the σ term is negligible. This simplified the solution if H does not enter the analysis and in the absence of any other quantity with the dimensions of length. With this assumption, a result of the form $W \propto g^{\frac{1}{2}} D^{\frac{5}{2}}$ was shown to be valid for radial flow. The velocity V is given by (A/r^2) in axisymmetric or (A/r) in plane strain, where A is a function of angular position only. Accordingly, the gradient function (dT/dr) is given in Equation **2.9**:

$$\frac{dT}{dr} = g\cos\theta - \frac{A^2}{r^5} \qquad \text{Equation } \mathbf{2.9}$$

It was assumed that (dT/dr) is positive throughout the region above the free arch. Hence Equation **2.10**:

$$A^2 = r_0^5 g\cos\theta \qquad \text{Equation } \mathbf{2.10}$$

where r_0 is radial distance to the orifice plane from the virtual apex.

Additionally, the radial acceleration at the arch can be calculated from Equation **2.11**:

$$V\frac{dv}{dr}\Big|_{r=0} = g\cos\theta \qquad \text{Equation } \mathbf{2.11}$$

Brown and Richards' (1965) analysis is based on continuum mechanics and can, therefore, give no information on the effect of particle diameter. Davidson and Nedderman (1973) presented the "hour-glass theory" wherein they considered a narrow-

angle, smooth-walled conical hopper as shown in Figure **2.23**. Since the shear stress is zero on the smooth wall and on the axis of symmetry, it is assumed to be zero throughout, and the radial, tangential, and circumferential stresses are, therefore, principal stresses.

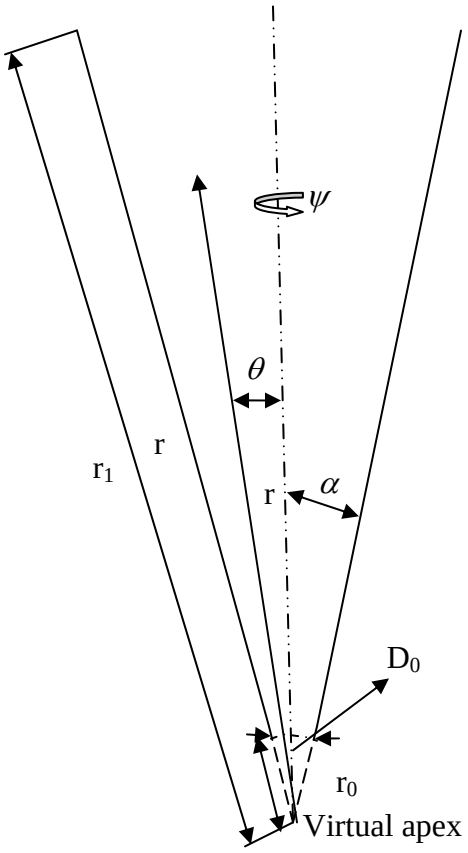

Figure **2.23**: Schematic and symbols for hour-glass theory of Davidson and Nedderman (1973)

As the particle flow converges toward the apex of the cone, a passive state of stress is assumed. Furthermore, invoking the Coulomb failure criterion, relationships between radial ($\sigma_{\theta\theta}$), circumferential ($\sigma_{\phi\phi}$) and radial stresses (σ_{rr}) were developed as shown in Equation **2.12:**

$$\sigma_{\phi\phi} = \sigma_{\theta\theta} = \left(\frac{1+\sin\phi}{1-\sin\phi}\right)\sigma_{rr} = k\sigma_{rr} \qquad \text{Equation } \mathbf{2.12}$$

where $\sigma_{\phi\phi}$ = circumferential component of normal stress (Pa)

$\sigma_{\theta\theta}$ = tangential component of normal stress (Pa)

σ_{rr} = radial component from normal stress (Pa)

ϕ = angle of internal friction or angle of repose

k= Janssen's or pressure ratio constant (dimensionless)

It is assumed that the velocities are radial and independent of angular position, this yields a first order differential equation in σ_{rr} that can easily be integrated. The two boundary conditions, $\sigma_{rr} = 0$ on r=r_0 (the free fall arch) and $\sigma_{rr} = 0$ on r=r_1 (the top surface) permit the evaluation of the constants of integration and the overall flow rate.

The mass flow rate is predicted in Equation **2.13**:

$$W = 2\pi\rho g^{\frac{1}{2}}(1-\cos\alpha)\left\{\frac{1+k}{2k-3}\right\}^{\frac{1}{2}} \cdot r_0^{\frac{5}{2}}\left\{\frac{1-y^{3-2k}}{1-y^{-2-2k}}\right\}^{\frac{1}{2}} \qquad \text{Equation } \mathbf{2.13}$$

where y=(r_1/r_0) and is normally large and α is hopper half angle.

k= Janssen's or pressure ratio constant

$r_{0=}$ radial distance to orifice plane from virtual apex

For commonly encountered materials, ϕ is in the range from 25^0 to 50^0, and hence k is in the range 2.5-7.5, and y is always raised to a large negative power. Replacing r_0 by the orifice diameter (D_0=2$r_0\sin\alpha$) yields Equation **2.14:**

$$W = \frac{\pi}{4} \frac{\rho g^{\frac{1}{2}} D_0^{\frac{5}{2}}}{\sin^{\frac{1}{2}} \alpha} \left\{ \frac{1+k}{2(2k-3)} \right\}^{\frac{1}{2}} \qquad \text{Equation } \mathbf{2.14}$$

It should be mentioned that this analysis is only valid for small α, since it has been assumed that the material is subjected to a radial body force of ρg. A similar analysis for an orifice of width b in a chisel-shaped hopper of thickness t gives Equation **2.15**:

$$W = \frac{\rho g^{\frac{1}{2}} t b^{\frac{3}{2}}}{\sin^{\frac{1}{2}} \alpha} \left\{ \frac{t+k}{2(k-2)} \right\}^{\frac{1}{2}} \qquad \text{Equation } \mathbf{2.15}$$

A key conclusion of these analyses was that the flow rate is independent of y and hence H. The dependence on the orifice dimension follows automatically. The effect of friction angle, via the term in k, is shown to be small, but this does not seem to have been tested experimentally in any satisfactory way. On the other hand, the analysis can give no information on the effect of particle size, and the dependence on the hopper half angle α is not in accord with experiments. In general, this analysis over predicts the flow rate by a factor of 1.5-2. This method cannot predict a velocity profile since it is necessary to assume that the velocities are independent of angular position.

2.5 Powder characteristics

2.5.1 Powder flowability

The flow properties (i.e., cohesion and slope of the yield locus) were investigated by Kamath et al. (1993). Two materials, wheat flour and sugar, were tested using four testers, namely, the triaxial cell, the direct shear cell, the Jenike shear cell, and the rotational split-level (RSL) shear cell over a range of loading conditions. The results showed that for wheat flour the flow properties were almost the same from all the four shear testers. For sugar, however, the test results from the RSL shear cell were significantly different from the other three testers.

Kamath and Puri (1997) built and calibrated a cubical triaxial tester to study the three-dimensional load-response of dry cohesionless and cohesive food powders at low pressures. They used a sample of wheat flour to load along isotropic, deviatoric, and mean effective stress paths. The isotropic (i.e. hydrostatic triaxial compression, HTC) test results were used to evaluate the state parameters, namely, the modified Cam-clay constitutive parameters λ (loading slope) and κ (unloading-reloading slope). Deviatoric and mean effective stress test results were used to evaluate the slope of the critical state line M. Test results yielded λ =0.046, κ =0.011, and M=0.98. The modified Cam-clay constitutive model was verified by comparing the model predicted stress-strain behavior of powder with the cubical triaxial tester experimental data.

2.5.2 Effect of powder characteristics on deposition related behavior

A general guideline for characteristic of bulk solids were developed by the European Materials Handling Equipment Manufactures Association. The general bulk properties for identification consist of eight groups of characteristics (Wilms and Kiihnemund, 1998):

1) Name of bulk solids and its chemical formula
2) Particle size
3) Particle shape
4) Angle of repose
5) Specific properties (i.e. cohesive, abrasive, corrosive, and explosive)
6) Moisture content
7) Bulk density
8) Additional information

Hoffmann et al. (1996) studied a series of industrial powders, most of them organic, were characterized in term of volumetric mean size, size distribution, density, particle shape, water retention characteristics (under a series of controlled ambient relative humidifies), and loosely packed and density packed voidage (giving the compressibility). The behavior of the powders in the powder handling apparatus (a precision powder filler) was also determined. Minimum and maximum bulk densities of the powders were related to the properties of the individual particles by means of a semi-empirical equation. Handling equipment used was a precision powder filler employing the auger principle, i.e., filling by means of a screw. The conical screw pushes the powder through an orifice

in the bottom of a small hopper. The powder level in this hopper is held constant by filling in turn from a larger feed hopper. Two aspects of the powder behavior are important in this type of equipment: the filling capacity and filling accuracy.

The values of the loosely packed and the tapped bed voidages for this range of mostly organic industrial powders could be corrected sufficiently well using the particle size, width of the size distribution, density, and shape index. The filling accuracy was related to the compressibility of the powder. For the range of powders investigated, an indication of the filling accuracy was gained directly from the particle properties using the equations and the table of values as given in Hoffmann et al. (1996). For completeness, some of the key equations are listed below:

$$compressibility = \frac{\varepsilon_{\max} - \varepsilon_{\min}}{1 - \varepsilon_{\min}} \qquad \text{Equation } \mathbf{2.16}$$

where

$\varepsilon_{\max}$ = void fraction of tapped packed bed

$\varepsilon_{\min}$ =void fraction of loosely packed bed

$$\varepsilon = 1 - \left\{1 - [(1 - \varepsilon_0)e^{a\rho\mu} + \varepsilon_0]e^{b\sigma}\right\}\psi \qquad \text{Equation } \mathbf{2.17}$$

where

a, b, c=constants, and c was taken as unity

ε =void fraction

ε_0 =void fraction for large, dense spheres of uniform size

ρ =particle specific gravity (the density divided by the density of water)

μ =mean particle diameter divided by a scale of 1 μm

σ =graphically determined standard deviation of log-normal particle size distribution

ψ =circularity of the projected particle squared

The parameter ε_0 signifies the voidage of uniform spheres for which the product $\rho\mu$ is so large that it does not influence the voidage in any significant way.

Hoffmann et al. (1996) used the Equation **2.18** for calculating the filling capacity for the handling equipment:

$$\overline{C} = K\rho_b \qquad \text{Equation } \mathbf{2.18}$$

where

$\overline{C}$ =average filling capacity over the range of 35-65% relative humidity (mg)

K=volumetric filling capacity per turn of screw (m^3)

ρ_b =bulk density (kg/m^3)

Table **2.3** summarizes values of fitted constants obtained for some powders by Hoffmann et al. (1996):

Table **2.3**: Fitted constants obtained for some powders (Hoffmann et al.,1996)

	ε_0	a	b	R^2
ε_{min}	0.338	-0.0114	-4.83	0.919
ε_{max}	0.535	-0.0128	-1.92	0.953

Suzuki et al. (2001) studied the effect of size distribution on tapping properties of fine powders. Fine powders with log-uniform size distribution were prepared by mixing

of mono-sized silica or fly ash powder. The tapping property of the powder packed beds was measured using the powder tester. The container for the packing was a stainless-steel cylinder with an internal diameter of 50.5 mm, depth of 50 mm, and capacity of 100 cm^3. The test powders were packed into the container to form a bed of 130-150 cm^3, which was then covered with a tapping cover, and the whole container including the tapping cover was allowed to fall freely 3, 5, 10, 30, 50, 100, 180, 300, 500, and 1000 times from a height of 18 mm. After the tapping operation, the tapping cover was removed and the piled powder on the container was cut away. The total mass of powder samples in the container was measured to determine the void fractions ε_j. Suzuki et al. (2001) presented a model equation for void fraction as shown in Equation **2.19**:

$$\varepsilon_j = \beta_j \sum_{k=1}^{m} Sa_k \varepsilon_{j,k} \qquad \text{Equation } \mathbf{2.19}$$

where $\varepsilon_{j,k}$ = partial void fraction around a particle *j* in direct contact with particle k

Sa_k is the fractional area of particle k.

β_j is a constant which is calculated from the following Equation **2.20**

$$\beta_j = \tilde{\varepsilon}_j / \varepsilon_{j,j} \qquad \text{Equation } \mathbf{2.20}$$

where $\tilde{\varepsilon}_j$ the void fraction in a bed of uniformity sized particle *j*, is obtained experimentally, and $\varepsilon_{j,j}$ is partial void fraction around a particle *j* in direct contact with particle *j*.

The effect of the packing process or the particles shape on the packing results can be considered in the experimental constant β_j. Suzuki et al. (2001) concluded that the

void fraction of the tapped powder bed is affected by size distribution for all tapping numbers. For log-uniform size distribution, the value of void fraction decreases with decreasing inclination of the size distribution.

Some of the known measuring techniques and equipment for the evaluation of the flowability of bulk solids which are simple, applicable, and used in practice were reviewed by Schulze (1998). Sixteen different measuring techniques or equipment were compared, including the Jenike shear tester, the ring shear tester, and the torsional shear tester, which is considered the versatile of all the sixteen techniques by Schulze (1998).

Abdullah and Geldart (1999) studied the relationship between bulk density of powders and flowability of porous and non-porous powders in which particle size changes as a result of controlling the percentage of fine components in the mixture. They concluded that the flowability of powder increases with the increase of particle size, and there appeared to be a critical size range above which flowability does not show any improvement.

2.6 Flow model

There has been extensive work done in the area of powder flow, using finite element model (FEM) and discrete element model (DEM). This section reviews some recent publications in the area of flow model using FEM and DEM.

2.6.1 Finite element model (FEM)

The finite element technique has long been used to model static and thermally induced loads in bins and silos. However, an area of research where little published work is found is that of finite element modeling of flow of cohesive granular materials in hoppers. To date, the bulk of the research has been confined to modeling of hopper flow using the finite elements model to cohesionless materials. A finite element model (FEM) was developed and validate for incipient flow analysis of cohesive powder from a hopper bin by Kamath and Puri (1999). A finite element model (FEM), using modified Cam-clay equations, was used to predict the incipient flow behavior of wheat flour in a mass flow hopper bin. The incipient flow regime in a hopper bin was characterized by the formation of the first dynamic arch. The first dynamic arch represented the transition between the static case, before opening the hopper outlet, and the dynamic case, when the powder was flowing out of the hopper. Experimental observation showed that an arch was formed after minimal discharge when the gate of the mass flow hopper bin was opened. This arch broke before the development of fully dynamic powder flow. To validate the FEM, a transparent plastic, laboratory size, mass flow hopper bin with an outlet size of 203 mm and a hopper angle of 15^0, with respect to the vertical was used. They concluded that the average relative difference (ARD) between the FEM predicted and the mean of the first experimentally observed dynamic arch location and profile was 14.2%, and the mean absolute difference was 5.8 mm.

Runesson and Nilsson (1986) modeled the flow of granular materials as a viscous-plastic fluid, with a Newtonian part and a plastic part. The Drucker-Prager yield rule was

used to represent purely frictional flow. Link and Elwi (1990) modeled the case of incipient flow of cohesionless materials in bins. An elastic perfectly-plastic, model was used along with a wall interface element to include wall friction in the formulation.

Meng and Jofriet (1992) presented a new secant constitutive relationship for bulk solids and used it to model cohesionless granular materials flow in silo or bin using FEM. The outflow velocity result seems reasonable when compared with preliminary experimental results. Diez and Godoy's model (1992) was intended for use with frictional cohesive materials. However, the simulations performed were for cohesionless materials for which they obtained fair agreement with other published results. The drawback of this model is the viscosity constant, γ, about which very little is known, and for neither experimental determination techniques could be found. Gallego et al. (2004) study has shown significant variation exists in pressure predictions in silos using the finite element model (FEM). The influence of Poisson's ratio on the lateral pressures expected in silo walls was analyzed by comparing the values obtained with two commercial finite element software packages, ANSYS and ABAQUS.

2.6.2 Discrete element model (DEM)

DEM was used by Masson and Martinez (1999) to simulate the filling and the discharge of the plane rectangular silo. Computer wall pressure at the end of filling was compared to analytical and finite element model (FEM) results. The results show that the friction and the stiffness of contacts play a major role in the flow kinematics and the stress field during filling and discharge process. Vidal et al. (2004) present a new

dynamic model for silo discharge using the Drucker-Prager plasticity model, surface-to-surface contact, and a flexible wall. Overpressure coefficients due to discharge were obtained in all cases. Vidal et al. (2004) summarizes the parametric studies developed to determine the influence of the flexibility of the wall and the internal coefficients.

The DEM was used by Yang and Hsiau (2001) to investigate the flow pattern of the filling and discharge process for two-dimensional plane silos. Conical and binsert were used in the silo to change the flow fields of the silo was studied. The effect of using differently shaped inserts on the flow pattern and wall stress was analyzed in Yang and Hsiau (2001). The controlling parameters include the silo half-angle, the orifice width, the shape of the insert, and the properties of the granular materials.

2.7 State-of-the-art

In summary, there are very few studies that have been done to investigate the uniformity of powder in multiple dies. Xie and Puri (2006) and Xie (2006) studied the uniformity of powder deposition in multiple dies by using the feed shoe filling method. But uniformity of powder in dies using other commonly used filling methods such as funnel, rainy, and pneumatic have not been systematically investigated. Therefore, investigation of this particular area is essential to determine the fill method most appropriate for a given powder.

2.8 References

1- Abdullah, E. C. and D. Geldart. 1999. The use of density measurement as flowability indicators. *Powder Technology 102 (2):151-165*.
2- Aulton E. Michael. 2002. *Pharmaceutics, the science of dosage form design.* Second edition. Churchill Livingstone publication.
3- Beverloo, W. A., H. A. Leniger and V. D. Velde. 1961. The flow of granular materials through orifices. *Chem. Eng. Sci. 15(3): 260-267*.
4- Bocchini, G. F. 1987. Influence of small die width on filing and compacting densities. *Powder Metallurgy 30(4): 261-266.*
5- Brown, R. L. and J. C. Richards. 1965. Kinematics of the flow of dry powders and bulk solids. *Rheologica Acta. 4(3):153-165*.
6- Bruff, W. and A. W. Jenike. 1967. A silo for ground anthracite. *Powder Technology 1(5): 252-255*.
7- Carleton, A. J. 1972. The effect of fluid-drag forces on the discharge of free-flowing solids from hoppers. *Powder Technology 6(2): 91-96.*
8- Cocks, A. C. F., L. Dihoru and F. Lawrence. 2001. A fundamental study of die filling. PM 2001: processing: October 22-24, 2001. Acropolis Convention Center, Nice, France *225-260*.
9- Danish, F. Q. and E. L. Parrot. 1971. Introduction to pharmaceutical powder processing. *J. Pharm. Sci. 66: 1235-1242*.
10- Davidson, J. F. and R. M. Nedderman. 1973. The hour-glass theory of hopper flow. *Trans. Instn. Chem. Eng. 51: 29-33*.
11- Dhanoa, P. S. and V. M. Puri. 1997. Experimental analysis of deposition of particulate materials into confined spaces. ASAE Paper No. 974106. ASAE, St Joseph, MI.
12- Dhanoa, P. S. and V. M. Puri. 1998. Deposition of particulate materials confined spaces-new tester development and experimental results. *KONA (Powder and Particle) 16:152-159.*
13- Diez, M. A. and L. A. Godoy. 1992. Viscoplastic incompressible flow of frictional-cohesive solids. *Int. J. Mech. Sci. 34:395-408.*
14- Fayed, M. E. and L. Otten. 1997. *Handbook of powder science and technology.* New York, N.Y.: Chapman & Hall.
15- Fowler, R. T. and J. R. Glastonbury. 1959. The flow of granular solids through orifices. *Chem. Eng. Sci. 10: 150-156.*
16- Franklin, F. L. and L. N. Johanson. 1955. Flow of granular material through a circular orifice. *Chem. Eng. Sci. 4: 119-129.*
17- Gallego, E., R. J. Goody, F. Ayuga and C. J. Brown. 2004. Some practical features in modeling silos with finite elements. ASAE paper no. 044150. ASAE Summer Mtg., Ottawa, Canada.
18- Harmens, A. 1963. Flow of granular material through horizontal apertures. *Chem. Eng. Sci. 18: 297-306.*

19- Hjortsberg. E. 2000. Density variations in iron powder caused by die filling. Proceeding of 2000 Powder Metallurgy World Congress. November 12-18. Kyoto International Conference Hall, Japan.
20- Hjortsberg, E. and B. Bergquist. 2002. Filling induced density variations in metal powder. *Powder Metallurgy 45(2): 146-153*.
21- Hoffmann, A. C., J. F. Hendrikus and A. S. Jacobus. 1996. Relationships between particle properties and bulk behavior for some industrial powders. Particle & Particle Systems Characterization *13: 354-361*.
22- Huntington, A. P. and N. M. Rooney. 1971. Discharge of granular materials from hoppers. Project Report, Department of Chemical Engineering, University of Cambridge UK.
23- Johanson, J. R. 1965. Method of calculating rate of discharge from hoppers and bins. *Trans. Min. Eng. AIME 232: 69-80*.
24- Kamath, S., V. M. Puri, H. B. Manbeck and R. Hogg. 1993. Flow properties of powders using four testers-measurement, comparison and assessment. *Powder Technology 76: 277-289.*
25- Kamath, S. and V. M. Puri. 1997. Measurement of powder flow constitutive model parameters using a cubical triaxial tester. *Powder Technology 90: 59-70*.
26- Kamath, S. and V. M. Puri. 1999. Finite element model development and validation for incipient flow analysis of cohesive powder from hopper bins. *Powder Technology 102: 184-193*.
27- Larid, B. W. and P. M. Roberts. 1979. Granular flow through hopper. Chemical Engineering Tripos Part 2. Research Project Report, University of Cambridge UK.
28- Li. J., C. Webb, S. S. Pandiella, G. M. Campbell, T. Dyakowski, A. Cowell, and D. McGlinchey. 2004. Solids deposition in low-velocity slug flow pneumatic conveying. *Chemical Engineering and Processing 44:167-173*.
29- Link, R. A. and A. E. Elwi. 1990. Finite element analysis of compressive cylinder tests. Proceedings of the Annual Conference and the First Biennial Environmental Speciality Conference, May 16-18, Hamilton,Canada.
30- Masson, S. and J. Martinez. 1999. Effect of particle mechanical properties on silo flow and stresses from distinct element simulations. *Powder Technology 109(3):164-178.*
31- Meng. Q. and J. C. Jofriet. 1992. Finite element analysis of bulk solids flow in silos. Paper no. 92-4016. ASAE Summer Mtg., Charlotte, California.
32- Mittal, B. and V. M. Puri. 1999. Correlation between powder deposition methods and green compact quality: part I mechanical properties of powders. *Particulate Science and Technology 17: 283-299.*
33- Mittal, B., V. M. Puri, and W. Shaffer. 2001. Analysis of feed shoe powder deposition method using a real-time cumulative mass deposition tester. *KONA (Powder and Particle) 19:144-154.*
34- Molenda, M., J. Horabik and I. J. Ross. 1993. Loads in model grain bins as affected by filling methods. *Trans. ASAE 36(3): 915-919.*
35- Molenda, M., J. Horabik and I. J. Ross. 1996. Effect of filling method on load distribution in model grain bins. *Trans. ASAE. 39(1): 219-224*.

36- Myers, M. E. and M. Sellers. 1978. Rate of discharge from wedge-shaped hoppers. Project Report, Department of Chemical Engineering, University of Cambridge UK.
37- Pecora Aria A. B, and Leonardo Goldstein. 1993. New particulate solids pneumatic feeding device with mass flowrate control. *Powder Technology 79: 265-268*.
38- Puri, V. M. 2001. Introduction to flowability via powder mechanics. Powder characterization short course note. Penn State. University Park. PA.
39- Rice. E. R. and J. Tengzelius. 1986. Die filling characteristics of metal powders. *Powder Metallurgy 29(3):183-184*.
40- Rietema, K. 1991. *The Dynamics of Fine Powders*. New York, N.Y.: Elsevier Science Publishers LTD.
41- Rose, H. F. and T. Tanaka. 1959. Rate of discharge of granular materials from bins and hoppers. The Engineer (London) *208: 465-469*.
42- Runesson, K. and L. Nilsson. 1986. Finite element modeling of the gravitational flow of a granular material. *Int. J. Bulk Solids and Handling 6:887-884*.
43- Schulze, D. 1998. Measurement of the flowability of bulk solids. *Silos-Fundamental of Theory, Behavior and Design*. E & Fn Spon, London *18-52*.
44- Shaxby, J. H. and J. C. Evans. 1923. On the properties of powders. The variation of pressure with depth in columns of powders. *Trans. Faraday Soc. 19: 60-72*.
45- Smid, J., P. V. Xuan and J. Thyn. 1993. Effect of filling method on the packing distribution of a catalyst bed. *Chem. Eng. & Tech. 16: 114-118*.
46- Suzuki, M., H. Sato, M. Hasegawa and M. Hirota. 2001. Effect of size distribution on tapping properties of fine powder. *Powder Technology 53-57*.
47- Tang, P. 2004. Percolation and sieving segregation patterns-quantification, mechanistic theory, model development and validation, and application. Ph.D. diss., University Park. PA. Pennsylvania State Univ: Agricultural and Biological Engineering Dept.
48- Tukiendorf, M. 2003. Characteristic of mixing granular materials achieved by using methods of variance analysis and geostatistical functions. *Journal of Polish Agricultural Universities 6(1): 265-278*.
49- Verghese, T. M. and R. M. Nedderman. 1995. The discharge of fine sands from conical hoppers. *Chem. Eng. Sci. 50(9): 3143-3153*.
50- Vidal, P., M. Guaita and F. Ayoga. 2004. Simulation of discharge processes in metallic silos. ASAE paper no. 044151. ASAE Summer Mtg., Ottawa, Canada.
51- Wilms, H. and B. Kiihnemund. 1998. Classification of bulk solids. Silos-Fundamentals of Theory, Behaviour and Design. E & Fn Spon, London. 104-110.
52- Wu, C. Y., A. C. F. Cocks and O. Gillia. 2003. Die filling and powder transfer. *Powder Metallurgy 39(4): 51-64*.
53- Xie, X., V. M. Puri and A. S. Grader. 2003. Evaluation of uniformity of simultaneous powder deposition in multiple containers of different cross sections. ASAE Paper. No. 034028. ASAE. Las Vegas, Nevada.
54- Xie, X., and V. M. Puri 2006. Uniformity of powder die filling using a feed shoe: A Review. *Partic. Science and Technology 24:411-426.*
55- Xie, X. 2006. Uniformity of Simultaneous Powder Deposition in Multiple Dies;

Measurement and Modeling. Ph.D. diss., University Park. PA. Pennsylvania State Univ: Agricultural and Biological Engineering Dept.

56- Yang C. S. and S. S. Hsiau. 2001. The simulation and experimental study materials discharge from a silo with the placement of inserts. *Powder Technology 120(3): 244-255*.

57- Zahrah, T. F., R. Rowland and G. Gasbarre Jr. 2001. Fluidized fill shoe uniform die filling. *Ind. Eng. Chem. Res. 30: 1977-1981*.

Chapter 3

Goal and Objectives

3.1 Goal

The overall goal of this research was to study the effectiveness of four different deposition methods: feed shoe, rainy, point feed, and pneumatic fill methods to deposit powder in shallow dies. The test materials were two powders that are widely used in industry, BPM (a battery powder mixture) and microcrystalline cellulose (Avicel PH102). This research also was used to develop a phenomenological model for deposition process in shallow dies. This general goal was completed through five specific objectives.

3.2 Objectives

1) To expand the capabilities of the current computer-controlled pressure deposition tester (PDT-II) for deposition of powder in shallow dies.
2) To design and fabricate rotational rainy, point feed, and pneumatic fill devices.
3) To employ deposition devices to collect data for the evaluation of four filling methods.
4) To use data in Objective 3 to compare different deposition methods in order to determine the best fill method.
5) To develop and verify a physics-based mathematical model to simulate the different deposition methods for die filling.

Chapter 4

Uniformity Discrimination Analysis, Part 1: Powder Deposition Characteristics in Rectangular Shallow Die Using Feed Shoe with Circular Cross-Section

4.1 Abstract

The process of die filling is a significant unit operation in many industries. The inhomogeneity of distribution such as, mass, bulk density, and pressure might cause many tablet and compact quality issues, such as lamination, capping, and distortion. No systematic investigations have been done to evaluate pressure distribution characteristics in dies with small aspect ratio (<0.5). In order to evaluate the pressure distribution during filling of shallow dies, factors influencing powder deposition were studied in this research. The factors included, particle size and shape, particle size distribution, and circular cross section feed shoe speed. The second generation pressure deposition tester (PDT-II) was used to measure two powders' pressure distribution characteristics. A battery powder mixture (BPM) and microcrystalline cellulose (Avicel PH102) were used to fill rectangular shallow die 32×30 mm in dimension and 6.5 mm deep. The feed shoe speeds of 20 and 100 mm/s were used to fill the die. Symmetry analysis, variance metrics, Gini coefficient, and uniformity analysis were used to quantify the deposition characteristics. The results showed that (1) contour plots were the most reliable method for measuring powder deposition characteristics; (2) the leeward-forward region generated larger symmetry index vs. the front-back region; (3) based on contour plot

analysis, BPM at 100 mm/s feed shoe speed resulted in the most uniform pressure distribution (64% uniformity at +/- 20 dm resolution) among all; (4) feed shoe speed highly influenced pressure distribution uniformity inside the die; (5) the high stress zone was mostly observed in forward and back regions inside the die.

4.2 Introduction

A non-uniformly distributed initial mass, bulk density, and/or pressure may cause many tablet and compact quality issues. Inhomogeneity may cause laminations, cracks, and non-uniform shrinkage on sintering. Creating an acceptable initial mass, bulk density, and/or pressure distribution inside the die or containers is an effective step to avoid tablet quality issues. Dhanoa and Puri (1997) designed and built a mass deposition tester (MDT) to evaluate the effect of filling method, rate of fill, die cross-section, and die size (aspect ratio, the ratio of die width to depth) on the spatial fill density distribution (Figure **4.1**). A funnel filling method and sieve filling method were used by Dhanoa and Puri (1998) to study the uniformity of particle material on small dies. They invented the real time spatial particulate mass deposition tester to determine the in-situ pre-compaction particulate density distribution.

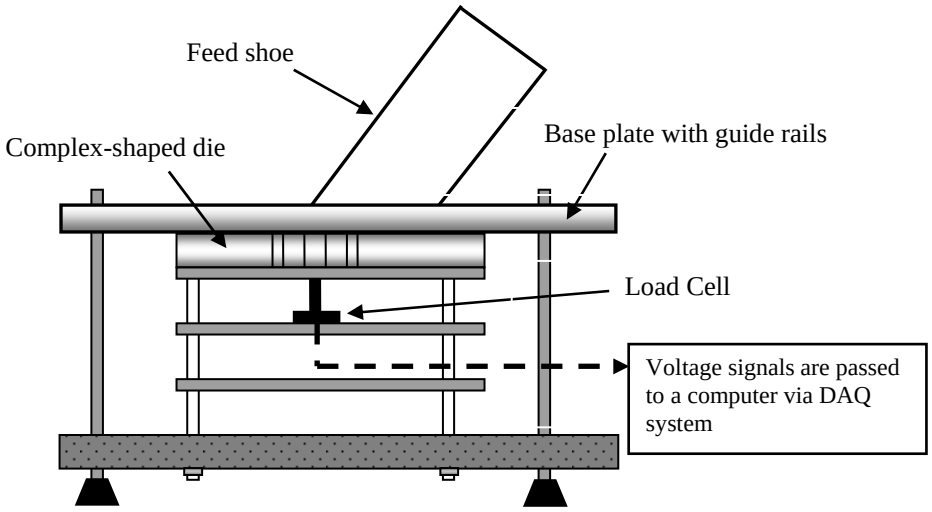

Figure **4.1**: Schematic of MDT along with feed shoe deposition method (Dhanoa and Puri, 1997)

A real time cumulative mass deposition tester (MDT) was used by Mittal et al., (2001) to study the deposition behavior of a free-flowing manganese zinc ferrite (MZF) powder. The feed shoe deposition method was used to fill the powder in toroid and E-shaped containers. Two different and one feed shoe approach regions were used for the E-die and one feed shoe approach for the toroid die was used, respectively. The results showed that powder deposition was affected by both fill region and die shape for the E-die. Each filling direction had unique powder deposition characteristics.

Xie and Puri (2007) conducted research with the second generation pressure deposition tester (PDT-II) (Figure **4.2**). They showed that PDT-II worked satisfactorily in terms of measurement of pressure distribution at the bottom of the die during the powder deposition process. They used three parallel cylindrical containers at three different speeds: 20 mm/s, 100 mm/s, and 500 mm/s. The results showed that at low feed shoe speeds (20 and 100 mm/s), the half circle close to the leeward region had higher final

pressure values than the forward half circle; the final within pressure distribution at the bottom of the dies was not always symmetrical about the center line of the feed shoe movement region; feed shoe speed at 500 mm/s resulted in higher final pressure values than lower feed shoe speed at most of the locations; and the final pressure distribution was more uniform in higher (500 mm/s) than the lower feed shoe speed (20 and 100 mm/s).

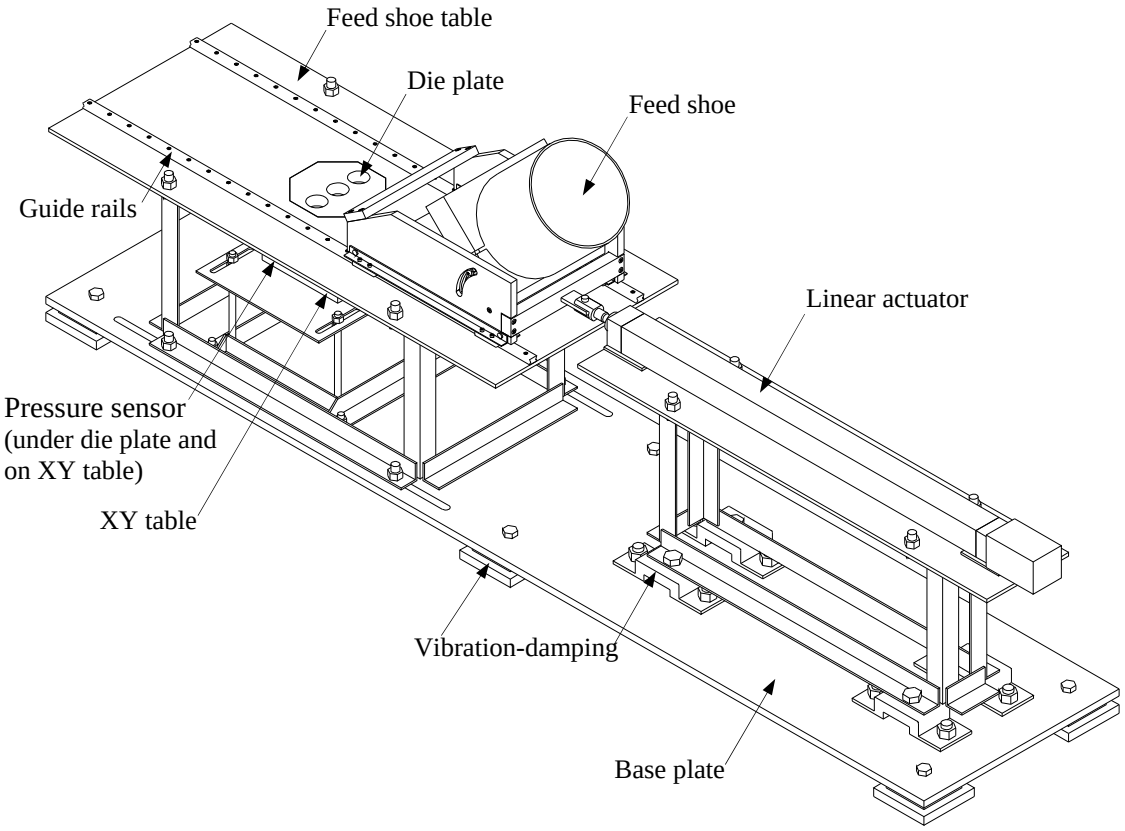

Figure **4.2**: A design schematic of the PDT-II (Xie, 2006)

4.3 Methodology

This section discusses pressure deposition tester (PDT-II) and experimental design for evaluating the fill quality of shallow rectangular dies with two powders, namely, microcrystalline cellulose, manufactured by FMC (Avicel PH102), and a battery powder mixture (BPM) supplied by an industrial sponsor. Throughout these experiments, a circular cross-section feed shoe at speeds of 20 mm/s and 100 mm/s were used. The experimental design and test characteristics are summarized in Table **4.1** .

Table **4.1**: Experimental design and test characteristics used in die filling study

Filling method	Test characteristics	Details
Feed shoe	Speed	20 mm/s
		100 mm/s
	Test materials	Avicel
		BPM
	Die shape	Rectangular (32×30 mm)
	Die depth	6.5 mm
	Feed shoe cross-section	Circular
	Number of replications	6

4.3.1 Second generation pressure deposition tester (PDT-II)

The PDT-II, designed and fabricated by Xie and Puri (2007), was used in this research (Figure 4.2). This device is capable of measuring pressure distribution at the bottom of the dies. The three major components of PDT-II are drive system, pressure sensor strip, and feed shoe to fill the die. The accessories of PDT-II include feed shoe table, guide rails, XY table, linear actuator, base plate, vibration-damping mounts and die plates.

The pressure sensor strip, P-1500 (Pressure Profile Systems Inc., Los Angles, CA), is the most important part of the measurement system. The P-1500 was connected to a data acquisition systems and data analysis software. There are 16 pressure sensors in one pressure sensor strip, the cross-section of each sensor is 2 mm× 5 mm with center-to-center spacing of 2 mm. The sensitivity of pressure sensor (P-1500) was 0.1% of the full scale range, or 5 Pa (4.8 mg on an area of 2 mm×5 mm). The highest pressure that the P-1500 can measure was 551.6 kPa (0.529 kg on an area of 2 mm×5 mm). The minimum time interval between two data points was 8.84 ms, i.e., the maximum data collection rate was 113 Hz. For protection of the pressure sensor strip from being damaged by the high force from die plate in use and the feed shoe container during filling process, a narrow gap (0.23 mm) was maintained between the pressure sensor strip and the die plate in use. A water column precision calibration system was used for pressure sensor strip (Xie, 2006). For each sensor element data, the regression line for pressure vs. voltage was drawn to obtain the best straight line passing through the origin. The sensor calibration was repeated every 50 PDT-II tests (Xie, 2006) to check and update the calibration based on previous tests of Xie (2006) and tests by the authors, i.e., it was determined that this frequency of calibration was sufficient to ensure valid and accurate measured pressure values.

4.3.2 Test of powder deposition into rectangular die

Avicel is widely used in the pharmaceutical industry as an excipient for direct compression because of its good flowability, compactibility, and compressibility (Schneider et al. 2007) and it is stable under ambient conditions. The bulk density and particle density of Avicel needed in this study were 0.28-0.33 g/cm3 and 1.53 g/cm3, respectively. The particle size range of Avicel powder was from +20 to 200 μm with median size (d_{50}) of 84 μm. The size distribution and micrograph of Avicel are shown in Figure **4.3**.

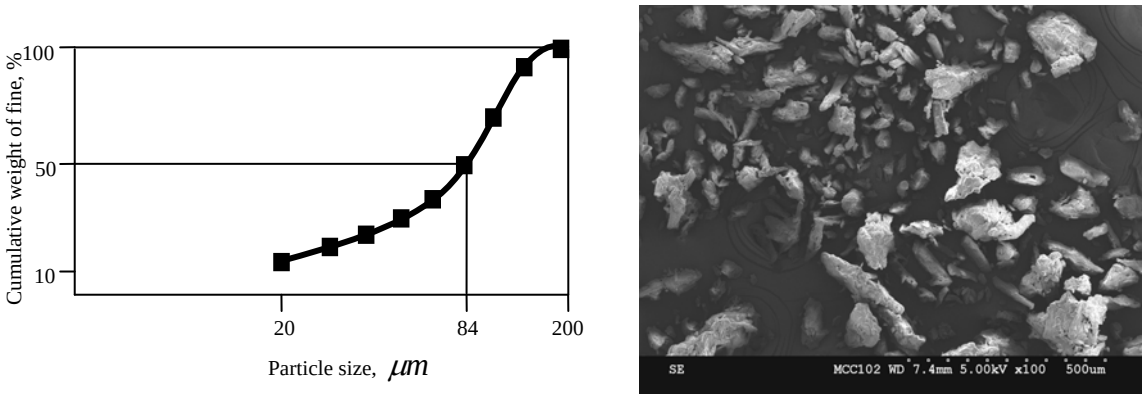

Figure **4.3**: Size distribution and micrograph of Avicel

The bulk density and particle density of BPM were 1.65 g/cm^3 and 4.7 g/cm^3, respectively (Xie, 2006). It is stable under ambient conditions. The granule size range of BPM powder was from less than 80 to 1000 μm with median size (d_{50}) of 600 μm. BPM powder is very friable; some granules easily fragment into finer granules during handling and transportation. Figure **4.4** shows the size distribution and micrograph of the BPM powder.

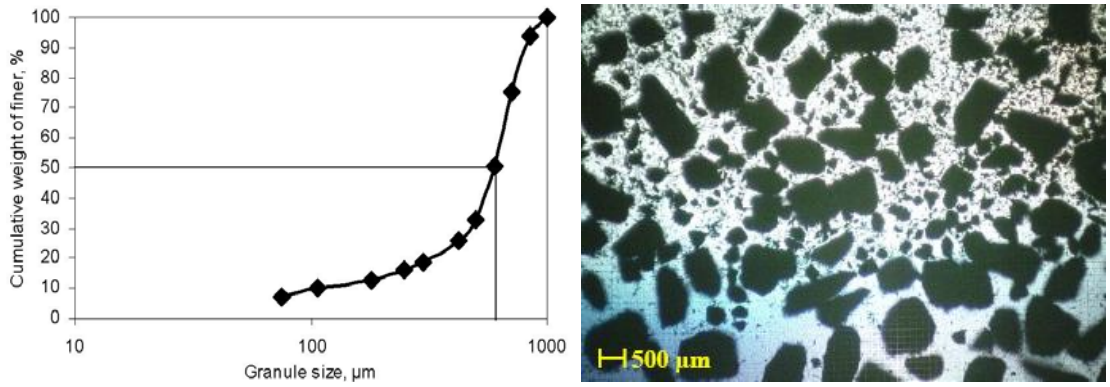

Figure **4.4**: Size distribution and micrograph of BPM powder (Xie, 2006)

The rectangular die configuration with respect to the feed shoe and the corresponding dimensions are shown in (Figure **4.5a**). The feed shoe was 158.7 mm in diameter (inner) and inclined at 45^0. Therefore, the cross-section in contact with feed shoe table was an ellipse. The movement of feed shoe was parallel to the long axis of the ellipse. A rectangular die with a dimension of 32×30 mm and 6.5 mm depth was configured along the long axis of the ellipse. The pressure sensor strip was positioned at six locations which covered the entire die cross section, i.e., 2.5, 7.5, 12.5, 17.5, 22.5, and 27.5 mm, with respect to forward region of the die (Figure **4.5b**). All sixteen sensors were exposed to record pressure increase profiles. Based on previous work of Dhanoa and Puri (1998) and Mittal et al. (2001), six replications were performed for each test, which resulted in coefficient of variation (COV) of about 20%. The feed shoe passed over the die from leeward to forward and filled the shallow die completely in one pass, i.e., there was no backward stroke.

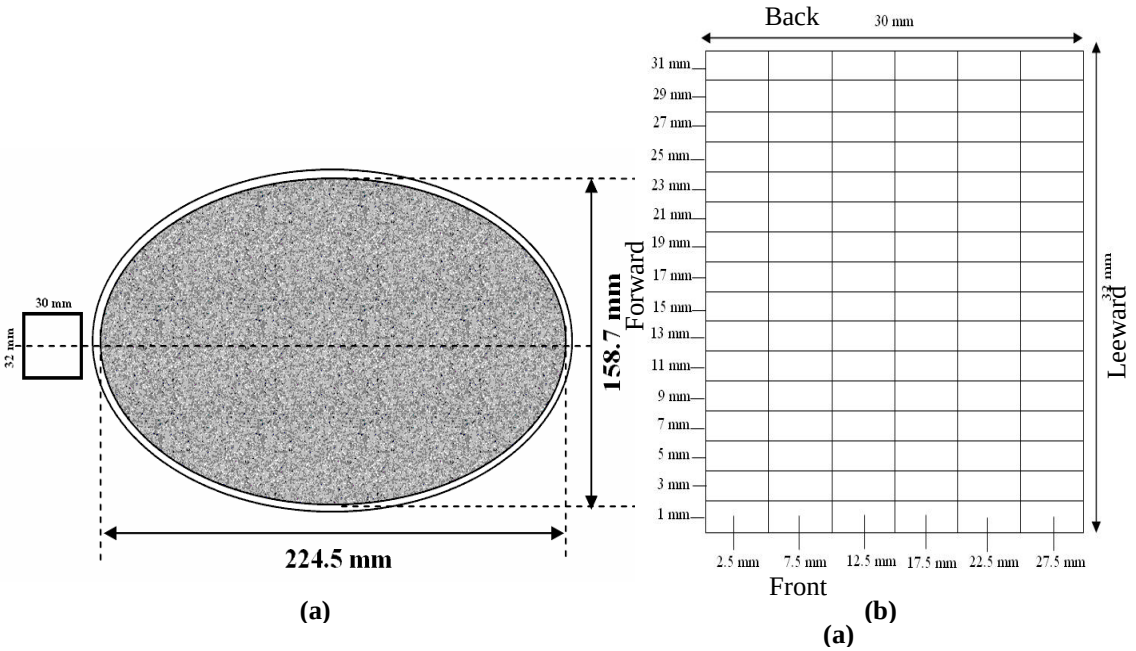

Figure **4.5**: Experimental set up: (a) dimensions of circular feed shoe cross-section in contact with table surface and rectangular die (drawn to scale) (b) rectangular die and the positions of pressure sensor strip at 2.5, 7.5, 12.5, 17.5, 22.5, and 27.5 mm from forward region; the sensors element centers are shown along the vertical.

4.4 Results and discussion

In order to quantitatively analyze the pressure distribution at the end of filling process, symmetry analysis, variance metrics, Gini coefficient, and uniformity analysis were used. Visual displays of the final pressure distributions as contour plots were quantitatively and qualitatively analyzed. Symmetry analysis was used to evaluate pressure distribution characteristics with respect to the centerline of the feed shoe movement region. Two types of symmetry analysis, namely, qualitative and quantitative, were used to evaluate the pressure distribution profile for front vs. back and leeward vs.

forward regions of the die. The qualitative analysis was done through the contour plots of the pressure distribution. In qualitative analysis, the symmetrical pressure distribution in front vs. back and leeward vs. forward regions were evaluated through the symmetry index. The symmetry index is defined as a ratio between 0 (least symmetrical distribution) and 100 (i.e., most symmetrical distribution).

Variance metrics, such as, coefficient of variation (COV), Max, Min, Min/Max, and (Max-Min)/Mean were used to assess the variability in measured pressure distribution profile. The usual COV is defined as a ratio between 0% and 100% was used for pressure distribution analysis. For this study, COV value of 0% was interpreted as ideal uniformity (i.e., most) and 100% as perfectly random non-uniform distribution (i.e., least uniform).

The Gini coefficient can measure inequality of a distribution, which is defined as a ratio between 0 (perfect equality) and 1 (perfect inequality); i.e., the numerator is the area between the Lorenz curve and the uniform (perfect) distribution line and the denominator is the area under the uniform distribution line (ABCDA/ABCOA) (Figure **4.6**). The Lorenz curve is generated when certain members of the population contribute more to the total pressure and certain members less.

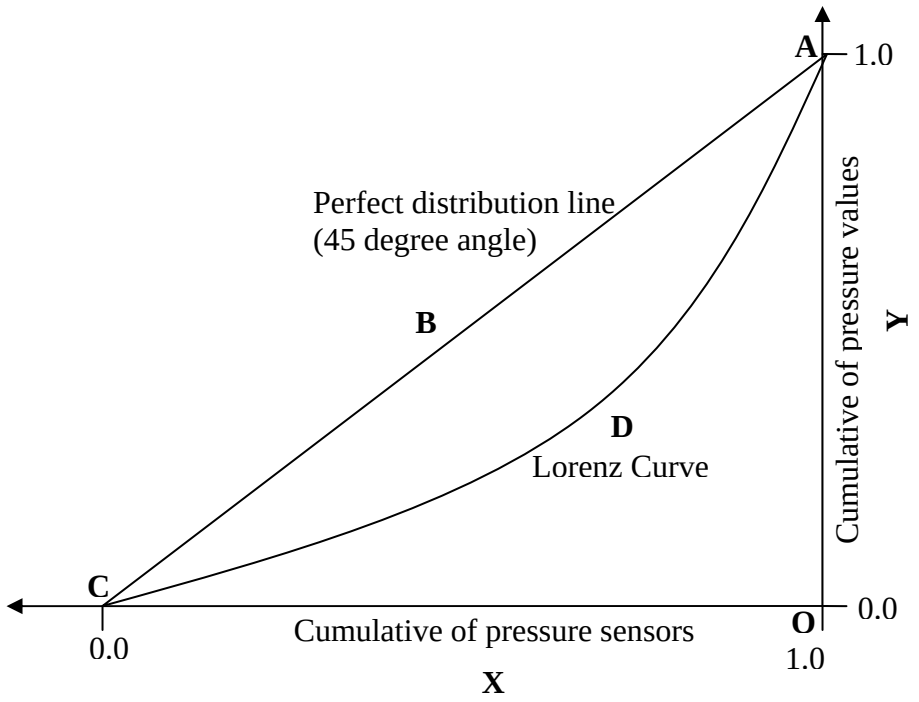

Figure **4.6**: Line of equality (45 degree line) and Lorenz curve for Gini coefficient (area ABCDA/ABCOA)

An estimate of Gini coefficient can be calculated, where the P_i s are the pressure readings ranked in order from least to greatest, by Equation **4.1** (Weiner and Solbrig, 1984).

$$G = \frac{\sum_{i=1}^{n} (2i - n - 1) P_i}{n^2 \overline{P}} \qquad \text{Equation } \mathbf{4.1}$$

where,

G= Gini coefficient, $0 \le G \le 1$
n= total number of pressure sensor readings
P_i = pressure reading for sensor i
$\overline{P}$ = mean pressure values

4.4.1 Symmetry analysis

Symmetry analysis evaluated the pressure distribution profile along long axis of the rectangular die. The reason for conducting a symmetry analysis was to assess the degree of equilibrium in pressure distribution at bottom of the die between front vs. back and leeward vs. forward regions of the die after completion of the filling process. The symmetry analysis is presented in qualitative form as contour plots, and quantitative form as symmetry index values.

The contour plots of pressure distribution profile for Avicel and BPM at locations 2.5, 7.5, 12.5, 17.5, 22.5, and 27.5 mm for 20 and 100 mm/s feed shoe speeds are shown in Figure **4.7** . In order to compare the results of Avicel with BPM, each pressure value was divided by the particle density multiplied by gravity ($\frac{p}{\rho.g}\times 10$). This can be interpreted as equivalent height (h), in this study the particle density (ρ) of Avicel and BPM used were 1.53 and 4.7 g/cc, respectively, and the gravity constant was 9.8 m/s^2. The scale of scrutiny was +/- 20 dm (corresponding to average COV of 20%); where, dm is decimeter, i.e., 1 dm=0.1 m.

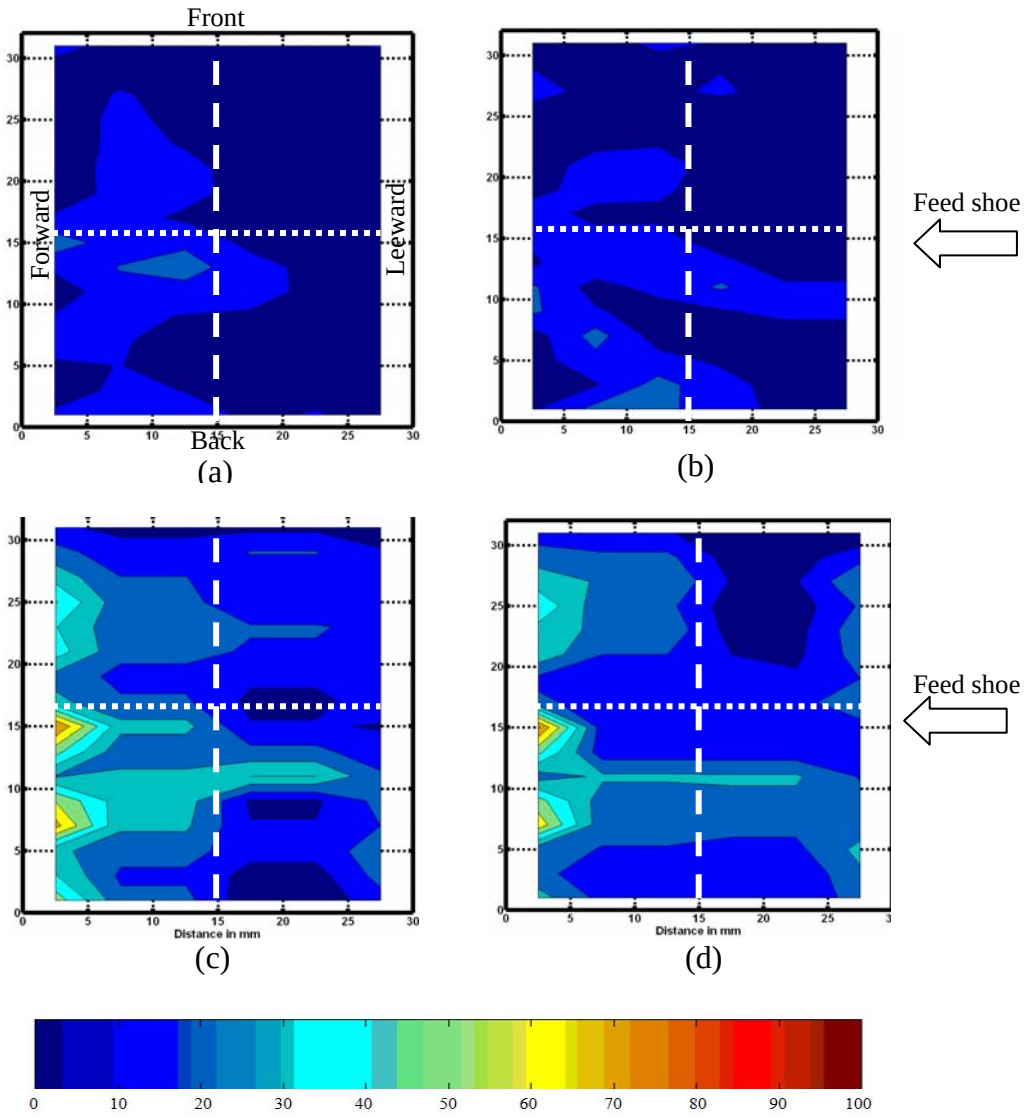

Figure **4.7**: Contour plots of final pressure as equivalent height (pressure/particle density*gravity) for Avicel (a) 20 mm/s, (b) 100 mm/s, and BPM (c) 20 mm/s. and (d) 100 mm/s feed shoe speed. (scale in dm)

The results showed that the mean final pressure values toward the leeward region (22.5 and 27.5 mm) are relatively lower than forward region (7.5 and 12.5 mm) in both powders. The reason for the increase in pressure values from forward to leeward regions

include: (1) feed shoe forward motion that launches particles toward the forward region, and (2) nose flow region rapidly fills the shallow die (Xie and Puri, 2006) followed by particles being pushed and dragged to the forward region by the feed shoe speed. The feed shoe speed of 20 mm/s in Avicel generated a more symmetrical final pressure distribution vs. 20 mm/s in BPM.

Even after normalization due to higher particle density of BPM, 4.7 g/cc compared to 1.53 g/cc for Avicel, the average pressure distribution is relatively high (Figure **4.7c** and **4.7d**). The locations 22.5 and 27.5 mm show less stress zones than the other locations inside the die. This can be attributed to the forward motion of the feed shoe which fills the die from the forward to the leeward region.

Symmetry Index (quantitative analysis): The symmetry index (η) (expressed as the difference percentage of uniformity in front vs. back and leeward vs. forward divided by the largest uniformity subtracted from 100) was used to evaluate the symmetrical pressure distribution inside the die (Table **4.2**).

Table **4.2**: The results for symmetry analysis for rectangular die for Avicel and BPM at 20 and 100 mm/s feed shoe speed

Filling method	Test materials	Feed shoe speed (mm/s)	Locations	% Uniformity	Symmetry index
Feed shoe-Rectangular die	Avicel	20	Front	75	72
			Back	55	
			Leeward	73	86
			Forward	63	
		100	Front	56	78
			Back	44	
			Leeward	59	81
			Forward	48	
	BPM	20	Front	39	65
			Back	60	
			Leeward	57	75
			Forward	43	
		100	Front	71	73
			Back	52	
			Leeward	68	81
			Forward	55	

Based on analysis and interpretation of results it was determined that: (1) Avicel at 20 mm/s at the front-back region had the lowest symmetry index (72%) which represented the least symmetrical pressure distribution among all; (2) the wall friction had greater influence on pressure distribution values of BPM vs. Avicel (higher pressure values of locations 2.5 and 27.5 mm in BPM vs. Avicel); (3) influence of wall friction became more pronounced with increase in the feed shoe speed for Avicel powder; (4) the lowest pressure values were mostly located in the leeward region for both powders; (5) the stress concentration zone increased with increasing feed shoe speed; and (6) the accumulation mostly observed in the back and forward region. The reason for this might be the leveling process that increased the shear stress in forward and back regions.

4.4.2 Variance metrics analysis

Table **4.3** shows variance metrics parameters for Avicel and BPM at 20 and 100 mm/s. Based on these values, BPM at 100 mm/s had the lowest COV and standard deviation (18.18% and 0.19, respectively); i.e., most uniform filling amongst all tested while Avicel at 20 mm/s had the highest COV and standard deviation (25.21% and 0.24, respectively), i.e., least uniform distribution. BPM at 100 mm/s also had the lowest Max/Min, and (Max-Min)/Mean, which represented more uniform pressure distribution vs. Avicel powder. Deposition of BPM with large particle size (particle size up to 1 mm) into shallow die (6.5 mm deep) markedly increased the non-uniform pressure distribution inside the die by minimizing the particle rearrangement and increased segregation ($\approx 5\%$ below 90 μm).

Table **4.3**: Variance metrics parameters for Avicel and BPM at 20 and 100 mm/s feed shoe with circular cross-section

Test material	Feed shoe speed mm/s	Max (dm)	Min (dm)	Mean (dm)	Max/Min	(Max-Min)/Mean	Standard deviation	COV%
Avicel	20	0.95	0.21	0.95	4.09	0.77	0.24	25.21
	100	0.86	0.23	0.89	3.70	0.70	0.22	24.71
BPM	20	1.26	0.52	0.89	2.40	0.83	0.21	24.51
	100	1.34	0.66	1.05	1.69	0.65	0.19	18.18

The results showed: (1) BPM at 100 mm/s feed shoe speed had the lowest Max, Min, (Max-Min)/Mean, standard deviation and COV which led to most uniform filling; (2) feed shoe speed highly influenced uniformity pressure distribution; (3) the uniformity increased with increasing feed shoe speed for both powders; (4) overall, variance metrics had low sensitivity for evaluating and discriminating uniformity in this study.

4.4.3 Gini coefficient

The Gini coefficient values for Avicel and BPM are shown in Table **4.4**. The results showed BPM at 100 mm/s had the lowest Gini coefficient or the highest uniformity among all (0.15 or 85% uniformity).

Table **4.4**: Gini coefficient within die for Avicel and BPM at 20 and 100 mm/s feed shoe speeds

Feed shoe speed	20 mm/s	100 m/s
Avicel	0.16	0.17
BPM	0.16	0.15

Based on the Gini coefficient, the following concluding remarks can be made: (1) Gini coefficient showed BPM had the highest uniformity distribution among all (0.15 or 85% uniformity); (2) Avicel and BPM generated the same uniformity at 20 mm/s feed shoe speed (0.16 or 84% uniformity); (3) there were only minor differences in Gini coefficient between Avicel and BPM at both feed shoe speeds; (4) the Gini coefficient is not sufficiently sensitive to measure and discriminate pressure distribution uniformity in this study.

4.4.4 Uniformity analysis

For uniformity evaluation of contour plot, the area of uniform color distribution was measured using AutoCAD 2005 (Autodesk Inc. San Rafael, CA, USA). The results showed that Avicel at 20 mm/s (Figure **4.7a**) had a 55% uniform pressure distribution, while at 100 mm/s (Figure **4.7b**) Avicel had a 59% uniform pressure distribution. The BPM powder at 20 mm/s had a 58% uniformity (Figure **4.7c**), while at 100 mm/s BPM

had a 64% uniformity in pressure distribution (Figure **4.7d**). Table **4.5** summarizes the uniformity analysis for the rectangular die using a feed shoe with a circular tube cross-section.

Table **4.5**: Uniformity analysis for rectangular and circular die at 20 and 100 mm/s feed shoe speeds

Filling method	Test materials	Speeds (mm/s)	% Uniformity
Feed shoe with circular tube cross-section	Avicel	20	55
		100	59
	BPM	20	58
		100	64

The following key results can be summarized based on contour plot analysis: (1) BPM at 100 mm/s had the highest uniformity (64%); (2) the feed shoe speed influenced the pressure distribution profile, i.e., the percent uniformity increased from 55% to 64%; (3) most particles accumulated near to the wall at forward region of the die; and (4) the areas of high pressure values were less than 5 percent of total area in BPM. The quantitative pressure difference between 20 and 100 mm/s feed shoe speed for Avicel were reduced with increasing feed shoe speed. The reason might be that the higher kinetic energy of particles collapsed local bridges and/or rearranged particles inside the die. However, there is a limitation to the upper feed shoe speed due to other parameters, such as air escape and minimum time to completely fill the die. This upper limit is expected to be unique to each different die shape, size, depth, and powder parameters, such as particle size, size distribution, and density.

4.5 Conclusions

The PDT-II is a suitable device to evaluate powder deposition characteristics inside shallow dies. The PDT-II data was used to study the influence of two distinct powders comprising different particle size, and particle shape, and feed shoe speed on the pressure distribution. The following conclusions were obtained from this study:

(1) More uniformity was observed toward front and leeward regions of the die due to particle trajectory during the forward motion in both powders.

(2) Feed shoe motion had a large influence on the uniformity inside the die based on the following observations:

- Uniformity increased with increasing feed shoe speed;
- The feed shoe speed at 20 and 100 mm/s had various symmetry indexes;
- Non-symmetrical distribution might be attributed to the complexity of the flow and deposition process;
- Avicel at 20 mm/s generated the least uniform pressure distribution among all (55%);
- BPM at 100 mm/s generated the most uniformity pressure distribution among all (64%);
- The Max/Min, (Max-Min)/Mean, standard deviation and COV, decreased with increasing feed shoe speed;

(3) Symmetry index is a reliable method for analyzing symmetry pressure distribution.

(4) Contour plots were a suitable method to analyze powder deposition characteristics in shallow dies.

4.6 References

1. Dhanoa, P. S. and V. M. Puri, 1997. Experimental analysis of deposition of particulate materials into confined spaces. ASAE Paper No. 974106. ASAE, St Joseph, MI.
2. Dhanoa, P. S. and V. M. Puri, 1998. Deposition of particulate materials confined spaces-new tester development and experimental results. *KONA (Powder and Particle) 16:152-159.*
3. Mittal, B., V. M. Puri, and W. Shaffer. 2001. Analysis of feed shoe powder deposition method using a real-time cumulative mass deposition tester. *KONA (Powder and Particle) 19:144-154.*
4. Schneider L. C. R., I. C. Sinka and A. C. F. Cocks, 2007. Characterization of the flow behavior of pharmaceutical powders using a model die-shoe filling system. *Powder Technology 173:59-71.*
5. Weiner, J. and O. T. Solbrig, 1984. The meaning and measurement of size hierarchies in plant populations. Oecologia (Berlin) *61:334-336.*
6. Xie, X., and V. M. Puri 2006. Uniformity of powder die filling using a feed shoe: A Review. *Partic. Science and Technology 24:411-426.*
7. Xie, X. 2006. Uniformity of Simultaneous Powder Deposition in Multiple Dies; Measurement and Modeling. Ph.D. diss., University Park. PA. Pennsylvania State Univ: Agricultural and Biological Engineering Dept.
8. Xie, X and V. M. Puri, 2007. Uniformity of Simultaneous Powder Deposition in Multiple Dies; *Parti. Science and Technology 25(3): 247-260.*

Chapter 5
Uniformity Discrimination Analysis: Development of Uniform Powder Deposition Method, Part 2: Circular Shallow Die

5.1 Abstract

The non-uniformity of pressure distribution generated during filling process might cause many tablet and compact quality issues, such as capping, cracking, and lamination. To avoid these issues, understanding the characteristics of the filling process and ensuring a uniform deposition into the die and cavity are necessary. The second generation pressure deposition tester (PDT-II) was used to investigate powder deposition characteristics into a circular and a rectangular shallow die (6.5 mm deep). The influence of die filling parameters, such as, die geometry, particle size and shape, and feed shoe speed were investigated in this research. Two types of powders, namely, microcrystalline cellulose (Avicel, PH102) and a battery powder mixture (BPM), with median size of 84 and 600 μm, respectively, were used as test materials. Symmetry analysis, variance metrics, and uniformity analysis were used to quantify the deposition characteristics. The results showed that: (1) die shape highly influenced the uniformity of pressure distribution inside the die; (2) the uniformity of pressure distribution increased with increasing feed shoe speed for both rectangular and circular dies; (3) the back and forward regions filled faster vs. front and leeward regions; (4) the front and leeward regions showed greater uniformity of pressure distribution vs. back and forward regions;

and (5) the areas of high pressure values (above 60 dm) were less than 5% of the total area for both rectangular and circular dies.

5.2 Introduction

Production of tablets, compacts, and briquettes can be performed by a number of techniques. The goal of these processes is to form the powder into a well defined shape. When the powder is placed into a die or cavity and the pressure is applied, a volume reduction occurs; this technique is referred to as the compaction process (Pietsch, 1997).

During the die filling process with a feed shoe to make tablets or compacts, non-uniformity or inhomogeneity of pressure distribution at different locations of the die may be created. This inhomogeneity has been attributed to various tablet quality problems, such as low strength, cracking, and shrinkage. Pressure gradients in the pressed parts may also lead to shrinkage on sintering (Reed, 1995). Besides physical properties, inhomogeneity may influence chemical and magnetic properties of the products.

Many methods and devices, such as high speed camera (Schneider et al., 2007), CT scanner (Xie and Puri, 2007), have been used to investigate the die filling process. However, the majority of them are expensive, and not user friendly; furthermore these methods only provide a qualitative assessment.

The PDT-II has the capabilities, such as controlling feed shoe speed and acceleration, sufficient flexibility and precision, and being user-friendly to be a better device to investigate the die filling process. The most important component of the

measurement system was a pressure sensor strip, P-1500. The detailed specifications of P-1500 were discussed in Part 1.

5.3 Objectives

The main objective of this research was to study the characteristics of the deposition process in a circular die and compare the results with a rectangular die (Part 1) using PDT-II with circular feed shoe cross-section.

5.4 Methodology

The second generation PDT-II, as discussed in Part 1, was used to evaluate the pressure distribution at the bottom of a circular shallow die. The PDT-II has the ability to quantify, with satisfactory sensitivity and precision, the distribution of pressure values across the die through the entire deposition process. Additional features of the PDT-II are summarized in Part 1 and by Xie (2006). Two types of powders, namely microcrystalline cellulose (Avicel PH102) and a battery powder mixture (BPM) with median size of 84 and 600 μm, respectively, were used in this study. A feed shoe with circular cross-section at speeds of 20 and 100 mm/s was used to fill a circular shallow die (6.5 mm deep and 35 mm diameter). The circular die configuration with respect to the feed shoe movement and orientations of the pressure sensor strip is shown in Figure **5.1**.

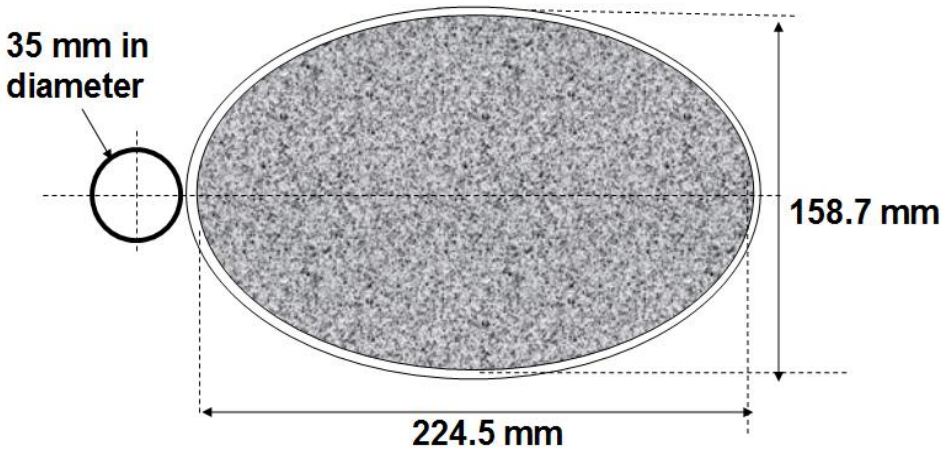

(a)

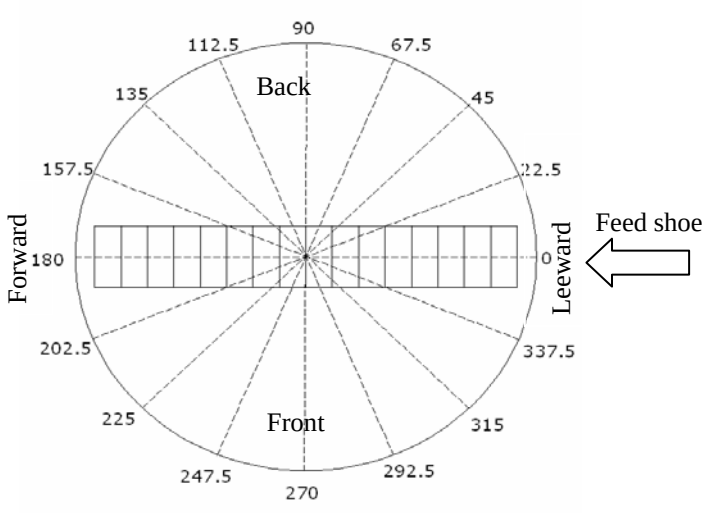

(b)

Figure **5.1**: (a) Dimensions of circular die and the circular feed shoe (drawn to scale) (b) orientations of the pressure sensor strip (angle)

The pressure sensor strip was positioned at eight different angles, 22.5 degrees apart, which covered the entire die; i.e., 0^0-180^0, 22.5^0-202.5^0, 45^0-225^0, 67.5^0-247.5^0, 90^0-270^0, 112.5^0-292.5^0, 135^0-315^0, and 157.5^0-337.5^0. All sixteen sensors were exposed to record the pressure increase profile. The experimental design is summarized in Table **5.1**

Table **5.1**: Experimental design and test characteristics

Filling method	Test characteristics	Details
Feed shoe	Speed	20 mm/s
		100 mm/s
	Test materials	Avicel
		BPM
	Die shape	Circular (diameter=35mm)
	Die depth	6.5 mm
	Feed shoe cross-section	Circular
	Number of replications	6

5.5 Results and discussion

Qualitative and quantitative analyses of the final pressure distribution for Avicel and BPM were accomplished through symmetry analysis, variance metrics, and uniformity analysis. Symmetry analysis was used to evaluate the uniformity of pressure distribution in the front vs. back and forward vs. leeward regions with respect to centerline of the die using contour plots. Symmetry index (η) was used as an indicator to illustrate the degree of symmetry after completion of the filling process. The symmetry index is defined in Equation **5.1** as below:

$$\eta = 100 - \left[\frac{A - B}{A} \times 100 \right] \qquad \text{Equation } \mathbf{5.1}$$

Where η = symmetry index, %

A= Large uniformity value;

B= Small uniformity value;

For example if the forward and leeward regions had 51% and 66% uniformity, the symmetry index is calculated as:

$$\eta = 100 - \left[\frac{66 - 51}{66} \times 100 \right] = 77\%$$

The symmetry index is defined as a ratio between 0 (least symmetrical distribution) and 100 (i.e., most symmetrical distribution).

Variance metrics demonstrate the statistical parameters, which is obtained for the circular die at 20 and 100 mm/s feed shoe speeds using the final pressure values. The Max, Min, Mean, Max/Min, (Max-Min)/Mean, StDev (standard deviation), and COV (coefficient of variation) were used as the statistical parameters in variance metrics analysis. The usual COV, defined as a ratio between 0% and 100% was used for pressure distribution analysis. For this study, a COV value of 0% was interpreted as ideal uniformity (i.e., most) and 100% as perfectly random non-uniform distribution (i.e., least uniform).

For uniformity analysis, the similarity percentage of the color distribution inside the die were measured using contour plots. In order to compare the results of Avicel with BPM, each pressure value was divided by the particle density multiplied by gravity ($\frac{p}{\rho.g}$). This can be interpreted as equivalent height (h); in this study the particle density (ρ) of Avicel and BPM, used were 1.53 and 4.7 g/cc, respectively and gravity constant (g) was 9.8 m/s^2. The scale of scrutiny was +/- 20 dm (corresponding to average COV of 20%) out of full scale of 100 dm; where, dm is decimeter, i.e., 1 dm=0.1 m.

5.5.1 Analysis of filling process

In order to enhance the understanding of the filling process, it was divided into various filling sequences. The feed shoe at 20 mm/s speed with Avicel powder was used to illustrate the die filling sequences. Data from a 20 mm/s feed shoe speed was selected because the air pressure and buoyancy effects of the two phase flow could be minimized at this speed. This set of data was used to illustrate the different sequences of the filling process. The relative positions of feed shoe tube with reference to the center line were used to mark the start and end point of different sequences and were represented by the positions of the feed shoe tube cross-section in contact with the table surface. These specific positions of the feed shoe tube were used to demonstrate the filling sequences as shown in Figure **5.2**. Corresponding to these positions, the specific time for the feed shoe tube to reach these positions are listed by the letter T and subscripts shown in Figure **5.2:**

T_1: the feed shoe started to move from its original (start) position (0 s).

T_2: the front wall of feed shoe tube reached the leeward region (0.44 s). The accumulation is observed in the back region. The reason for the accumulation may be caused by more particles entering the back region.

T_3: the feed shoe tube front wall reached the center of the die (0.88 s). Accumulation is observed in the leeward and back region, toward the die walls.

T_4: the feed shoe tube front wall reached the forward region (1.32 s). The particles covered the die's entire bottom. Accumulations are expanded to the forward region of the die.

T_5: the front wall of the feed shoe tube passed the forward region (1.76 s). The

particle accumulation is expanded in the forward and back regions of the die. The cause is thought to be due to more particles entering to the back region of the circular die (the back region filled first).

T_6: the middle of the feed shoe tube reached the die center (6.55 s). At this time, no filling is accomplished because the die was fully filled and could not accommodate more particles. The accumulation, or stress concentration zone, in the back region increased due to the increasing shear stress and particle-particle forces.

T_7: the back wall of the feed shoe tube reached the leeward region (12.15 s).. The accumulation area in the front region increased and expanded toward the center of the die.

T_8: the back wall of the feed shoe tube reached the middle of the die (13 s). The surcharge powder started to be removed from the die (leveling process), which generated high shear stress in the forward region.

T_9: the back wall of feed shoe tube reached the forward region (the filling process ended) (13.44 s). The area of particle accumulation or stress zone, mostly concentrated in the forward and front regions. The particles began to rearrange themselves, which decreased the stress points in accumulation areas.

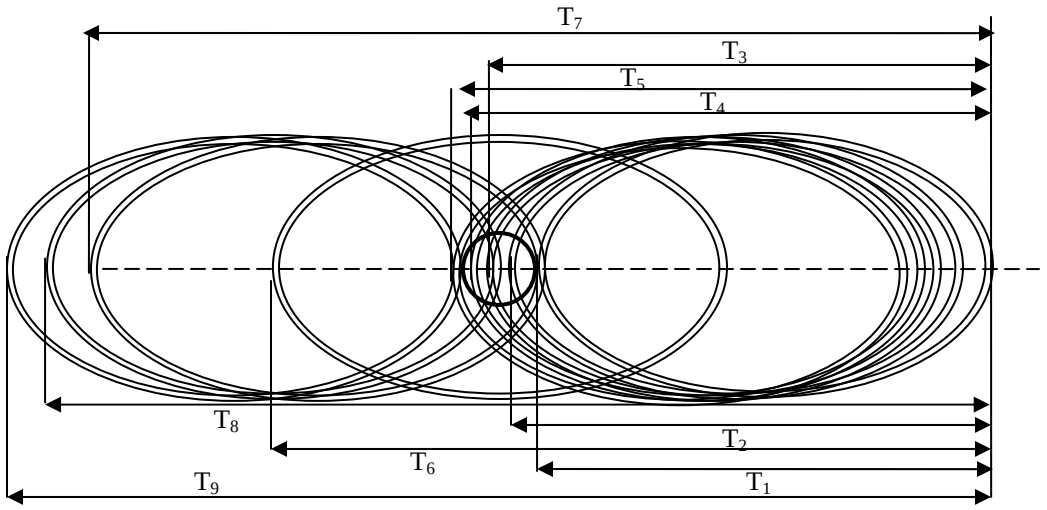

Figure **5.2**: Feed shoe tube positions at different filling sequences for circular shallow die

As Cocks et al. (2001) and Wu et al. (2003) studied, during the forward stroke of feed shoe movement, the powder in the feed shoe was forced to the back of the feed shoe due to inertia during the feed shoe acceleration from rest, which generated a space between the feed shoe tube front wall and powder inside the tube (Figure **5.3**).

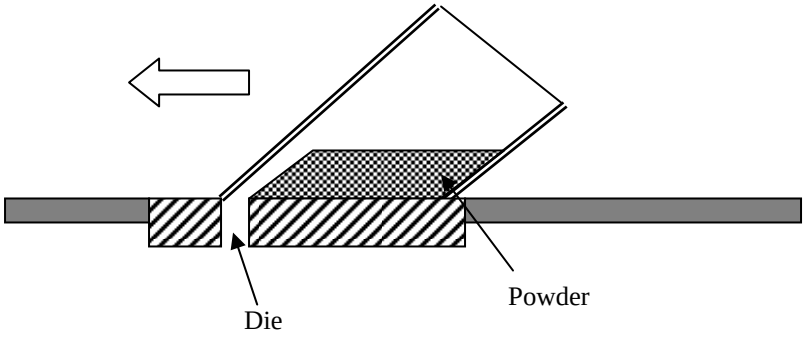

Figure **5.3**: Feed shoe tube and powder position inside the tube at forward stroke

The contour plots of filling sequences for Avicel powder at 20 mm/s feed shoe speed at different time sequences are shown in Figure **5.4**. The feed shoe tube filled the die from leeward toward forward region.

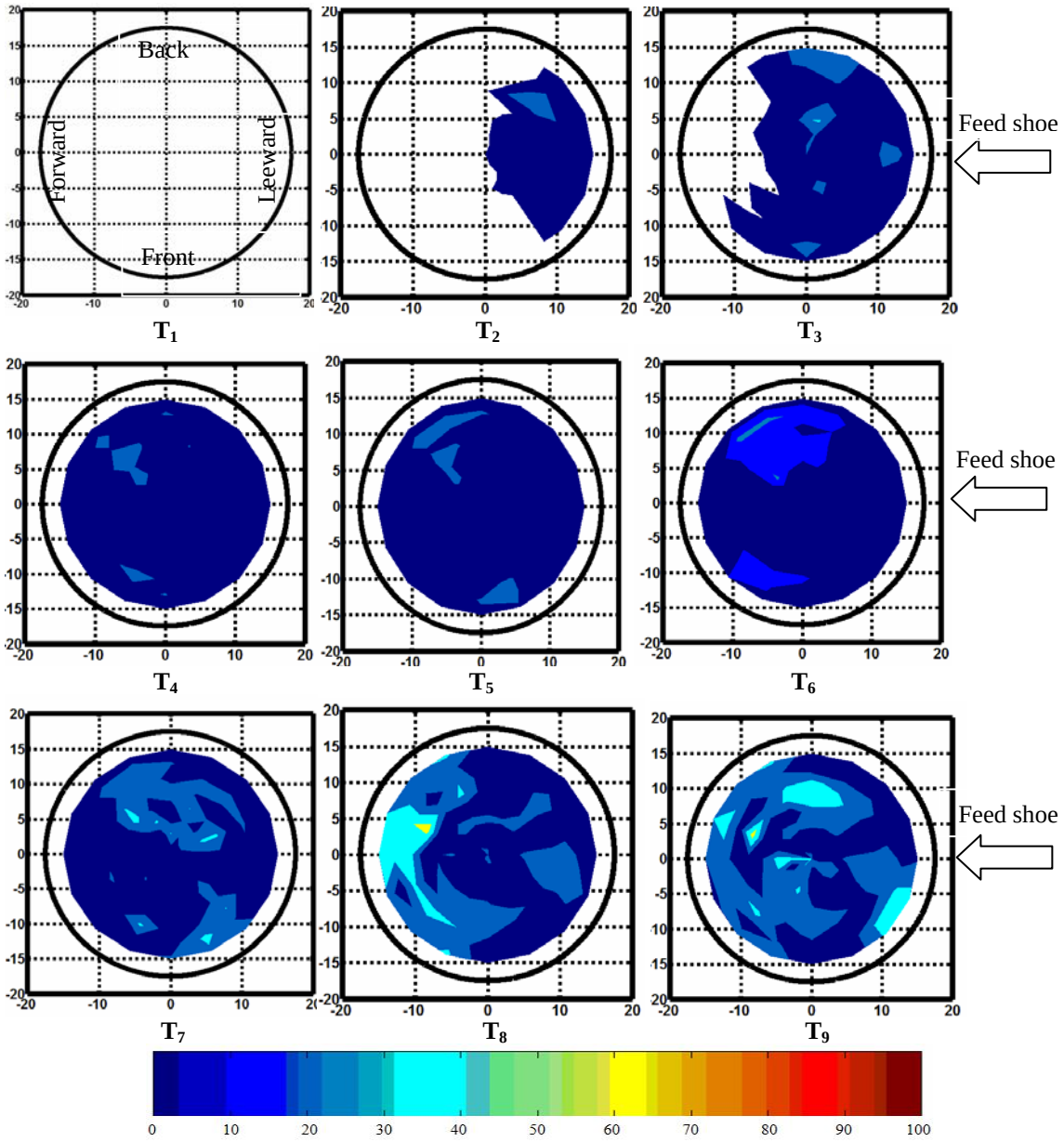

Figure **5.4**: Contour plots of filling sequences as equivalent height in dm (pressure/particle density*gravity) in circular shallow die for BPM powder at 20 mm/s feed shoe speed using a feed shoe tube with circular cross-section at time T_1=0 s, T_2=0.44 s, T_3=0.88 s, T_4= 1.32 s, T_5=1.76 s, T_6=6.55 s, T_7=12.15 s, T_8=13 s, and T_9=13.44 s (scale in dm).

During the filling process with the feed shoe tube, the powder in tube remains stationary and most of the flow takes place in the wedge of tube which is falling freely

under gravity. During the initial filling process (filling under gravity, T1-T5) and subsequent process (T6- T9), only 6-10 layers of particles are actively involved in filling procedures (Brown and Richards, 1959). Therefore, the feed shoe filling process can be divided into two filling zones, namely active and stagnant zones. The active zone is located at the contact points between the particles in the feed shoe tube and particles on the surface of the die. The active zone included 6-10 layers of particles which were continuously in contact with each other during the feed shoe tube movement. The estimated thickness of active zone for Avicel and BPM were 0.84 and 10 mm, respectively. The stagnant zone includes the stationary particles which surround the active zone. Figure **5.5** demonstrates the filling zones which are generated during the feed shoe movement.

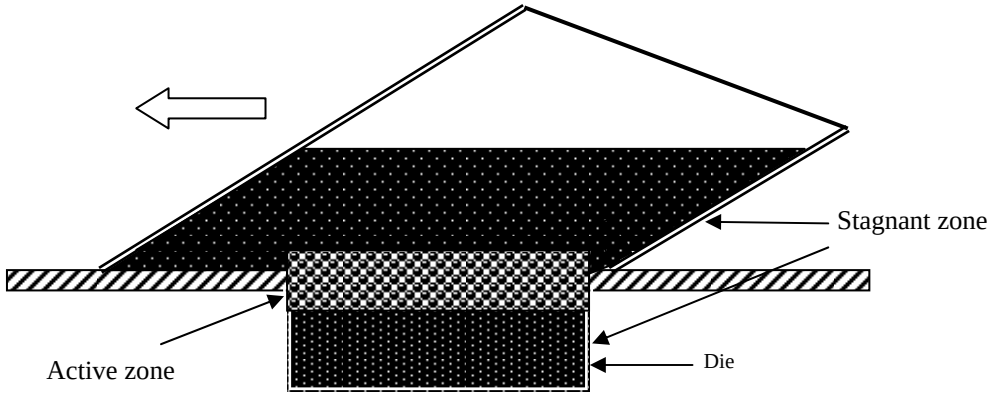

Figure **5.5**: Filling zones during feed shoe tube movement

5.5.2 Symmetry analysis

Figure **5.6** shows the contour plots of circular shallow die which is divided into front-back and leeward-forward regions. The feed shoe tube approaches the die from leeward to forward region. The areas of uniform color distribution in front vs. back and forward vs. leeward regions were compared and analyzed.

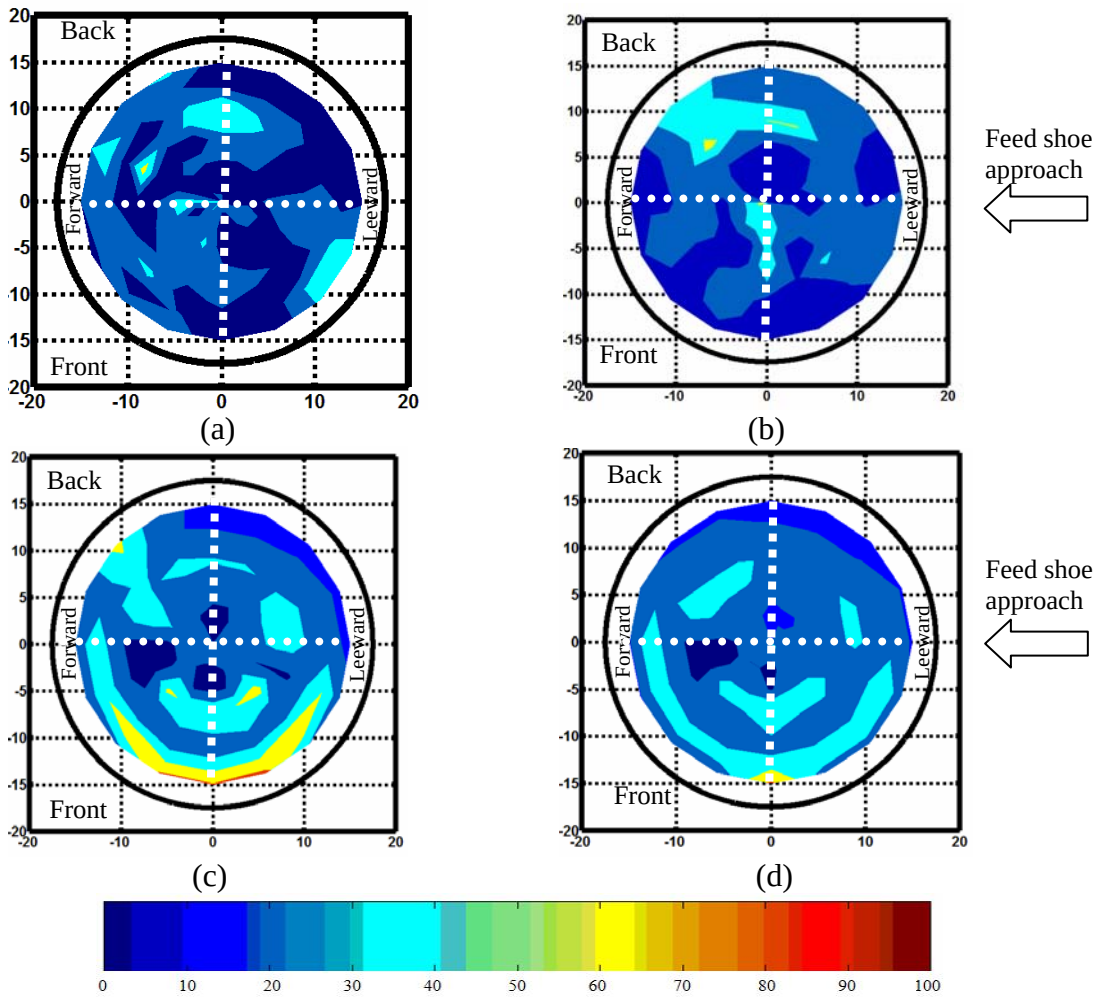

Figure **5.6**: Contour plots of final pressure as equivalent height in dm (pressure/particle density*gravity) for Avicel (a) 20 mm/s, (b) 100 mm/s, and BPM (c) 20 mm/s, and (d) 100 mm/s feed shoe speed (scale in dm).

Front and back analysis: The results showed that Avicel deposited at 20 mm/s (Figure **5.6a**) had 58% and 44% uniformity, respectively, for front and back regions, while at 100 mm/s (Figure **5.6b**) had 46% and 43% uniformity based on the same color distribution, respectively. The symmetry indexes for front-back region at 20 and 100 mm/s feed shoe speed were 76% and 93%, respectively. As already discussed in section 5.5.1, the main reason for higher uniformity in the back region was because the front region accepted more particles during the filling process, which increased the accumulation area.

BPM at 20 mm/s (Figure **5.6c**), in the front and back regions had 64% and 38% uniformity, respectively, while 100 mm/s (Figure **5.6d**), had 69% and 52% uniformity, respectively. The symmetry index for front-back region for BPM powder at 20 and 100 mm/s feed shoe speed were 59% and 79%, respectively. The results showed that symmetry index increased with increasing feed shoe speed. This may be caused by a higher feed shoe speed helping to densify the particles by collapsing bridges and/or rearranging particles inside the die (Wu et al. 2003).

BPM powder generated higher stress points inside the die (87 Pa). This could be due to the relatively larger particle size of BPM, which for small fill depth (6.5 mm), caused higher forces to be applied from each particle to neighboring particles and dramatically increased the stress points inside the die.

Forward and leeward analysis: Avicel at 20 mm/s (Figure **5.6a**) in the leeward and forward regions had 56% and 49% uniformity, respectively, while at 100 mm/s (Figure **5.6b**) had 32% and 28% uniformity, respectively The symmetry index for forward-leeward regions for Avicel powder at 20 and 100 mm/s feed shoe speed were

88% and 88%, respectively. As discussed in section 5.5.1, the reason for less uniformity in forward region is that the forward region filled first which generated higher accumulation areas and increased the non-uniformity. Another plausible reason for higher accumulation in forward region might be the increased rolling, dragging, and sliding of the particles increased during the leveling process (T_8), which generated higher shear stress in forward region. Overall, despite the low uniformity in the forward and leeward regions, the forward-leeward region had high symmetry index at both feed shoe speeds.

BPM powder at 20 mm/s (Figure **5.6c**) in forward and leeward regions had 56% and 59% uniformity, respectively, while BPM at 100 mm/s (Figure **5.6d**) had 65% and 67% uniformity, respectively. The symmetry index for the forward-leeward region at BPM at 20 and 100 mm/s feed shoe speeds were 95% and 99%, respectively. The results showed that the stress concentration zones decreased with increasing feed shoe speed. As already discussed, one of the reasons might be due to high kinetic energy at 100 mm/s feed shoe speed; the particles collapsed the local bridges and increased the particles' rearrangement inside the die. Table **5.2** summarizes the symmetrical analysis of Avicel and BPM at 20 and 100 mm/s feed shoe speed using symmetry index.

Table **5.2**: The results for symmetry analysis for circular die for Avicel and BPM at 20 and 100 mm/s feed shoe speeds

Filling method	Test materials	Feed shoe speed (mm/s)	Locations	% Uniformity	Symmetry index
Feed shoe	Avicel	20	Front	58	76
			Back	44	
			Leeward	56	88
			Forward	49	
		100	Front	46	93
			Back	43	
			Leeward	32	88
			Forward	28	
	BPM	20	Front	64	59
			Back	38	
			Leeward	59	95
			Forward	56	
		100	Front	69	75
			Back	52	
			Leeward	67	99
			Forward	65	

Based on the analysis and interpretation of the results, it was determined that: (1) the forward-leeward region for BPM at 100 mm/s feed shoe speed generated the highest symmetrical distribution (symmetry index=99%), while front-back region for BPM at 20 mm/s had the least symmetrical distribution (symmetry index= 59%), which may be caused by the feed shoe filling the die more symmetrically in the forward-leeward region than front-back region since the region of feed shoe tube moved from leeward to forward; and (2) the feed shoe speed highly influenced the symmetrical pressure distribution particularly for BPM.

5.5.3 Variance metrics analysis

The statistical parameters of pressure distribution inside the circular die for Avicel and BPM after completion of the filling process are shown in Table **5.3** (each pressure

value was divided by the particle density multiplied by gravity, $\frac{p}{\rho.g}$). Based on the results, BPM generated the highest pressure distribution inside the die (6.20 and 5.43 dm) due to the higher particle density (4.7 g/cc). BPM at 20 mm/s had the highest COV (24.3%), i.e., least uniformity among all, while BPM at 100 mm/s had the lowest COV (12.4%), i.e., the highest uniformity. BPM at 100 mm/s feed shoe speed had the lowest Max/Min, (Max-Min)/Mean, standard deviation and COV, led to the most uniform filling.

Table **5.3**: Variance metrics parameters for Avicel and BPM at 20 and 100 mm/s for circular die

Test Material	Feed shoe speed mm/s	Max (dm)	Min (dm)	Mean (dm)	Max/Min	(Max-Min)/Mean	Standard Deviation	COV%
Avicel	20	3.0	0.3	2.10	10.03	1.29	0.46	22.2
	100	4.0	0.5	2.11	8.03	3.05	0.41	19.6
BPM	20	6.20	2.10	2.79	2.95	1.47	0.67	24.3
	100	5.43	1.99	2.65	2.72	1.28	0.32	12.4

The following concluding remarks can be made as: (1) BPM at 20 mm/s generated higher pressure inside the die vs. Avicel, (6.2 and 3.0 dm, respectively) due to higher particle density; (2) BPM at 100 mm/s feed shoe speed generated the lowest Max/Min, (Max-Min)/Mean, standard deviation and COV and led to the most uniform filling among; (3) variance metrics provided valuable information about pressure distribution inside the die; however, it had low sensitivity for evaluating and discriminating uniformity in this study.

5.5.4 Uniformity analysis

For uniformity analysis, the uniform color distribution for the entire die was measured using a contour plot. As discussed in section 5.5.1, the pressure mostly accumulated in front and forward regions of the die (for reasons already discussed). The results showed that, Avicel, at 20 and 100 mm/s (Figure **5.6a** and **5.6b**), had 44% and 52% uniformity, respectively, while the BPM at 20 and 100 mm/s (Figure **5.6c** and **5.6d**), had 51% and 66% uniformity, respectively. BPM powder generated higher stress concentration zone than Avicel powder. The stress zones were mostly located in front and forward regions of the die (for reasons already discussed). In Table **5.4**, the uniformity pressure distribution values for Avicel and BPM at 20 and 100 mm/s feed shoe speed are summarized.

Table **5.4**: Uniformity analysis for circular die using contour plot

Test Materials	Speeds (mm/s)	% Uniformity
Avicel	20	44
	100	52
BPM	20	51
	100	66

The following key observations were obtained from this study: (1) the uniformity increased with increasing feed shoe speed for both Avicel and BPM, most likely due to higher kinetic energy of particles collapsing local bridges and/or rearranging particles inside the die; (2) there is a limitation to upper feed shoe speed due to factors, such as air escape and minimum time to completely fill the die, this upper limit was expected to be different for various die shapes, size, depth, and powder parameters, such as particle size, size distribution, and density; (3) the highest accumulation or stress concentration zones

occurred in the forward and front regions of the die; (4) the areas of high pressure values was less than 5% of total area in BPM; whereas its was 9% for Avicel.

5.6 Uniformity comparison between rectangular and circular die at 20 and 100 mm/s feed shoe speed

PDT-II with a circular feed shoe cross-section was used to study the filling characteristics in rectangular and circular shallow dies. The results were discussed in Chapters 4 (Part 1) and 5 (Part 2), respectively. In order to compare the uniformity pressure distribution in the rectangular and circular dies, the values of uniformity pressure distributions are summarized in Table **5.5.**

Table **5.5**: Uniformity comparison in rectangular and circular shallow die using circular feed shoe cross-section at 20 and 100 mm/s filling speed

Die shape	Test Materials	Feed shoe speed (mm/s)	% uniformity pressure distribution
Rectangular	Avicel	20	55
		100	59
	BPM	20	58
		100	64
Circular	Avicel	20	44
		100	51
	BPM	20	51
		100	66

The following concluding remarks were obtained from this study:

(1) die shape influenced the uniformity pressure distribution inside the die, this was seen as differences in uniformity percentage between circular and rectangular die at the same conditions, i.e., Avicel at 20 mm/s feed shoe speed in rectangular die had 55% uniformity while at the same conditions the circular die had 44% uniformity.

(2) The uniformity increased with increasing feed shoe speed for both rectangular and circular dies.

(3) The circular die generated a higher uniformity inside the die than a rectangular die for both Avicel and BPM. The main reason for a lower pressure distribution uniformity can be found in die geometry. The wall in the rectangular die has sharp regions and corners, which held the particles at its corners during the filling process and led to increase in stress concentration zone and, therefore, a decrease in uniformity.

(4) The highest pressure distribution uniformities for rectangular and circular die were observed for BPM at 100 mm/s feed shoe speed with 47% and 61% uniformity, respectively.

5.7 Conclusions

In this study, the filling characteristics of Avicel (a pharmaceutical powder) and BPM (supplied by an industrial sponsor) at 20 and 100 mm/s filling rate were evaluated. PDT-II, with highly sensitive and precise pressure sensors, was used to measure the pressure values after filling process. The circular shallow die, with 35 mm diameter and 6.5 mm depth, was used and compared to a rectangular die with dimenssion of $32 \times 30 \times 6.5$ mm (deep). The following conclusions were arrived at from this study:

(1) Feed shoe speed highly influenced the pressure distribution uniformity as noted in the following observations:

- high feed shoe speed (100 mm/s) increased uniformity for both dies;
- symmetry index increased with increasing feed shoe speed for both dies.

(2) Die geometry highly influenced the uniformity pressure distribution inside the die.

(3) Non-symmetrical distribution might be attributed to the complexity of the flow and filling process.

(4) During the filling process, the forward and front regions of the die filled faster vs. the back and leeward regions.

(5) The ratio of particle size to die depth highly increased the stress concentration zone inside the die.

5.8 References

1- Brown, R. L. J. C. Richards. 1965. Kinematics of the flow of dry powders and bulk solids. *Rheologica. Acta*. *4(3): 153-165*.

2- Cocks, A. C. F., L. Dihoru, and Lawrence. 2001. A fundemental study of die filling. In *PM 2001 Proceesings*, 225-260. Acropolis center, Nice, France. *22-24* October.

3- Pietsch, J. E. 1997. Size enlargement by aggromeration. *In Handbook of Powder Science and Technolog.* Ed. M. E. Fayed and L. Otten, ch. 6, 202-377. New York: Chapman & Hall.

4- Reed, J. S. 1995. *Principles of Ceramic Processing*. New York: John Wiley & Sons, Inc.

5- Schneider L. C. R., I. C. Sinka and A. C. F. Cocks, 2007. Characterization of the flow behaviour of pharmaceutical powders using a model die-shoe filling system. *Powder Technology 173:59-71*.

6- Wu, C., A. C. F. Cocks, and O. T. Gillia. 2003. Die filling and powder transfer. *The International Journal of Powder Metallurgy 39(4):51-64*.

7- Xie, X., and V. M. Puri. 2006. Uniformity of powder die filling using a feed shoe: A Review. *Partic. Science and Technology 24:411-426.*

8- Xie, X., and V. M. Puri. 2007. Simultaneous deposition of powder in three parallel-oriented cylindrical dies. *Partic. Science and Technology 25(4): 247-260*

9- Xie, X. 2006. Uniformity of Simultaneous Powder Deposition in Multiple Dies; Measurement and Modeling. Ph.D. diss., University Park. PA. Pennsylvania State Univ: Agricultural and Biological Engineering Dept.

Chapter 6

Uniformity Discrimination Analysis - Powder Deposition Characteristics in Circular and Rectangular Shallow Dies Using Feed Shoe with Square Cross-Section

6.1 Abstract

The inhomogeneity of the pressure distribution after completion of the filling process might create many tablet and compact quality issues. Generating a uniform pre-compaction powder deposition into a die would help to alleviate many tablet quality problems. This chapter determines the characteristics of the deposition process into a rectangular die and a circular shallow die, using a feed shoe with a square cross-section tube. A series of experiments were performed that determined the cumulative influence of particle size, particle size distribution, die geometry, and feed shoe speed on uniformity pressure distribution at the end of filling process. For uniformity comparison, the profiles of pressure distribution at the end of filling process were displayed as contour plots. The symmetry analysis, variance metrics, and uniformity analysis were implemented to quantify the deposition characteristics. Feed shoe speeds of 20 and 100 mm/s were used to fill the die. A pharmaceutical based powder (microcrystalline cellulose- Avicel PH102) and an industrial based powder designated as a battery powder mixture (BPM) were used as test materials. The results showed that: (1) feed shoe speed highly influenced the uniformity pressure distribution inside the die; (2) die shapes highly influenced the pressure distribution uniformity inside the die; (3) higher stress was

generated inside the rectangular die than in the circular die; (4) the back region of the die received more particles during the filling process; and (5) a circular die generated higher COV than a rectangular die.

6.2 Introduction

Powder and granular materials are widely used in industry, and yet the understanding of such systems is quite limited. These materials are difficult to use, handle, and manage because of their size, weight, and shape (unwieldy structure). It is evident that (Kestenbaum, 1997) in all of the operations for processing or handling powders and granules, accurate knowledge of the behavior of powders and granules is required.

The density and pressure gradients in a tablet or briquette is known to lead to many quality problems. For example, inhomogeneous powder assembly might show different strengths at different regions or locations, which cause lamination, cracking, distortion, low strength and shrinkage (Reed, 1995). To avoid quality problems, generating a uniform pre-compaction particle deposition in dies is an effective first step, since manufacturing processes have a tendency to magnify variation (Mittal and Puri, 1999).

In order to evaluate the filling process and uniformity in shallow dies, the second generation pressure deposition tester, PDT-II, was designed and fabricated (Xie and Puri, 2007). This device measures the pressure distribution at bottom of the die. A pharmaceutical based powder (Avicel, PH102) and an industrial powder designated as a

battery powder mixture (BPM) with median particle size of 84 and 600 μm, respectively, were used in this study.

6.3 Objectives

The objective of this study was to investigate the characteristics of the deposition process in a circular and a rectangular die using PDT-II when filled using a square cross-section feed shoe.

6.4 Methodology

The major components of PDT-II were a feed shoe tube, a measurement system and a drive system. There were some other components to support or improve the performance of the major components, including linear actuator table, base plate, guide rails, and feed shoe table. The PDT-II and dimensions of square cross-section feed shoe are shown in Figure **6.1**.

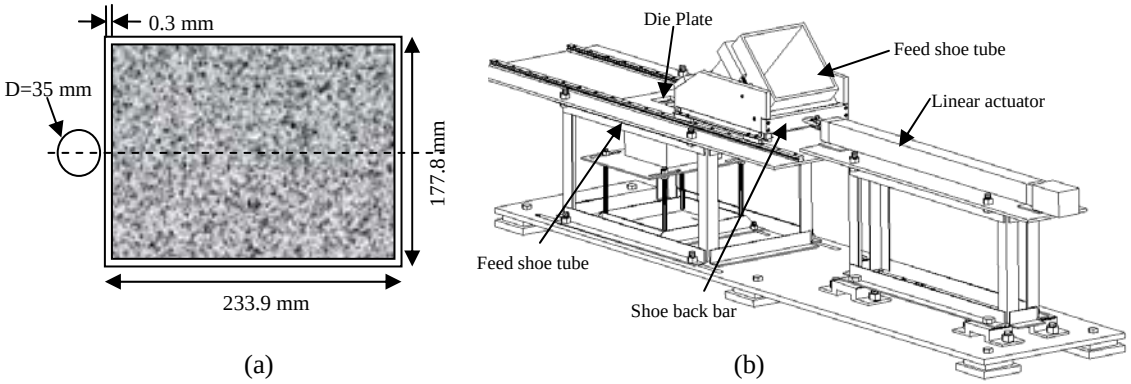

(a) (b)

Figure **6.1**: (a) Dimensions of square feed shoe cross section with circular die (drawn to scale), (b) An AutoCAD drawing of the assembled PDT-II

A rectangular die with the dimension of 32×30 mm and 6.5 mm depth was configured along the feed shoe tube. The pressure sensor strip was positioned at six locations which covered the entire die cross section, i.e., 2.5, 7.5, 12.5, 17.5, 22.5, and 27.5 mm, with respect to forward region of the die (Figure **6.2a**), all sixteen sensors were exposed to record the pressure increase profile. For circular die, the pressure sensor strip was positioned at eight different angles, 22.5 degrees apart, which covered the entire die, i.e., 0^0-180^0, 22.5^0-202.5^0, 45^0-225^0, 67.5^0-247.5^0, 90^0-270^0, 112.5^0-292.5^0, 135^0-315^0, and 157.5^0-337.5^0 (Figure **6.2b**). Based on previous studies (Dhanoa and Puri, 1998; Mittal et al., 2001), each test combination was repeated six times. Their tester consisted of a tiered arrangement of load cells with resolution of +/- 200 Pa. It allowed a mean value with a coefficient of variation (COV) less than 20, thus indicating that the data obtained from six replications was consistent. Accordingly, the experimental design with six replications per treatment is summarized in Table **6.1**.

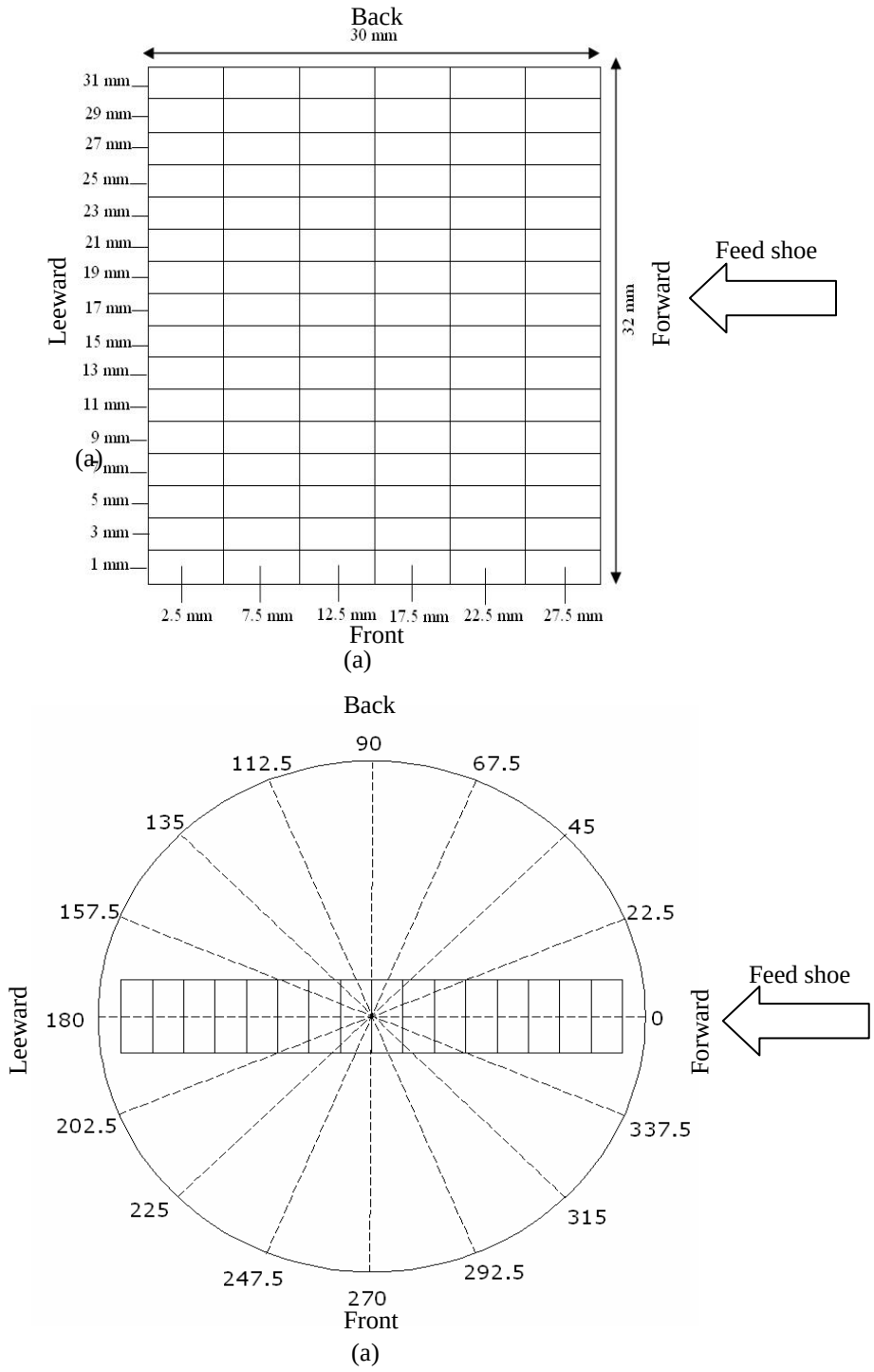

Figure **6.2**: Orientations of pressure sensor strip, (a) rectangular die, (b) circular die

Table **6.1**: Experimental design and test characteristics

Filling method	Test characteristics	Details
Feed shoe with square cross-section	Speed	20 mm/s
		100 mm/s
	Test materials	Avicel
		BPM
	Die shape	Rectangular (32 × 30 mm)
		Circular (diameter=35 mm)
	Die depth	6.5 mm
	Feed shoe cross-section	Square
	Number of replications	6

6.5 Results and discussion

In order to quantify the data, three types of analyses, namely, symmetry analysis, variance metrics, and uniformity analysis were used to evaluate the pressure distribution profile at the end of filling process.

Symmetry analysis was used to evaluate the uniformity of pressure distribution in the front vs. back and forward vs. leeward regions with respect to centerline of the die using contour plots. The symmetry index is defined as a ratio between 0 (least symmetrical distribution) and 100 (i.e., most symmetrical distribution).

Variance metrics summarize the values of statistical parameters which were obtained for the rectangular and circular dies at 20 and 100 mm/s feed shoe speeds using the final pressure values. The Max, Min, Mean, Max/Min, (Max-Min)/Mean, StDev (standard deviation), and COV (coefficient of variation) were used as the statistical parameters in variance metrics analysis as a means to evaluate uniformity.

For the uniformity analysis, the uniform color distribution for the entire die was measured using contour plot. For the symmetry and uniformity analyses, the area of uniform color distribution was measured using AutoCAD 2005 (Autodesk Inc. San Rafael, CA, USA). In order to compare the results of Avicel with BPM, each pressure value was divided by the particle density multiplied by gravity ($\frac{p}{\rho.g}$). This can be interpreted as equivalent height (h); in this study the particle density (ρ) of Avicel and BPM were 1.53 and 4.7 g/cc, respectively, and the gravitical constant was 9.8 m/s^2. The scale of scrutiny was +/- 20 dm (corresponding to average COV of 20%) out of full scale of 100 dm.

6.5.1 Analysis of filling process

The rectangular die at 20 mm/s feed shoe speed using BPM powder was used to demonstrate the filling process at different time sequences. Data from 20 mm/s feed shoe speed was selected because the air pressure and buoyancy effects of the two phase flow could be minimized at this speed. The relative positions of feed shoe tube with reference to the center line were used to mark the start and end point of different sequences. These specific positions of the feed shoe tube were used to demonstrate the filling sequences as shown in Figure **6.3**. Corresponding to these positions, the specific time for the feed shoe tube to reach these positions are listed by the letter T. The corresponding sequences of filling is shown in Figure **6.4**.

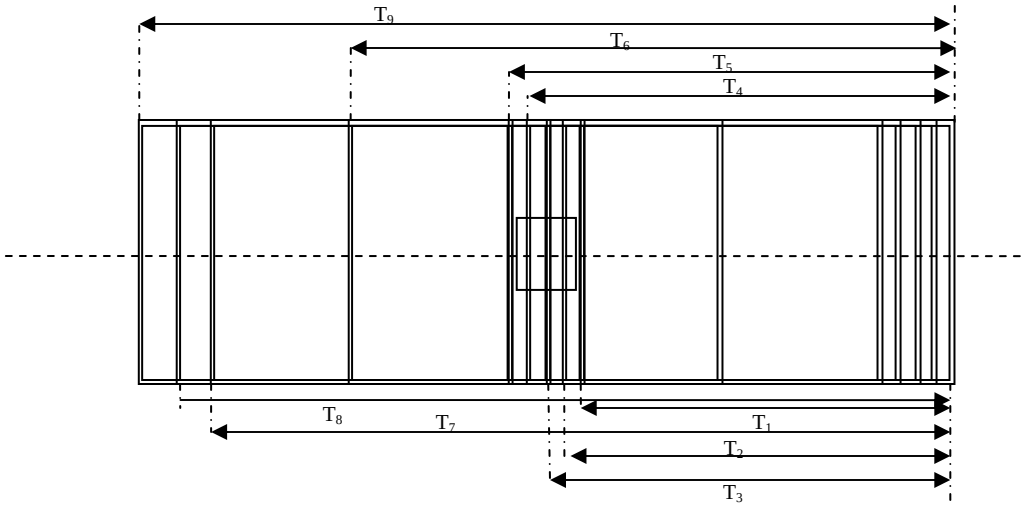

Figure **6.3**: Feed shoe tube positions at different time sequences and corresponding positions for rectangular shallow die (T_1=0 s, T_2=0.37 s, T_3=0.75 s, T_4= 1.12 s, T_5=1.5 s, T_6=5.8 s, T_7=10.20 s, T_8=10.94 s, and T_9=11.70 s)

T_1: the feed shoe started to move from its original (start) position (0 second).

T_2: the front wall of the feed shoe tube reached the leeward region (0.37 second). Accumulation is observed at back region closest to the wall, which may be caused by more particles entering the back region of the die (Figure **6.4**).

T_3: the front wall of feed shoe tube reached the middle of the die (0.75 second). The accumulation expanded toward the forward region.

T_4: the front wall of the feed shoe tube reached the forward region (1.12 second). The particles covered the die's entire bottom. The accumulation expanded toward the forward region.

T_5: the front wall of the feed shoe tube passed the forward region of the die (1.5 second). More particles entered the back region of the die which expanded the accumulation area.

T_6: the center of the feed shoe tube reached the center of the die (5.8 second). As the feed shoe tube moved from leeward to forward region, the particle-particle force increased; hence, the shear stress dramatically increased inside the die. Due to the rectangular die's sharp regions and corners, the majority of stress was observed in forward and back regions. In addition to the sharp corners, another possible reason for the higher stress may be caused by the ratio of die depth to particle size for BPM. The large particle size (up to 1 mm) and shallow die depth (6.5 mm) considerably increased the particle-particle force during the filling process, especially in the corners of the die.

T_7: the back wall of the feed shoe tube reached the leeward region (10.2 second). The stress zone in the forward and back regions increased and expanded toward the die center.

T_8: the back wall of the feed shoe tube reached the middle of the die (10.94 second). The surcharge powder started to be removed from the die (leveling process). The stress point reached the highest point inside the die.

T_9: the back wall of the feed shoe tube reached the forward region (the filling process ended) (11.7 second). The stress zone areas in the forward and back regions decreased due to particle rearrangement. The accumulation areas or stress zone were mostly concentrated in the forward and front regions.

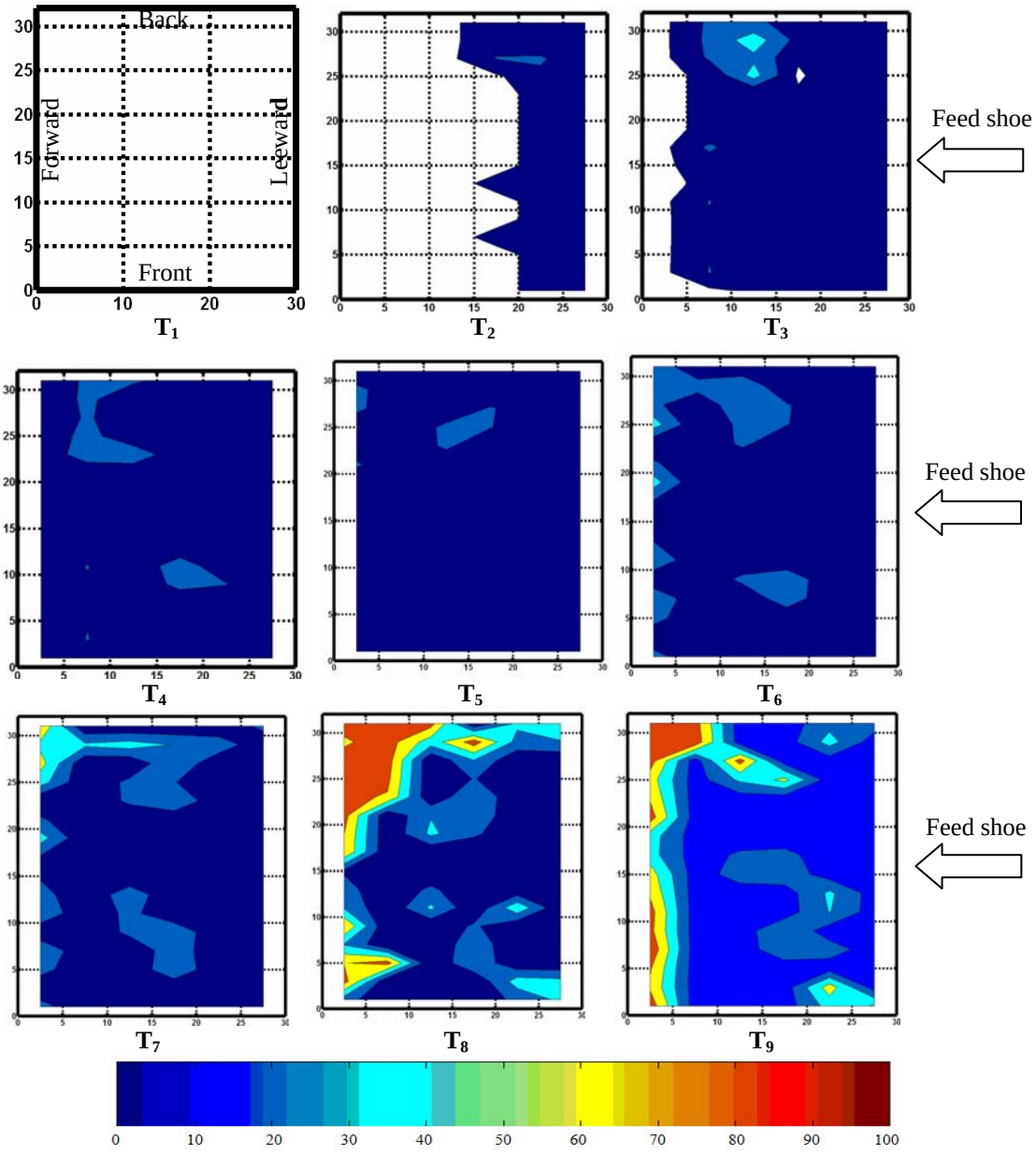

Figure **6.4**: Contour plots of filling sequences as equivalent height in dm (pressure/particle density*gravity) in rectangular shallow die for BPM powder at 20 mm/s feed shoe speed using a feed shoe tube with square cross-section at time T_1=0 s, T_2=0.37 s, T_3=0.75 s, T_4=1.12 s, T_5=1.5 s, T_6=5.8 s, T_7=10.2 s, T_8=10.94 s, and T_9=11.7 s (scale in dm).

6.5.2 Symmetry analysis

Figure **6.5** shows the contour plots of the rectangular shallow die, which is divided into the front-back and leeward-forward regions. The feed shoe tube approaches the die from the leeward to forward region. The areas of uniform color distribution in the front vs. back and forward vs. leeward regions were compared and analyzed.

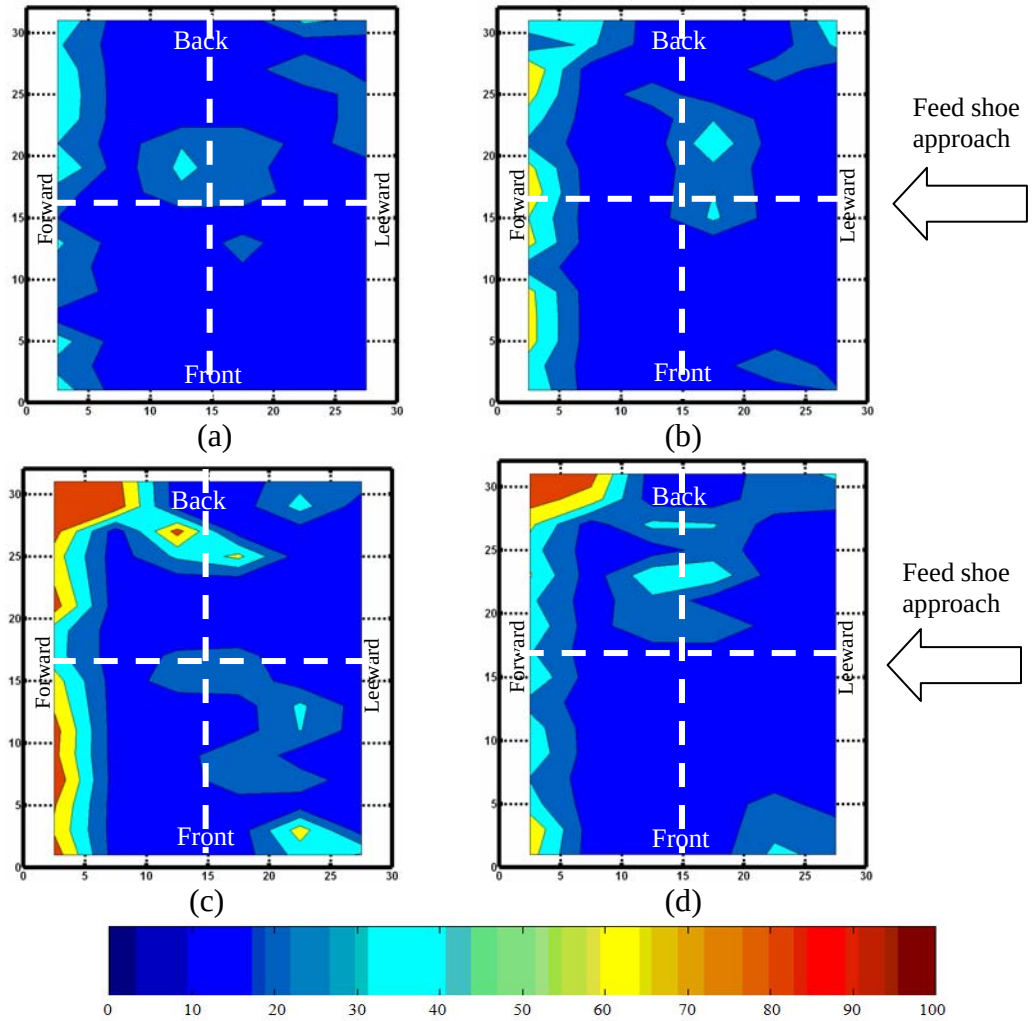

Figure **6.5**: Contour plots of the final pressure as equivalent height in dm (pressure/particle density*gravity) in rectangular die for Avicel (a) 20 mm/s, (b) 100 mm/s, and BPM (c) 20 mm/s, and (d) 100 mm/s feed shoe speed (scale in dm).

Rectangular die: The rectangular die was divided into the front-back and leeward-forward regions. The results showed that Avicel at 20 mm/s feed shoe speed (Figure **6.5a**) had a front and back uniformity of 73% and 50%, respectively, while the forward and leeward regions had 61% and 75% uniformity, respectively. As already discussed in section 6.5.1, the forward and back regions accumulated more particles, which generated higher stress and eventually decreaed the uniformity of pressure distribution. The symmetry index values for the front-back and leeward-forward regions were 68 % and 81%, respectively.

Avicel at 100 mm/s feed shoe speed (Figure **6.5b**), had a front and back uniformity of 48% and 58%, respectively, while the leeward and forward had 56 and 48% uniformity, respectively. The symmetry index values for front-back and leeward-forward regions were 82% and 85%, respectively.

For BPM powder at 20 mm/s (Figure **6.5c**), the front and back had 59% and 41% uniformity, respectively, and the leeward and forward had 36% and 59% uniformity, respectively. The symmetry index values for the front-back and leeward-forward regions were 69% and 61%, respectively.

For BPM at 100 mm/s (Figure **6.5d**), the front and back had 68% and 49%, uniformity respectively, while the leeward and forward had 65% and 55% uniformity, respectively. The symmetry index values for front-back and leeward-forward region were 72% and 84%, respectively.

The results showed that: (1) the highest accumulation area was observed in the forward and back regions, the reason being that during the filling process; more particles enter the forward and back regions (the back and forward regions filled first) which

increased the stress zone in these areas; (2) the symmetry index values increased with increasing feed shoe speed, possibly due to the particle collapsing the local bridges during the filling process, which generated more uniformity inside the die; and (3) the leeward region of the die at Avicel powder at 20 mm/s generated the highest uniformity (75%). Table **6.2** summarizes the symmetrical analysis of Avicel and BPM at 20 and 100 mm/s feed shoe speed using symmetry index.

Table **6.2**: The results for the symmetry analysis for rectangular die for Avicel and BPM at 20 and 100 mm/s feed shoe speeds

Filling method and die	Test materials	Feed shoe speed (mm/s)	Locations	% Uniformity	Symmetry index
Feed shoe-Rectangular die	Avicel	20	Front	73	68
			Back	50	
			Leeward	75	81
			Forward	61	
		100	Front	58	82
			Back	48	
			Leeward	56	85
			Forward	48	
	BPM	20	Front	59	69
			Back	41	
			Leeward	36	61
			Forward	59	
		100	Front	68	72
			Back	49	
			Leeward	65	84
			Forward	55	

Circular die: Figure **6.6** shows the contour plots for symmetry analysis for a circular die at 20 and 100 mm/s feed shoe speeds using Avicel and BPM. The results showed that for Avicel at 20 mm/s feed shoe speed (Figure **6.6a**), the front and back had 55% and 41% uniformity, respectively, while the leeward and forward had 51 and 46% uniformity, respectively. The symmetry index values for the front-back and leeward-forward regions for Avicel at 20 mm/s feed shoe speed were 74% and 90%, respectively.

Avicel at 100 mm/s (Figure **6.6b**), the front and back had 48 and 42% uniformity, respectively, while the leeward and forward had 42% and 37% uniformity, respectively. The symmetry index values for the front-back and leeward-forward regions for Avicel at 20 mm/s feed shoe speed were 86% and 88%, respectively.

BPM at 20 mm/s (Figure **6.6c**), had uniformity of 42% and 33% for the front and back, respectively, while the leeward and forward had 39% and 34% uniformity, respectively. The symmetry index values for the front-back and leeward-forward regions for BPM at 20 mm/s feed shoe speed are 78% and 87%, respectively. BPM at 100 mm/s (Figure **6.6d**), had a front and back uniformity of 72% and 59%y, respectively, while the leeward and forward had 69 and 68% uniformity, respectively. The symmetry index values for the front-back and leeward-forward regions for BPM at 100 mm/s feed shoe speed were 81% and 99%, respectively.

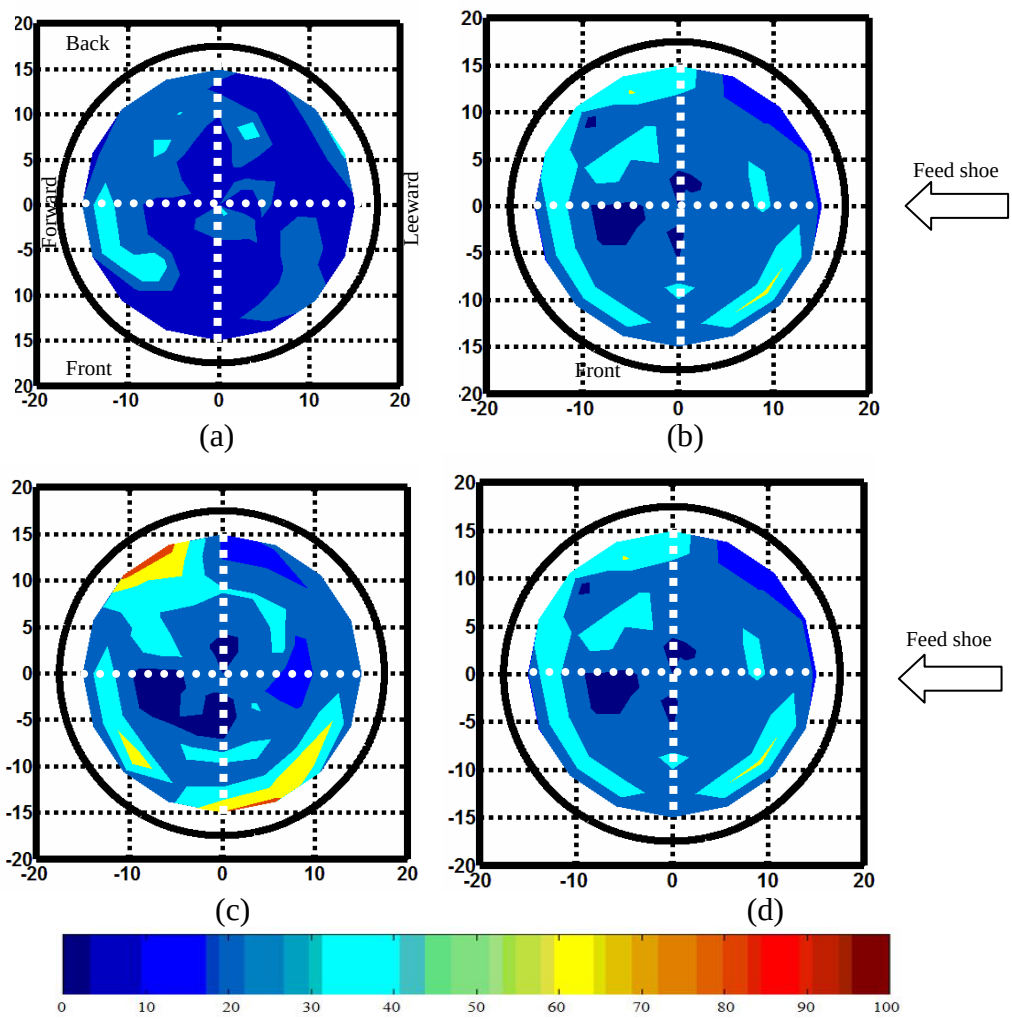

Figure **6.6**: Contour plots of final pressure as equivalent height in dm (pressure/particle density*gravity) for Avicel (a) 20 mm/s, (b) 100 mm/s, and BPM (c) 20 mm/s. and (d) 100 mm/s feed shoe speed (scale in dm).

The results showed that: (1) both Avicel and BPM in the front and leeward regions had higher uniformity vs. back and forward regions, respectively. The stress zone or accumulation area was located toward the center of the die which probably was caused by the curvature in the circular die, less accumulation was seen along the wall; (2) BPM at 100 mm/s at the leeward and forward generated the maximum symmetrical pressure

distribution among all (symmetry index=99); (3) the symmetry index values increased with increasing feed shoe speed for both Avicel and BPM, possibly due to the higher feed shoe speed collapsing the local bridges, which generated more uniformity inside the die; (4) BPM in 100 mm/s at the front region generated the highest uniformity among all (72%); and (5) BPM at 20 mm/s at the back region generated the least uniformity among all (33%). The results for a circular die are summarized in Table **6.3**.

Table **6.3**: The results for the symmetry analysis for circular die for Avicel and BPM at 20 and 100 mm/s feed shoe speeds

Filling method	Test materials	Feed shoe speed (mm/s)	Locations	% Uniformity	Symmetry index
Feed shoe – circular die	Avicel	20	Front	55	74
			Back	41	
			Leeward	51	90
			Forward	46	
		100	Front	48	87
			Back	42	
			Leeward	42	88
			Forward	37	
	BPM	20	Front	42	78
			Back	33	
			Leeward	39	87
			Forward	34	
		100	Front	72	81
			Back	59	
			Leeward	69	99
			Forward	68	

6.5.3 Variance metrics analysis

The statistical parameters, such as Max, Min, Mean, Max/Min, (Max-Min)/Mean, standard deviation (StDev), and coefficient of variation (COV) were used in this study. The usual COV defined as the ratio between 0% (ideal, most uniform) and 100 % (non-uniform, least uniform) (each pressure value was divided by the particle density

multiplied by gravity, $\frac{p}{\rho.g}$) was used. Table **6.4** summarizes the statistical parameters for Avicel and BPM at 20 and 100 mm/s for a rectangular and a circular die.

Table **6.4**: Variance metrics parameters for Avicel and BPM at 20 and 100 mm/s for rectangular and circular dies

Die	Test material	Feed shoe speed mm/s	Max (dm)	Min (dm)	Mean (dm)	Max/Min	(Max-Min)/Mean	Standard deviation	COV%
Rectangular	Avicel	20	3.00	0.44	2.17	6.80	1.18	0.54	24.9
		100	5.17	0.66	2.43	7.80	1.56	0.56	23.4
	BPM	20	7.01	2.11	3.14	3.32	1.55	1.04	33.2
		100	8.21	2.33	3.23	3.52	1.82	0.58	18.2
Circular	Avicel	20	2.43	0.33	2.34	7.30	0.90	0.58	25.0
		100	4.87	0.47	2.53	10.36	1.73	0.58	23.2
	BPM	20	7.11	3.05	4.11	2.33	0.98	1.20	29.1
		100	7.77	4.04	4.33	1.92	0.86	0.63	14.7

The following concluding remarks were made from this study: (1) BPM at 100 mm/s at both rectangular and circular die generated the smallest COV, which was interpreted as the highest uniformity among all (COV=18.2% and 14.7 %, respectively); (2) BPM at 20 mm/s with a rectangular die had the largest COV, or the least uniformity (COV=33.2%), probably due to the sharp regions and corners of the rectangular die, which trapped the particles and increased the stress zone inside the die; (3) BPM at 20 mm/s for both rectangular and circular die had the highest standard deviation (1.04 and 1.20, respectively); (4) the (Max-Min)/Mean were almost the same for both Avicel and BPM; (5) BPM at 100 mm/s had the lowest Max/Min, and (Max-Min)/Mean, which led to the most uniform filling for the circular die.

6.5.4 Uniformity analysis

Table **6.5** summarizes the uniformity comparison between rectangular and circular dies. For rectangular die, the Avicel powder at 20 mm/s feed shoe speed had 56% uniformity (Figure **6.5a**), while at 100 mm/s feed shoe speed had 59% uniformity (Figure **6.5b**). BPM at 20 mm/s feed shoe speed had 58% uniformity (Figure **6.5c**), while at 100 mm/s feed shoe speed had 61% uniformity (Figure **6.5d**). The reason for the higher uniformity seen with a higher feed shoe speed might be by higher speed collapsing the local bridges, which generated more uniformity inside the die.

For circular die the Avicel powder at 20 mm/s feed shoe speed had 46% uniformity (Figure **6.6a**), while at 100 mm/s feed shoe speed had 50% uniformity (Figure **6.6b**). BPM at 20 mm/s feed shoe speed had 52% uniformity (Figure **6.6c**), while at 100 mm/s feed shoe speed had 64% uniformity (Figure **6.6d**).

For the circular die, the accumulation was located toward the center of the die. However, in the rectangular die, most of the accumulation was observed next to the wall. The reasoning for this is that during the filling process for a circular die, the particles with high kinetic energy hit the die's curvature and were able to spread within the die. The sharp regions and corners of the rectangular die trapped the particles which then accumulated next to the wall and corners.

Table **6.5**: Uniformity analysis for rectangular and circular die at 20 and 100 mm/s feed shoe speeds

Filling method	Die	Test materials	Feed shoe speed, mm/s	% Uniformity
Feed shoe with square cross-section	Rectangular	Avicel	20	56
			100	59
		BPM	20	58
			100	61
	Circular	Avicel	20	46
			100	50
		BPM	20	52
			100	64

6.6 Uniformity comparison between a rectangular and a circular die

The results showed that: (1) die shapes highly influenced the uniformity pressure distribution; (2) the rectangular die generated higher stress zone than the circular die; (3) the feed shoe speed highly influenced the uniformity distribution inside the die, the reason might be that for the different feed shoe speeds, particles enter the die with different kinetic energies which cause varying pressure distributions inside the die.

6.7 Conclusions

The filling characteristics of Avicel and BPM at 20 and 100 mm/s feed shoe speeds using PDT-II with square feed shoe cross-section were studied and analyzed. The following concluding remarks were obtained from this study:

(1) The symmetry index values increased with increasing the feed shoe speed;

(2) The leeward-forward region for both circular and rectangular dies had higher symmetrical pressure distribution than the front-back regions;

(3) BPM at 100 mm/s feed shoe speed with a circular die had the lowest Max/Min, (Max-Min)/Mean, and COV (coefficient of variation), which led to the most uniform filling among all;

(4) Particle size highly influenced the uniformity pressure distribution inside the die;

(5) Die shape highly influenced uniformity distribution;

(6) The ratio of the particle size to die depth influenced the uniformity due to the lack of space for rearrangement during filling process. (the particle-die ratio for BPM and Avicel were 0.1 and 0.01, respectively);

(7) Uniformity increased with increasing the feed shoe speed in both dies.

6.8 References

1- Dhanoa, P. S. and V. M. Puri, 1998. Deposition of particulate materials confined spaces-new tester development and experimental results. *KONA (Powder and Particle) 16:152-159.*
2- Kestenbaum, D. 1997. Sand castles and cocktail nuts. *New Science 2083:25-28.*
3- Mittal, B. and V. M. Puri. 1999. Correlation between powder deposition methods and green compact quality: part II compact quality and correlations. *Partic. Science and Technology 17:301-315*.
4- Mittal, B., V. M. Puri, and W. Shaffer 2001. Analysis of feed shoe powder deposition method using a real-time cumulative mass deposition tester. *KONA (Powder and Particle) 19: 144-154*.
5- Puri, V. M. and P. S. Dhanoa. 2000. Real-time spatial particulate mass deposition testers. United States Patent. Patent number: 6,089,100.
6- Reed, J. S. 1995. *Principles of Ceramic Processing*. New York: John Wiley & Sons, Inc.
7- Xie, X. and V. M. Puri. 2007. Simultaneous deposition of powder in three parallel-oriented cylindrical dies. *Partic. Science and Technology 25(4): 247-260*.

Chapter 7

Uniformity Discrimination Analysis - Powder Deposition Characteristics in Circular and Rectangular Shallow Dies Using a Rotational Rainy Fill Device

7.1 Abstract

Study of the particulate material deposition into dies, bags, and containers represents a critical step in numerous industrial processes. However, there have been no systematic investigations wherein different methods have been compared. Herein, results from an experimental study dealing with filling of powders into shallow dies (aspect ratios less than 0.25) are presented. An innovative rotational rainy filling device was designed and fabricated. This versatile device can be used to evaluate deposition characteristics for various particles sizes, particles size distributions, die shapes, and deposition rates. In this research, a rotational rainy fill device was used to investigate the uniformity of powder deposition into a rectangular die (32×30 mm), and a circular (35 mm in diameter) die each 6.5 mm in depth, respectively. The test materials used in this study were microcrystalline cellulose (Avicel-PH102), a pharmaceutical powder, and a battery powder mixture (BPM), an industrial powder. Two different deposition rates were used, i.e., 26 and 132 g/min. Symmetry analysis, variance metrics, and uniformity analysis were implemented to quantify the deposition characteristics. The results showed that: (1) die geometry highly influenced the pressure uniformity distribution; (2) the circular die generated higher uniformity than the rectangular die; (3) rotational speed of 8.5 rpm was determined to be the best angular speed for the rotational rainy fill device;

(4) deposition rates did not substantially influence the uniformity pressure distribution inside the die; and (5) leveling procedures (removing surcharge powder) markedly increased non-uniformity within the die.

7.2 Introduction

Powders are processed in numerous industries, such as agriculture, ceramic, chemical, food, pharmaceutical, powder metallurgy, mineral, and mining. Many complex processes, for example, conveying, mixing, and pelletizing, are employed in the particulate industries. Most of these industries are migrating toward the use of materials in particulate form as major products. However, anisotropy is a major problem in some powder compaction processes because it creates quality problems, such as, shrinkage, cracking, low strength, and warpage of compacts. The anisotropism is ascribed, in part, to the deposition process because of the non-uniform bulk distribution within the die that may occur during this process. Having a uniform density distribution in a die, or powder uniformity, is an important first step in avoiding undesirable quality for pellets, tablets, and compacts. Deposition uniformity is correlated to filling process parameters, such as, filling rate, filling method, die geometric characteristics, and powder characteristics, such as absolute size distribution, shape, and bulk density, and also environmental conditions (Dhanoa and Puri, 1998; Mittal et al., 2001). Within the past few years, a number of researchers in the rapidly growing powder mechanics field have turned their attention to filling methods in dies and load distributions in large storage structures. In contrast, very few researchers have systematically studied the filling process into small dies.

7.3 Objectives

The objective of this research was to study the powder deposition characteristics in a rectangular and a circular shallow die using an innovative rotational rainy fill method.

7.4 Methodology

This section discusses the design of a stationary and a rotational rainy fill device. In addition, the methods for using these devices to study the pressure change and distribution at the bottom of the dies during the powder filling process and are summarized.

Deposition of powder into a rectangular and a circular shallow die with a depth of 6.5 mm and dimensions of 32×30 mm, and 35 mm in diameter, respectively, shown in Figure **7.1**, were used in this study. The volumetric capacity of the rectangular and circular dies was the same (6245 mm^3).

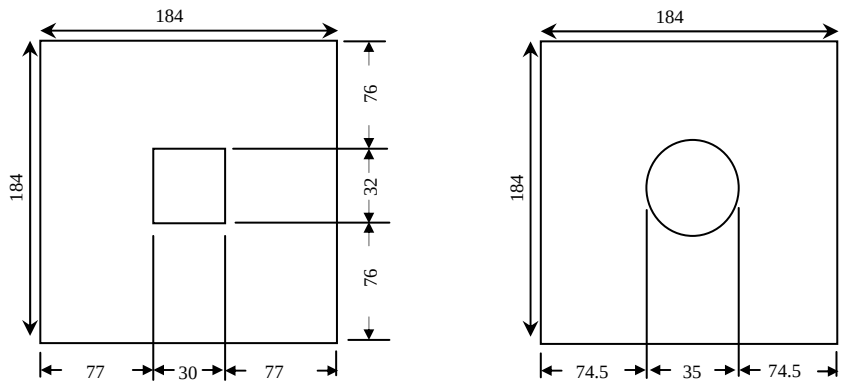

(a) (b)

Figure **7.1**: AutoCAD drawing of rectangular (a) and circular (b) dies including dimensions (drawn to scale, all dimensions are in mm)

The test materials: 1) microcrystalline cellulose (Avicel, PH102) with d_{50}=84 μm and, 2) battery powder mixture (BPM) with d_{50}=600 μm. Two different deposition rates were used which corresponded to the deposition rate noted at 20 and 100 mm/s feed shoe speeds, namely, 26 and 132 g/min.

7.4.1 Stationary rainy fill device

An initial design of a rainy filling device consisted of five screens (Figure **7.2**), each 2 cm apart. Each screen had an opening size of 3.352 mm (wire diameter 0.889 mm). Each screen was oriented 45^0 with respect to the screen wires above and below. By trial-and-error, five layers were determined to be sufficient to spread a line feed of powder into a rainy fill. Table **7.1** lists the characteristic dimensions of wire mesh used in fabrication of the stationary rainy device.

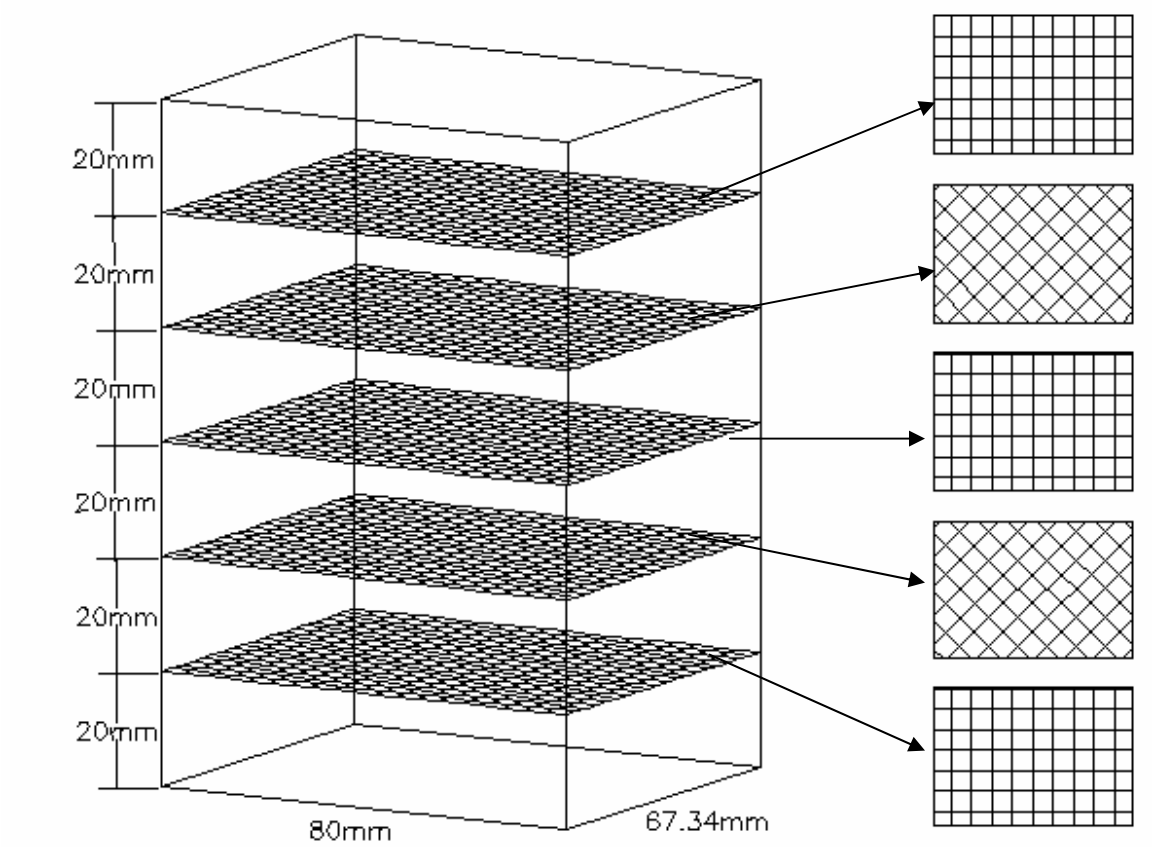

Figure **7.2**: Stationary rainy fill device with dimensions

Table **7.1**: Wire mesh characteristic used for rainy filling device

	Type	Mesh per centimeter	Wire diameter (mm)	Opening width (mm)	Open area (%)
Wire mesh	304 stainless steel	3×3	0.889	3.352	62.7%

7.4.2 Rotational rainy fill device

Based on extensive initial tests with the stationary rainy fill device shown in Figure **7.2**, a new and improved design of rainy device was developed (Roudsari and Puri, 2005). The new design, called rotational rainy fill, contains one screen (3.352 mm opening and 0.889 mm wire diameter) that was sufficient to pass the largest BPM particle (1.00 mm). The screen was mounted in the middle of a Plexiglas cylinder. Using trial-and-error, the optimal cylinder dimensions were determined to be 6.35 cm inner diameter x 15.24 cm height. These dimensions were satisfactory to spread uniformly the BPM powder above the die. The cylinder was placed inside a PVC ring and plate to prevent from any axial or lateral movements. The purpose of PVC ring was to minimize friction during rotation. A DC electric gear motor with an adjustable rotational speed (1-10 rpm) was used to rotate the Plexiglas cylinder. A timing belt transferred the motion from electric motor to the cylinder. A cut-away 3D view and photograph of the assembled rainy fill device are shown in Figure **7.3** and Figure **7.4**, respectively.

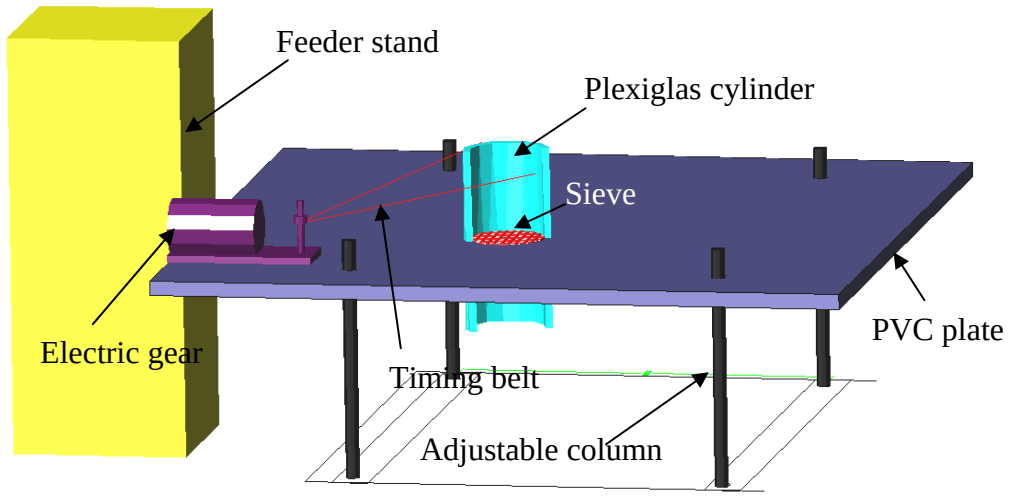

Figure **7.3**: Overall AutoCAD rendition of the rotational rainy fill device

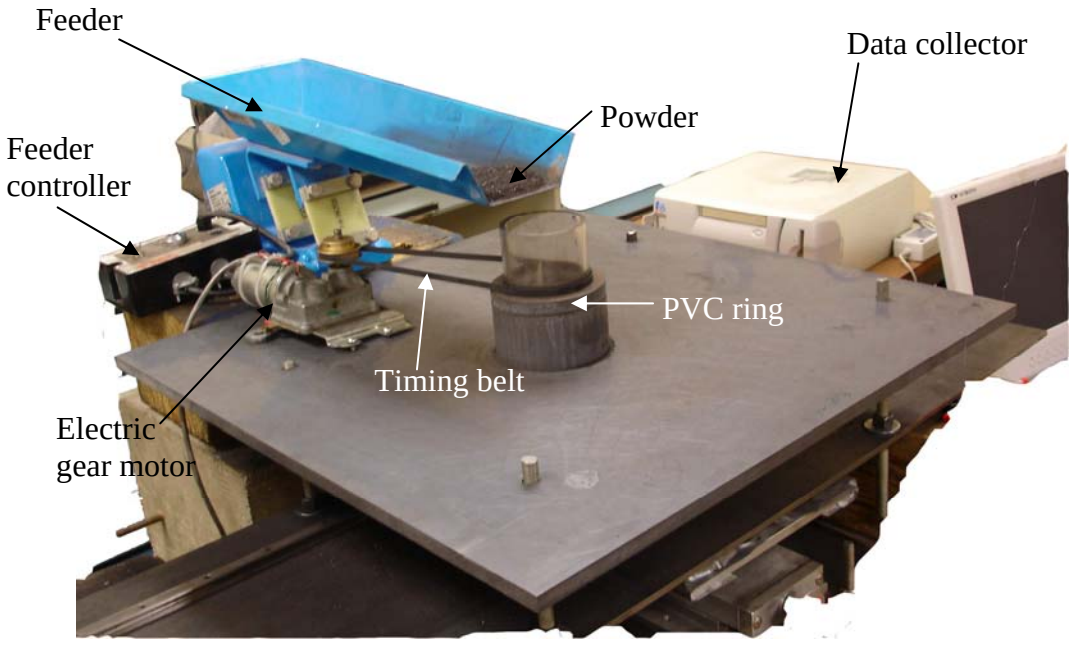

Figure **7.4**: Photograph of the assembled rotational rainy fill device

In order to determine the optimum rotational speed, which results in a uniform fill, preliminary tests were done using an open top and bottom rectangular box with dimension of 94.01 mm × 53.72 mm with 28 equal-sized compartments (each 13.43 ×13.43 mm). This rectangular box was sufficient to cover the area of a rectangular die. Figure **7.5** shows the rectangular box and the compartments in comparison with a circular die area. The tests were carried out by varying RPMs from 1 through 10. For each RPM, the amount of powder mass deposited inside each compartment was measured.

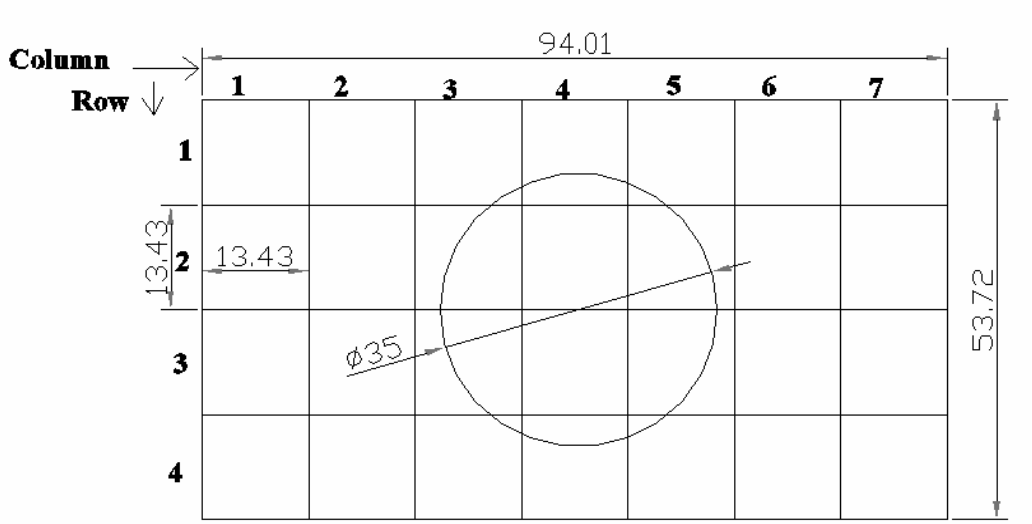

Figure **7.5**: Rectangular cells in comparison with circular die (middle), all dimensions in mm (drawn to scale)

A syntron F-010 vibrating feeder with a standard 12.7×50.8 cm flat pan trough was used to feed the rainy device. The feeder was set to 2.81 and 3.35 mm amplitude and 60 Hz to be comparable to a feed shoe filling at 20 and 100 mm/s, respectively. The feeder was placed at the closest possible distance (5 mm) above the upper region. The pile (mound) of powder inside the die reached about 7 mm during the filling process; the

cylinder was located 10 mm above the die. The feeder had a maximum capacity of four tons per hour, though the actual capacity of the vibration feeder varies according to the density of the bulk material being handled and the feeder trough size.

For the rectangular die, the pressure sensor strip was positioned at six locations which covered the entire die cross section, i.e., 2.5, 7.5, 12.5, 17.5, 22.5, and 27.5 mm, with respect to the forward region of the die (Figure **7.6a**). For the circular die, the pressure sensor strip was positioned at 8 different angles, 22.5 degrees apart, which covered the entire die, i.e., 0^0-180^0, 22.5^0-202.5^0, 45^0-225^0, 67.5^0-247.5^0, 90^0-270^0, 112.5^0-292.5^0, 135^0-315^0, and 157.5^0-337.5^0 (Figure **7.6b**). Based on previous studies (Dhanoa and Puri, 1998; Mittal et al., 2001), each test combination was repeated six times. Their tester consisted of a tiered arrangement of load cells with resolution of +/- 200 Pa. It allowed a mean value with coefficient of variation (COV) less than 20, thus indicating that the data obtained from six replications was consistent. Table **7.2** summarizes the experimental design with six replications per treatment for this study.

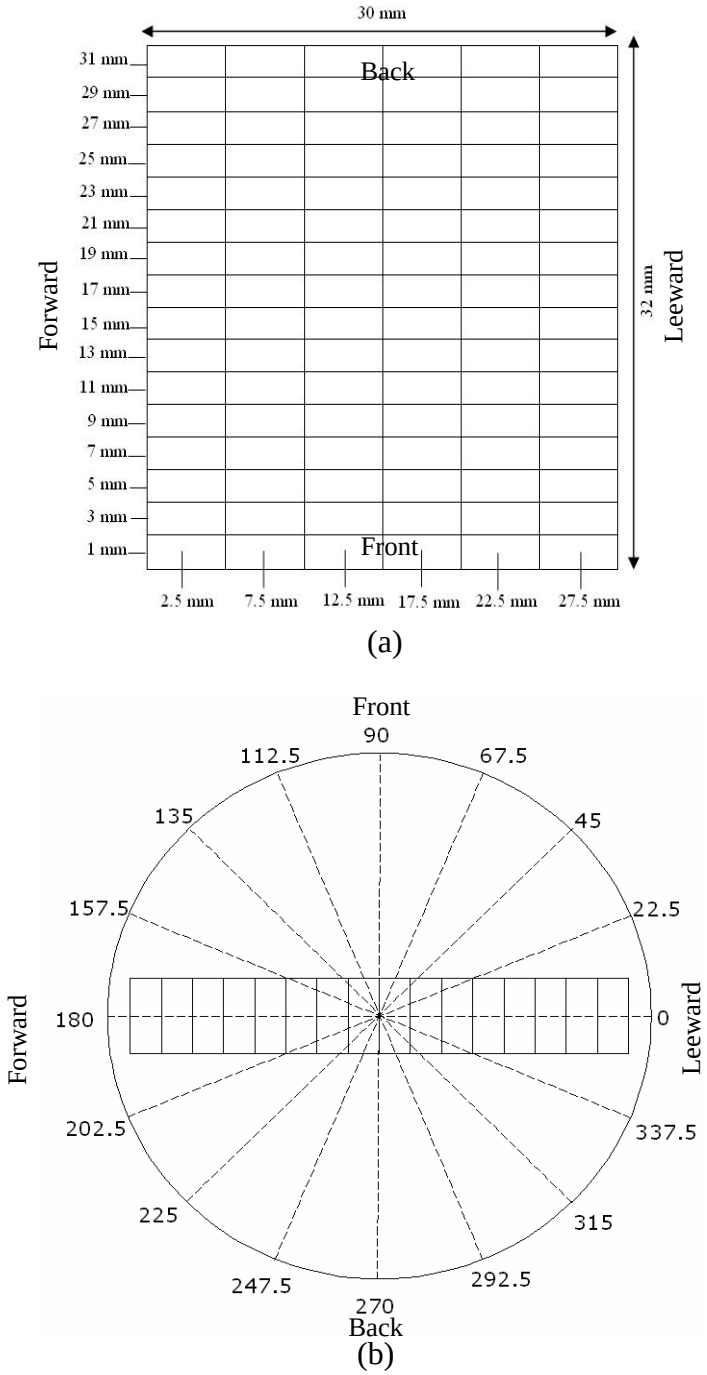

Figure **7.6**: Orientations of pressure sensor strip, (a) rectangular die, (b) circular die

Table **7.2**: Experimental design of rotational rainy fill

Filling method	Test characteristics	Details
Rotational rainy	Filling rate (g/min)	26
		132
	RPM	8.5
	Die shape	Circular
		Rectangular
	Die depth (mm)	6.5
	Number of replications	6

7.5 Results and discussion

The amount of powder mass inside each cell of the rectangular boxes for different RPMs, was compared and analyzed. For a rainy fill, this was based on the quantity of powder weight that was deposited into six equi-sized 13.43 mm x 13.43 mm compartments at RPMs, of 2 to 10. The results showed, for Avicel, in highest and lowest COVs of 70% and 12% were obtained at RPMs 3.5 and 8.5, respectively, and for BPM, in highest and lowest COVs of 69% and 24% at RPMs 2 and 8.5, respectively.
Figure **7.7** shows the relationship between represented the COV (coefficient of variation) at different RPM for Avicel and BPM. Based on these values, a rotational speed of 8.5 rpm, which had the lowest COV for both powders, was inferred as the most uniform distribution among the ten RPMs.

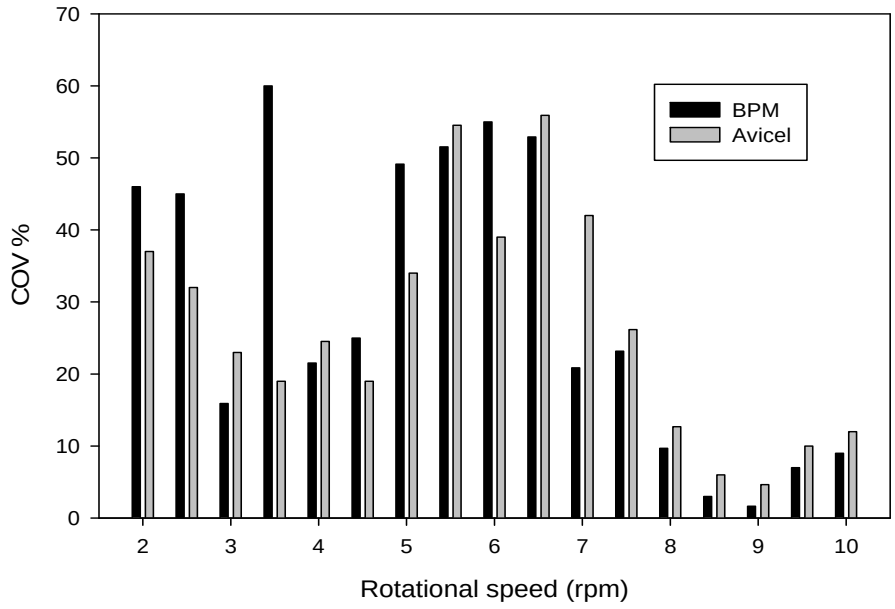

Figure **7.7**: The relationship between rotational speed (rpm) and coefficient of variation (COV) for Avicel and BPM

Qualitative and quantitative analyses of the final pressure distribution for Avicel and BPM were accomplished through symmetry analysis, variance metrics, and uniformity analysis. Symmetry analysis was used to evaluate the uniformity of pressure distribution in the front vs. back and forward vs. leeward regions with respect to the centerline of the die using AutoCAD (Autodesk Inc. San Rafael, CA, USA). The symmetry index was defined as a ratio between 0 (least symmetrical distribution) and 100 (most symmetrical pressure distribution).

Variance metrics involved determining the statistical parameters which were obtained for the rectangular and circular dies at 26 and 132 g/min filling rates using the final pressure values converted to equivalent height in decimenter (pressure/particle density*gravity). The Max, Min, Mean, Max/Min, (Max-Min)/Mean, StDev (standard

deviation), and COV (coefficient of variation) were used as the statistical parameters in variance metric analysis.

In order to compare the uniformity results of Avicel with BPM, each pressure value was divided by the particle density multiplied by gravity ($\frac{p}{\rho.g}$). This can be interpreted as equivalent height (h); in this study the particle density (ρ) of Avicel and BPM used were 1.53 and 4.7 g/cc, respectively, and the acceleration due to gravity was 9.8 m/s^2. The scale of scrutiny was +/- 20 dm based on average COV of 20%; where, dm is decimeter (1 dm=0.1 m).

7.5.1 Analysis of filling process

The BPM powder at 26 g/min was used to demonstrate the filling process at different time sequences. The average filling time for a rotational rainy fill was approximately 55 seconds, which was divided into 9 time sequences. The contour plots of filling process for a rectangular and a circular die are shown in Figures **7.8** and **7.9**, respectively. The specific times for rotational rainy fill are listed by the letter T and subscripts as listed below.

T_1: prior to starting the filling process, the die was divided into four regions, namely, front, back, forward, and leeward.

T_2: fourteen percent completion of filling process (7 second). The particles covered the entire bottom of the die.

T_3: twenty-eight percent completion of filling process (14 second). Accumulation started to build up at the back region of the die.

T_4: forty-two percent completion of filling process (21 second).

T_5: fifty-seven percent completion of filling process (28 second). The particles accumulated at the back region by the wall.

T_6: seventy-one percent completion of filling process (35 second). The pressure reached 30 dm inside the die.

T_7: eighty-five percent completion of filling process (42 second). The accumulation increased at the die's corner regions.

T_8: one hundred percent completion of die filling (49 second). The die was fully filled. The particles were mostly accumulating in forward and back regions.

T_9: leveling process (54 second). The excess powder was removed from the die. The majority of particles accumulated in the forward and back regions. The stress peaked to 90 dm within the die.

For a rectangular die, more particles accumulated at the regions and corners of the die. This probably was caused by the rectangular die's sharp regions trapping the particles during the filling process, which then created high accumulation areas at the corner regions of the die. The leveling process increased the non-uniformity inside the die for both the rectangular and circular dies due to an increase in shear stress and dragging of particles while removing the surcharge powders with plastic straight edge (to maintain the same final height and thickness as a feed shoe apparatus).

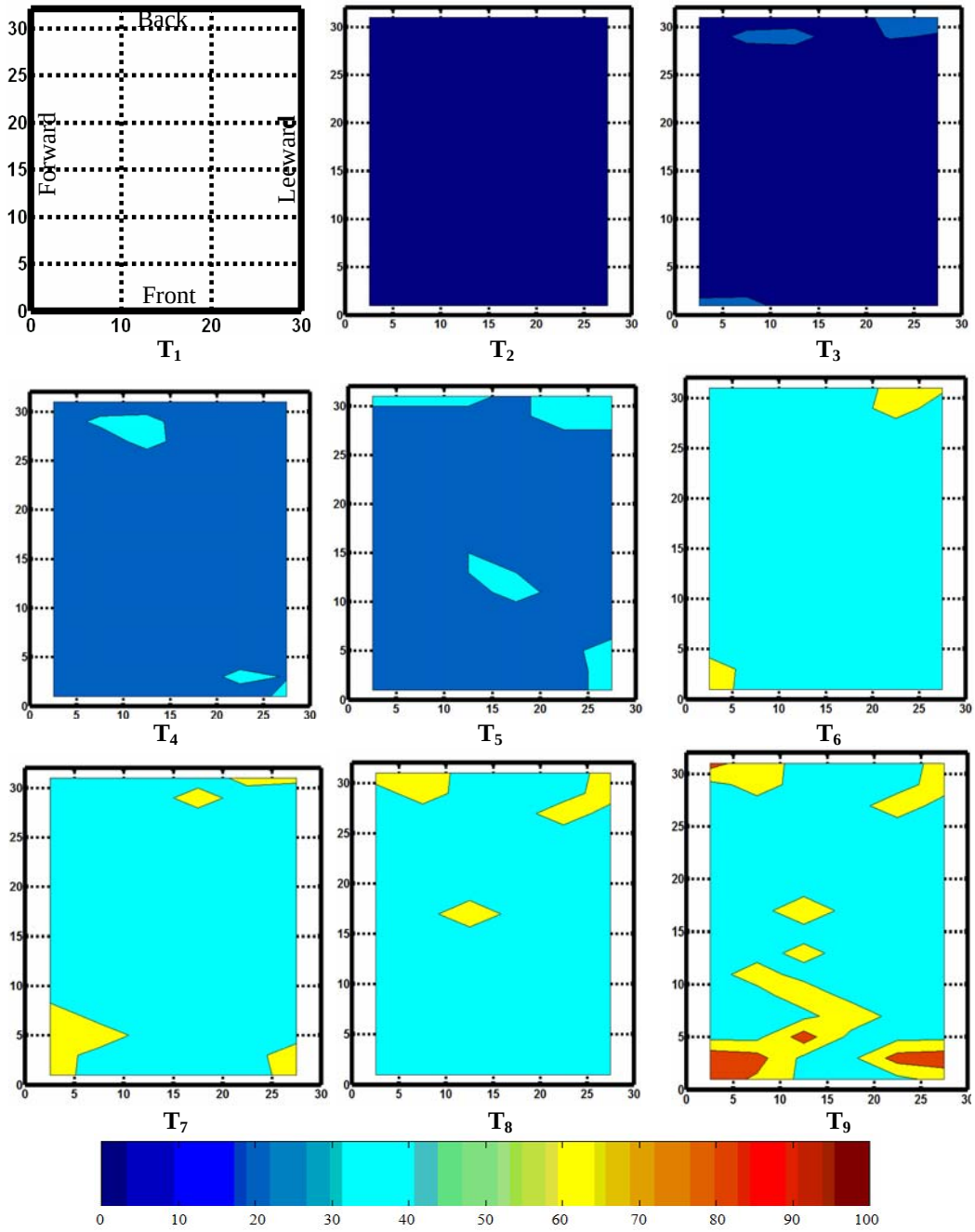

Figure **7.8**: Filling sequences in equivalent height units in dm (pressure/particle density*gravity) for rectangular shallow die with BPM powder at a 26 g/min filling rate using rotational rainy fill at time T_1=0 s, T_2=7 s, T_3=14 s, T_4= 21 s, T_5=28 s, T_6=35 s, T_7=42 s, T_8=49 s, and T_9=54 s (scale in dm).

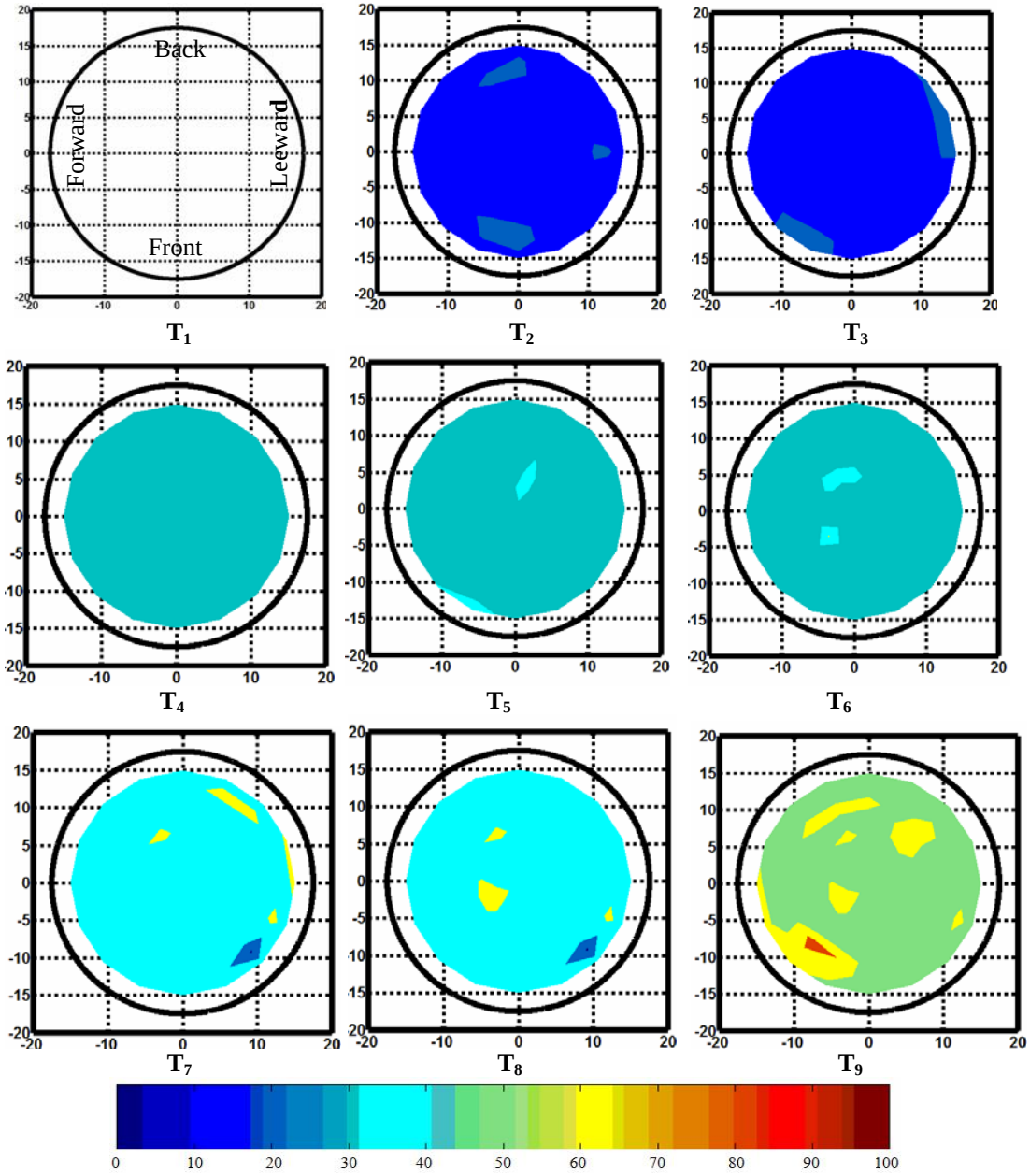

Figure **7.9**: Filling sequences in equivalent height units in dm (pressure/particle density*gravity) for circular shallow die with BPM powder at a 26 g/min filling rate using rotational rainy fill at time T_1=0 s, T_2=7 s, T_3=14 s, T_4= 21 s, T_5=28 s, T_6=35 s, T_7=42 s, T_8=49 s, and T_9=54 s (scale in dm).

7.5.2 Symmetry analysis

Rectangular die: Figure **7.10** shows the contour plots of the rectangular shallow die for Avicel and BPM using the rotational rainy filling device. For symmetry analysis, the contour plots were divided into front vs. back and forward vs. leeward regions. The uniformity of the same color distributions in front vs. back and forward vs. leeward were measured and analyzed using AutoCAD.

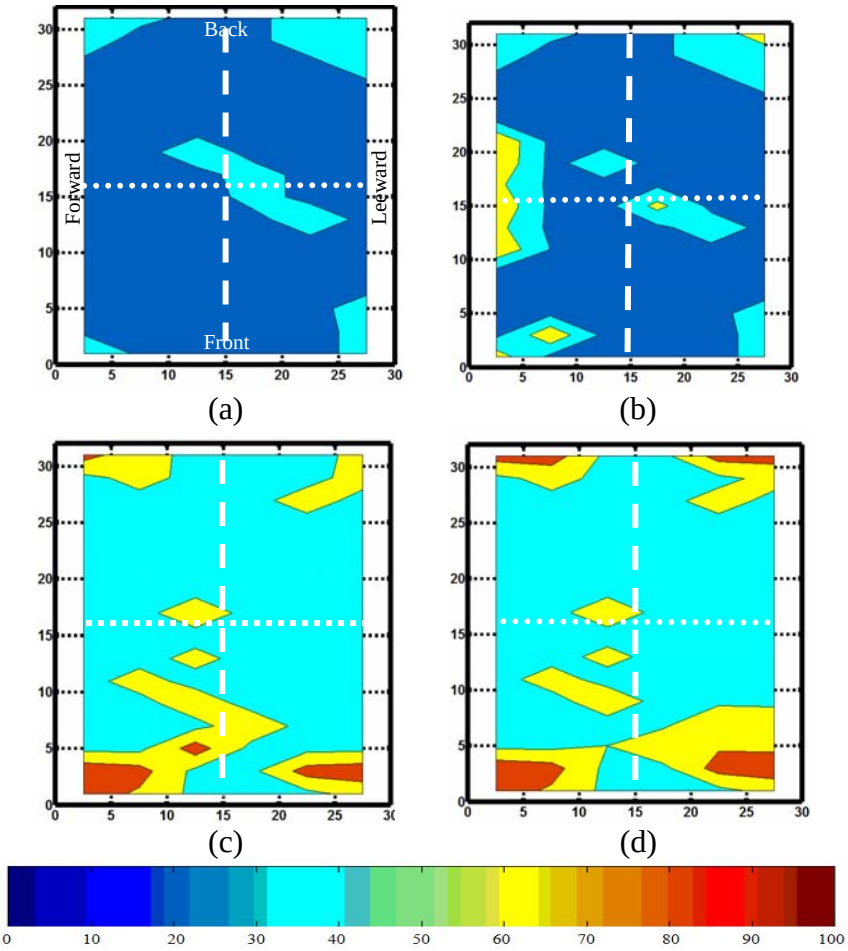

Figure **7.10**: Isopressure contour plots of the final pressure distribution in rectangular dies as equivalent height in dm with Avicel (a) 26 g/min, (b) 132 g/min, and BPM (c) 26 g/min, and (d) 132 g/min (scale in dm).

Front-back analysis: The results showed that for Avicel at filling rate of 26 g/min, the front and back had 92% and 89% uniformity respectively (Figure **7.10a**), while at 132 g/min had 77% and 68% uniformity, respectively (Figure **7.10b**). The symmetry index values for the front-back at 26 and 132 g/min were 96% and 88%, respectively.

For the BPM powder at 26 g/min, the front and back regions had 55% and 67% uniformity, respectively (Figure **7.10c**), while at 132 g/min had 44% and 65% uniformity, respectively (Figure **7.10d**). The symmetry index values for front-back at 26 and 132 g/min were 82% and 67%, respectively.

Forward-leeward analysis: For Avicel at filling rate of 26 g/min, the forward and leeward regions had 83% and 88% uniformity, respectively (Figure **7.10a**), while at a filling rate of 132 g/min had 61% and 68%, uniformity (Figure **7.10b**). The symmetry index values for forward-leeward region at 26 and 132 g/min filling rates were 94% and 89%, respectively.

For the BPM powder, at a 26 g/min filling rate, the forward and leeward regions had 58% and 64% uniformity, respectively (Figure **7.10c**), while at 132 g/min these regions had 57% and 52% uniformity, respectively (Figure **7.10d**). The symmetry index values for BPM at the forward-leeward region at 26 and 132 g/min filling rates were 90% and 91%, respectively. Table **7.3** summarizes the symmetry analysis results for Avicel and BPM for rectangular die.

Table **7.3**: The results for symmetry analysis for rectangular die for Avicel and BPM at 26 and 132 g/min filling rates

Filling method and die	Test materials	Deposition rate (g/min)	Locations	% Uniformity	Symmetry index %
Rotational rainy-Rectangular die	Avicel	26	Front	92	96
			Back	89	
			Leeward	83	94
			Forward	88	
		132	Front	77	88
			Back	68	
			Leeward	68	89
			Forward	61	
	BPM	26	Front	55	82
			Back	67	
			Leeward	58	90
			Forward	64	
		132	Front	44	67
			Back	65	
			Leeward	57	91
			Forward	52	

The results showed that the leeward and front regions had higher uniformity pressure distribution than the forward and back regions. The reason might be that during the leveling process, more particles enter the forward and back regions which increased the accumulation area and generated a higher stress zone. The most uniformity is observed in front-back region at 26 g/min filling rate for Avicel powder (96%), while the least uniformity is seen in front-back region at 132 g/min for BPM powder (67%). Generally, the BPM powder generated lower uniformity vs. Avicel. The cause might be due to the ratio of particle size to the die depth; this ratio is considerably higher in BPM than Avicel powder (the ratio of particle size to die depth for BPM and Avicel are 0.1 and 0.01, respectively), which decreases the degrees of freedom that the particles have for rearrangement inside the die.

Circular die: Figure **7.11** shows the contour plots for a circular shallow die with front vs. back, forward vs. leeward regions for Avicel and BPM powders at 26 and 132 g/min filling rates.

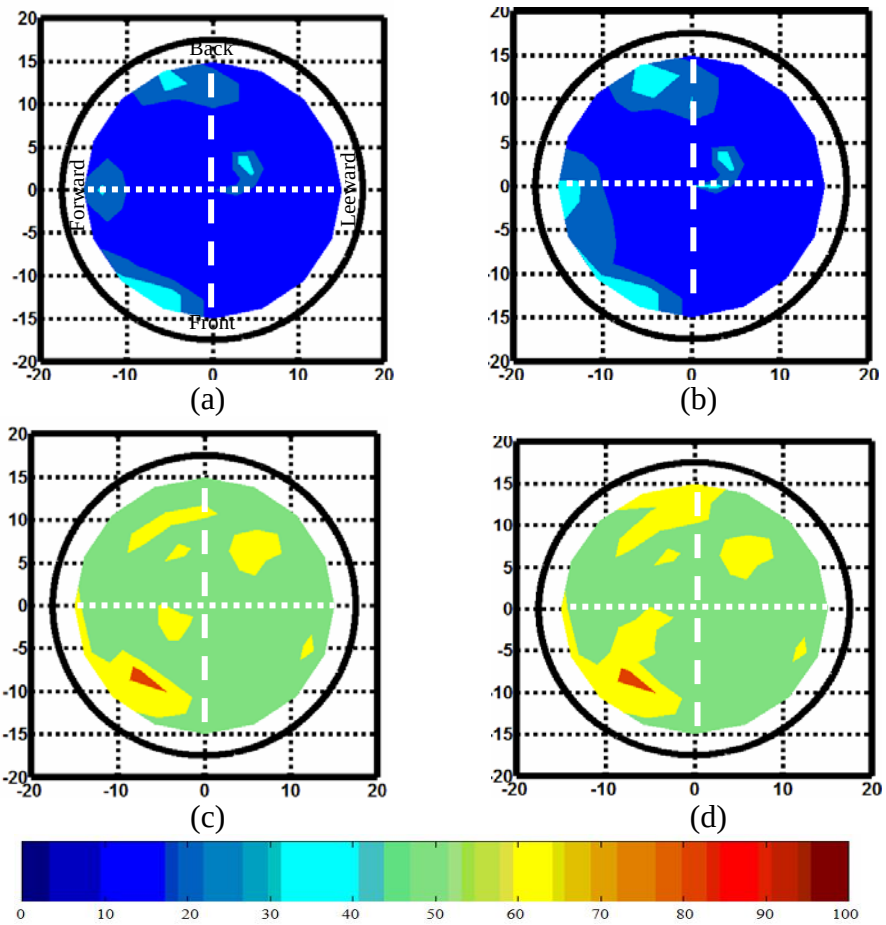

Figure **7.11**: Contour plots of the final pressure distribution in circular dies as equivalent height in dm with Avicel (a) 26 g/min, (b) 132 g/min, and BPM (c) 26 g/min, and (d) 132 g/min (scale in dm).

Front and back analysis: The results showed that for Avicel powder at 26 g/min, the front and back regions had 93% and 91% uniformity (Figure **7.11a**), while at 132 g/min these regions had 86% and 84% uniformity (Figure **7.11b**), respectively. The

symmetry index values for front-back at 26 and 132 g/min were 97% and 97%, respectively. For the BPM powder, the front and back regions had 89% and 83% uniformity (Figure **7.11c**), respectively, while at 132 g/min they had 80% and 74% uniformity (Figure **7.11d**), respectively. The symmetry index values for BPM powder for the front-back region at filling rates of 26 and 132 g/min were 93% and 92%, respectively.

Forward and leeward analysis: Avicel at a filling rate of 26 g/min had uniformity of 88% and 96% for the forward vs. leeward regions (Figure **7.11a**), respectively, while at a filling rate of 132 g/min the uniformity values were 79% and 95% uniformity (Figure **7.11b**), respectively. The symmetry index values for the forward-leeward region at 26 and 132g/min were 91% and 83%, respectively. For the BPM powder, the forward and leeward regions at 26 g/min had 78% and 90% uniformity (Figure **7.11c**), respectively, while at 132 g/min had 48% and 70%, uniformity. The symmetry index values for the forward-leeward region at 26 and 132 g/min were 87% and 60% (Figure **7.11d**), respectively. Table **7.4** summarizes the symmetry analysis results for BPM and Avicel for a circular die.

Table **7.4**: The results for symmetry analysis for circular die for Avicel and BPM at 26 and 132 g/min filling rates

Filling method and die	Test materials	Deposition rate (g/min)	Locations	% Uniformity	Symmetry index %
Rotational rainy-Circular die	Avicel	26	Front	93	97
			Back	91	
			Leeward	96	91
			Forward	88	
		132	Front	86	97
			Back	84	
			Leeward	95	83
			Forward	79	
	BPM	26	Front	89	93
			Back	83	
			Leeward	90	87
			Forward	78	
		132	Front	80	92
			Back	74	
			Leeward	70	60
			Forward	48	

The results showed that the leeward and front regions had greater more uniformity of pressure distribution. As already discussed, during the leveling process more particles entered the forward and back region, which increased the accumulation area. Another plausible reason might be the leveling process (leeward to forward regions) that generated shear stress in the top layer of the die, which caused an increase in non-uniformity in the forward and back regions (due to the leveling region which moved from the leeward to forward region). Also, Avicel had higher uniformity vs. BPM powder. The maximum equivalent pressure height for Avicel and BPM were 37 and 87 dm, respectively. This difference is probably due to the different particle densities, i.e., Avicel and BPM had densities of 1.53 and 4.7 g/min, respectively. The highest symmetry index values were observed in the front-back region for Avicel at both 26 and 132 g/min filling rates (97%), while the forward-leeward region for BPM at 132 g/min had the lowest symmetry index value (60%).

7.5.3 Variance metrics analysis

The variance metrics included the statistical parameters, such as Max, Min, Mean, Max/Min, (Max-Min)/Mean, standard deviation (StDev), and coefficient of variation (COV) were used in this study. Table **7.5** summarizes the statistical parameters for a rectangular and circular die for Avicel and the BPM powder.

Table **7.5**: Variance metrics parameters for Avicel and BPM at 26 and 132 g/min filling rates for rectangular and circular dies using rotational rainy fill

Die	Test Material	Filling rate g/min	Max (dm)	Min (dm)	Mean (dm)	Max/Min	(Max-Min)/Mean	Standard Deviation	COV%
Rectangular	Avicel	26	1.33	0.23	0.34	3.90	3.20	0.07	20.6
		132	1.72	0.29	0.44	5.05	3.25	0.09	20.5
	BPM	26	2.41	0.67	0.88	3.60	1.97	0.22	25.0
		132	2.75	0.77	0.89	3.57	2.22	0.24	26.9
Circular	Avicel	26	1.27	0.38	0.41	3.34	2.17	0.09	21.9
		132	1.10	0.33	0.44	3.33	1.75	0.08	18.1
	BPM	26	1.36	0.67	1.05	2.02	0.65	0.20	19.6
		132	2.48	0.88	1.13	2.81	1.41	0.22	19.7

The results showed: (1) BPM generated higher Max pressure distribution than Avicel for both the rectangular and circular dies which is due to BPM's higher particle density; (2) the standard deviation increased with increasing filling rate; (3) Avicel at 132 g/min filling rate for both circular and rectangular dies had the lowest COV%, which implied the maximum uniform filling (18.1% and 20.5%); (4) the circular die had lower COV, (Max-Min)/Mean, and Max/Min values compared to the rectangular die, which implied a more uniform filling in the circular die; and (5) generally, the circular die generated more uniformity compared to rectangular die, the reason probably being due to the fact the particles were trapped in the rectangular die's sharp regions and corners, which increased the non-uniformity within the die.

7.5.4 Uniformity analysis

Rectangular die: For uniformity analysis, the area of uniform color distribution for the entire die was measured using AutoCAD and analyzed. The results showed that Avicel at 26 and 132 g/min had 84% (Figure **7.10a**) and 79% (Figure **7.10b**) uniform color distribution, respectively, while BPM at the same filling rates had 76% (Figure **7.10c**) and 69% (Figure **7.10d**) uniformity, respectively. Avicel generated higher uniformity at both filling rates.

Circular die: For Avicel at 26 and 132 g/min filling rates had 85% (Figure **7.11a**) and 81% (Figure **7.11b**) uniformity, respectively, while BPM at the same filling rates had 79% (Figure **7.11c**) and 69% (Figure **7.11d**) uniformity, respectively. The Avicel powder had higher uniformity vs. BPM at both filling rates.

For both rectangular and circular dies, the accumulation area or high stress zone was mostly located in the forward region. The uniformity analysis of a rectangular and a circular die for Avicel and BPM at 26 and 132 g/min filling rates are summarized in Table **7.6.**

Table **7.6**: Uniformity analysis for rectangular and circular die 26 and 132 g/min filling rates using rotational rainy fill

Filling method	Die	Test materials	Filling rates, g/min	% Uniformity
Rotational rainy fill	Rectangular	Avicel	26	84
			132	79
		BPM	26	76
			132	69
	Circular	Avicel	26	85
			132	81
		BPM	26	79
			132	69

The results showed that: (1) filling rates did not influence the pressure distribution uniformity for both rectangular and circular dies; (2) BPM generated a lower uniformity compared to Avicel powder; (3) the ratio of particle size to the die depth highly influenced the pressure uniformity inside the die; (4) the die's shape highly influenced the pressure distribution uniformity; and (5) the leveling procedure increased non-uniformity pressure distribution within the die.

7.6 Conclusions

The filling characteristics of Avicel and BPM at 26 and 132 g/min deposition rates for a circular and a rectangular die were evaluated and analyzed. An innovative rotational rainy fill with a rotational speed of 8.5 rpm was used to fill the powder into the dies. The following concluding remarks can be made based on this study:

1) The ratio of particle size to the die depth markedly influenced the uniformity of pressure distribution inside the die.
2) Die geometry highly influenced the uniformity of pressure distribution.
3) The accumulation areas were generally observed in the forward and back regions.
4) The leveling procedures (removing surcharge powder) generally increased the non-uniformity inside the die.
5) The circular die generated higher uniformity than the rectangular die.
6) Filling rates did not substantially influence the uniformity of pressure distribution.
7) A rotational speed of 8.5 rpm, generated the lowest COV for both Avicel and BPM.

8) The front-back region generated a higher symmetry index values than a forward-leeward region.

7.7 References

1- Dhanoa, P. S. and V. M. Puri, 1998. Deposition of particulate materials confined spaces-new tester development and experimental results. *KONA (Powder and Particle) 16:152-159.*
2- Mittal, B., V. M. Puri, and W. Shaffer 2001. Analysis of feed shoe powder deposition method using a real-time cumulative mass deposition tester. *KONA (Powder and Particle) 19: 144-154*.
3- Roudsari, S. Saed, and V. M. Puri. 2005. Uniformity evaluation of different filling method for deposition of powders on containers. ASABE Technical. Portland, OR. Paper # 064005.

Chapter 8

Uniformity Discrimination Analysis - Powder Deposition Characteristics in Circular and Rectangular Shallow Dies Using Point Feed Filling Method

8.1 Abstract

The production of powder based compacts, and tablets are carried out by many industries. Deposition of uniform pressure distribution into a die is a critical step to avoid many tablet and compact quality issues. The aim of this research was to determine the charcteristics of powder deposited into a shallow die using a point feed (funnel) filling method. In this research the deposition of two powders, namely, microcrystalline cellulose (Avicel PH102) and a battery powder mixture (BPM) were studied using a rectangular and a circular shallow die with dimensions of $32 \times 30 \times 6.5$ mm and 35 mm in diameter$\times 6.5$ mm deep, respectively. Two different deposition rates of 26 and 132 g/min were used to fill the dies. Symmetry analysis, variance metrics, and uniformity analysis were implemented to quantify the deposition characteristics. The results showed that: 1) filling rates of 26 and 132 g/min did not influence the uniformity distribution inside the die; 2) the circular die generated a higher uniformity compared to rectangular die (average uniformity percentage in a circular and rectangular die were 70% and 64%, respectively); and 3) the leveling process (from leeward to forward) markedly increased the non-uniformity inside the die.

8.2 Introduction

Particulate technology is a science that impacts a large number of industries including advanced materials, agricultural, ceramics, chemicals, foods, minerals, and pharmaceuticals. One of the prominent research areas amongst particulate technology is that of powder mechanics. The processing and handling of powders play a major role in the production of materials and constitute a large volume of high value industry. Almost all processing of operations in a powder industry (namely, synthesis, characterization, and handling) require a precise knowledge of the behavior of powder systems in order to achieve the desired process control. Some of the typical industrial processes that involve powders are storage, flow, deposition/filling, mixing, and compaction. Of these processes, powder deposition is a very important unit operation in industries. The aim of powder deposition is to generate uniform bulk density and pressure distribution inside the die or containers. During the filling process, inhomogeneity can be created, due to non-uniform bulk density and pressure distributions at different locations. These inhomogeneities may cause many product quality problems such as capping, low strength, shrinkage, lamination, and distortion. Density and stress gradients in the compacted parts may also lead to non-uniform shrinkage (Reed, 1995), and they may also influence non-uniformity in other properties of the product that affect normal function and performance, such as magnetic and chemical properties. Ensuring uniform pre-compaction particle deposition in dies

is a first step to avoid these quality problems and enhance the economics of tablet, pellet, and compact formulation.

8.3 Objectives

The objective of this research was to study the powder deposition characteristics in a rectangular die and a circular shallow die using a point feed fill device.

8.4 Methodology

This section discusses the design of the point feed fill device and the methods utilized to use this device to study the pressure change and pressure distribution at the bottom of a rectangular die and a circular shallow dies during the powder filling process.

8.4.1 Point feed device

A PVC funnel with 80 mm distance from a 4.2 mm diameter outlet was used in this study. Based on the height of the powders' mound (conical heap), which was generated during the filling process, the filling height (distance from funnel outlet to die bottom) was determined to be 21.5 mm. This is the closest filling height which can be used to fill the die. A schematic and photograph of the 3D AutoCAD drawing of the point fill device used in this study are given in Figure **8.1**.

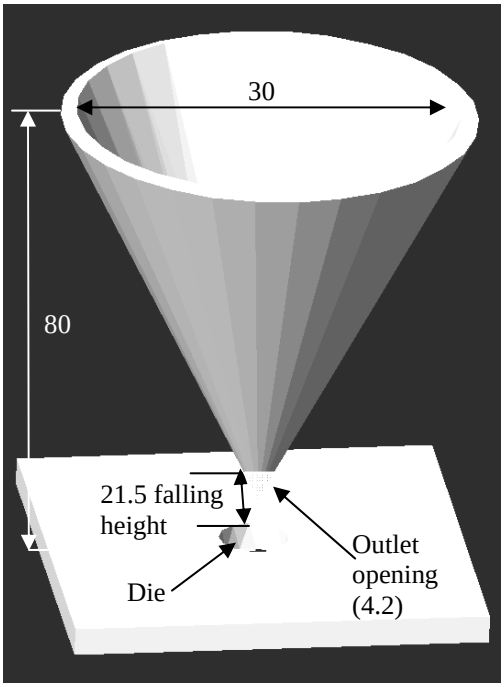

(a)

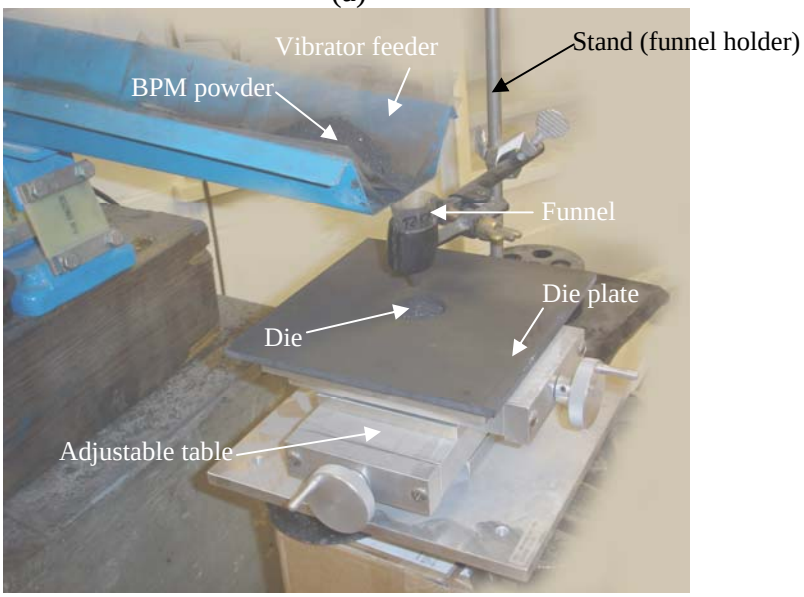

(b)

Figure **8.1**: (a) Overall AutoCAD rendition of the point feed fill device (all dimensions are in mm), (b) photograph of point feed set-up.

Two types of shallow dies were used, a rectangular and a circular die with dimensions of $32 \times 30 \times 6.5$ mm deep, and 35 (diameter) $\times 6.5$ mm deep, respectively. In order to fill the dies, two different filling rates were used, 26 and 132 g/min. For a rectangular die, the pressure sensor strip was located at six different locations, 2.5, 7.5, 12.5, 17.5, 22.5 and 27.5 mm (Figure **8.2a**). For a circular die, the pressure sensor strip was positioned at eight different angles, 22.5 degrees apart, which covered the entire die, i.e., 0^0-180^0, 22.5^0-202.5^0, 45^0-225^0, 67.5^0-247.5^0, 90^0-270^0, 112.5^0-292.5^0, 135^0-315^0, and 157.5^0-337.5^0 (Figure **8.2b**). Each test combination was repeated six times for reasons discussed in earlier chapters. Table **8.1** summarizes the experimental design for this study.

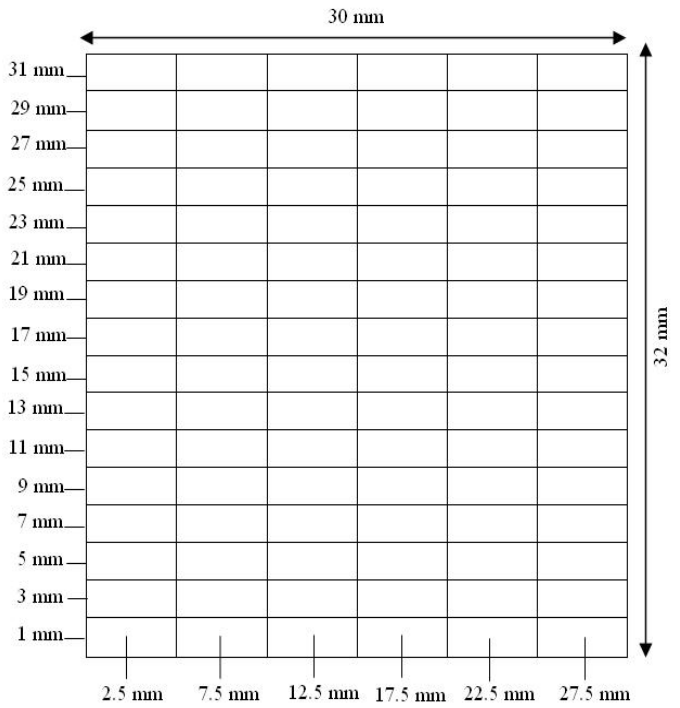

(a)

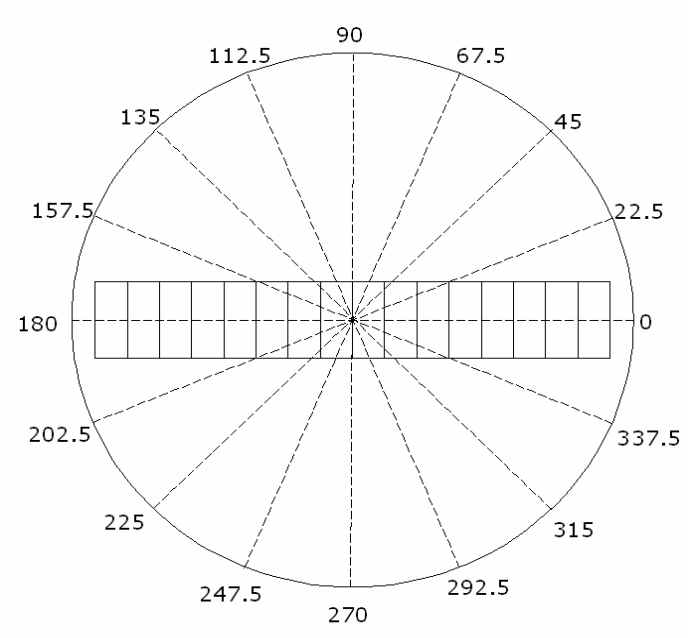

(b)

Figure **8.2**: Orientations of pressure sensor strip, (a) rectangular die, (b) circular die

Table **8.1**: Experimental design of point feed filling method

Filling method	Test characteristics	Details
Point feed	Filling rate (g/min)	26
		132
	Die shape	Circular
		Rectangular
	Die depth (mm)	6.5
	Number of replications	6

8.5 Results and discussion

In this section, the results obtained for point feed fill method are discussed and analyzed. Qualitative and quantitative analyses of the final pressure distribution for Avicel and BPM were accomplished through symmetry, variance metrics, and uniformity analyses. Symmetry analysis was used to evaluate the uniformity of pressure distribution in the front vs. back and the forward vs. leeward regions with respect to centerline of the die using contour plot. The terminology front-back, and forward-leeward regions are being used so that the comparison of different filling methods can be done. The symmetry index is defined as a ratio between 0 (least symmetrical distribution) and 100 (i.e., most symmetrical pressure distribution).

Variance metrics demonstrate the statistical parameters which are obtained for the rectangular and circular dies at 26 and 132 g/min filling rates using the final pressure values. The Max, Min, Mean, Max/Min, (Max-Min)/Mean, StDev (standard deviation), and COV (coefficient of variation) were used as the statistical parameters. In order to compare the results of Avicel with BPM, each pressure value was divided by the particle

density multiplied by gravity ($\frac{p}{\rho.g}$). This can be interpreted as an equivalent height (h), in this study, the particle density (ρ) of Avicel and BPM used were 1.53 and 4.7 g/cc, respectively, and gravity constant was 9.8 m/s^2. The scale of scrutiny was +/- 20 dm based on average COV of 20%; where, dm is decimeter (1 dm=0.1m).

8.5.1 Analysis of filling process

The BPM powder with a filling rate of 26 g/min was used to demonstrate the filling process at different times. The average filling time for the point feed method is approximately 64 seconds, which is divided into nine time sequences. The contour plots of filling process for a rectangular and a circular die and the specific times are listed by the letter T and subscripts and are shown below and in Figures **8.3** and **8.4**, respectively.

T_1: prior to starting the filling process with the die was divided into regions: front, back, forward, and leeward regions.

T_2: fourteen percent of completion of filling process (8 s). The filling process started from center of the die.

T_3: twenty-eight percent completion of filling process (16 s). The areas of filling process containes to expand.

T_4: forty-two percent of completion of filling process (24 s).

T_5: fifty-seven percent of filling completion of process (32 s). The highest pressure was observed at center of the die.

T_6: seventy-one percent completion of filling process (40 s). The particles almost reached the die's wall.

T_7: eighty-five percent completion of filling process (48 s). The accumulation increased at the center of the die.

T_8: one hundred percent completion of die filling (56 s). The die was fully filled. The particles mostly accumulated at center of the die.

T_9: leveling process (64 s). The surcharge powder was removed from the die. The accumulation was mostly located in forward region of the die. The reason for this might be due to the leveling process, which dragged the particles toward forward region and generated areas of high accumulation.

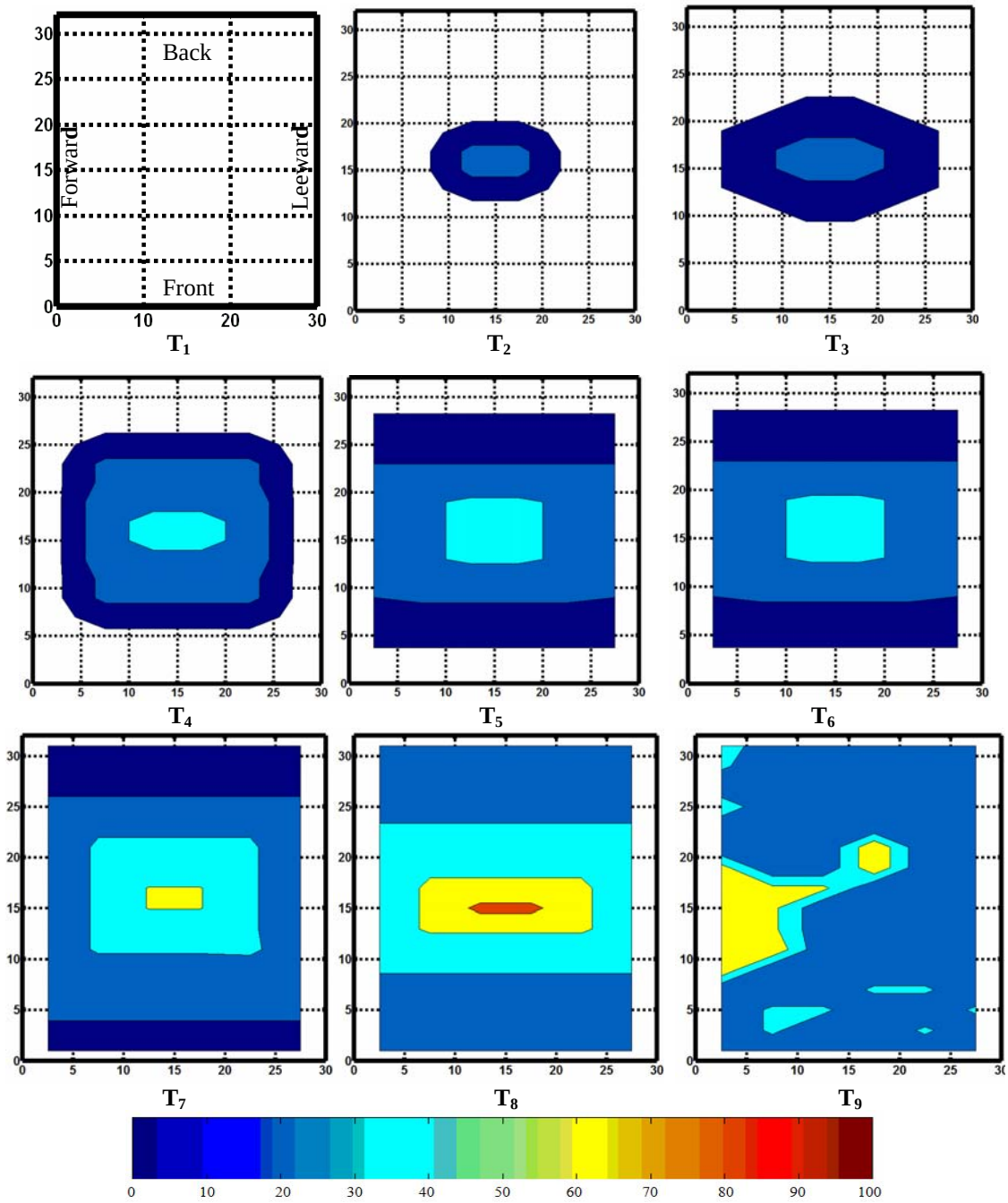

Figure **8.3**: Filling sequences in a rectangular shallow die for BPM powder at a 26 g/min filling rate using a point feed fill at time T1=0 s, T2=8 s, T3=16 s, T4= 24 s, T5=32 s, T6=40 s, T7=48 s, T8=56 s, and T9=64 s (contour plots are in equivalent height for pressure values in dm, i.e., scale in dm).

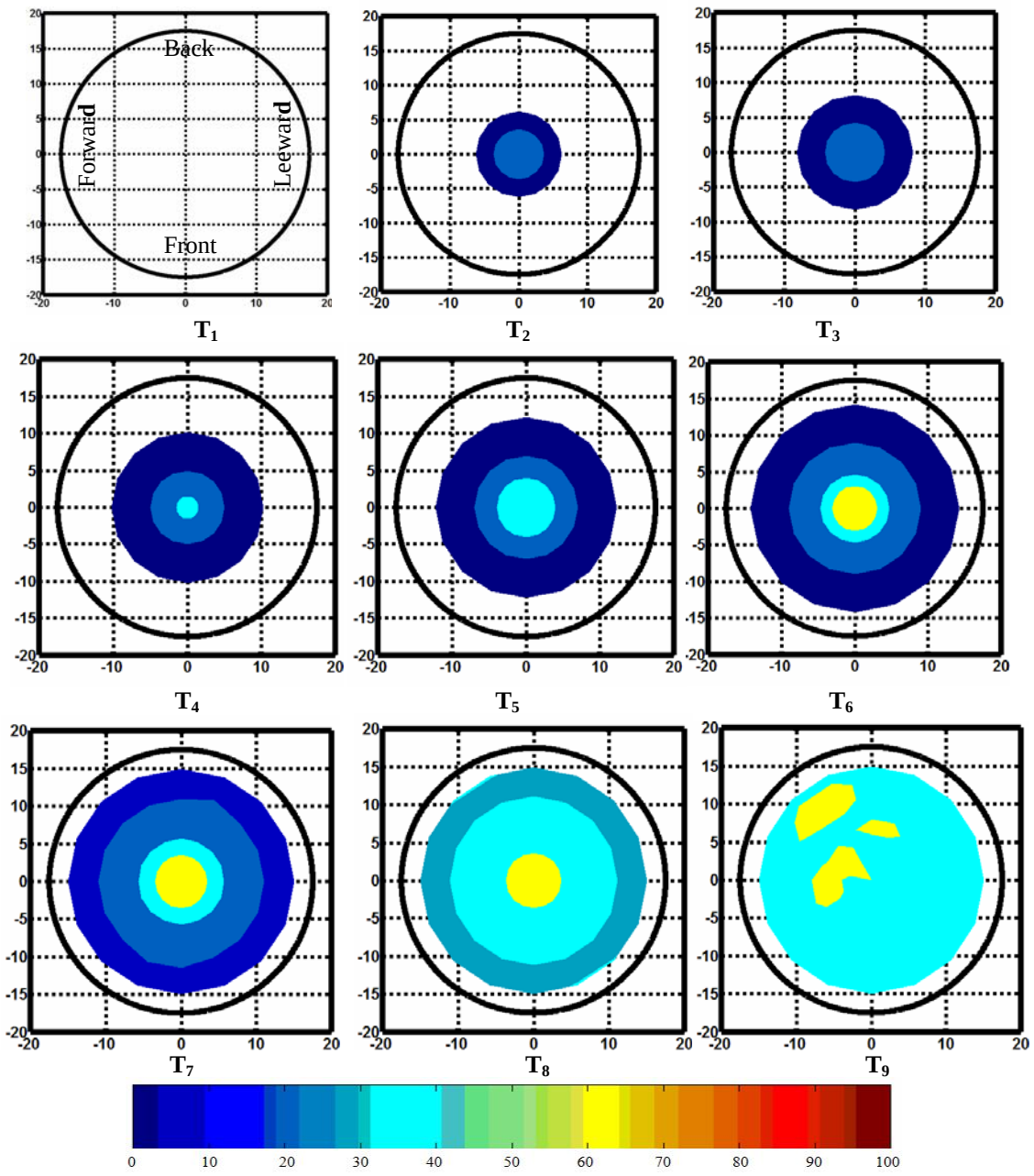

Figure **8.4**: Filling sequences in a circular shallow die for BPM powder at a 26 g/min filling rate using point feed fill at time T1=0 s, T2=8 s, T3=16 s, T4= 24 s, T5=32 s, T6=40 s, T7=48 s, T8=56 s, and T9=64 s (contour plots are in equivalent height for pressure values in dm, i.e., scale in dm).

The following observations can be made from filling analysis: (1) for both rectangular and circular dies, the pressure increase profile expanded from the center toward the die walls; (2) the center of the dies generated the highest pressure during the filling process; (3) the leveling procedures markedly changed the pressure distribution inside the die (from T8 to T9 in Figures **8.3** and **8.4**); and (4) more accumulation was observed in the forward region for reasons already discussed.

8.5.2 Symmetry analysis

Point feed for rectangular die: Figure **8.5** shows the contour plots of the rectangular shallow die at 26 and 132 g/min filling rates. For symmetry analysis each contour plot was divided into the forward-leeward and the front-back regions. The uniformity of same color distributions in the front vs. back and the forward vs. leeward regions were evaluated.

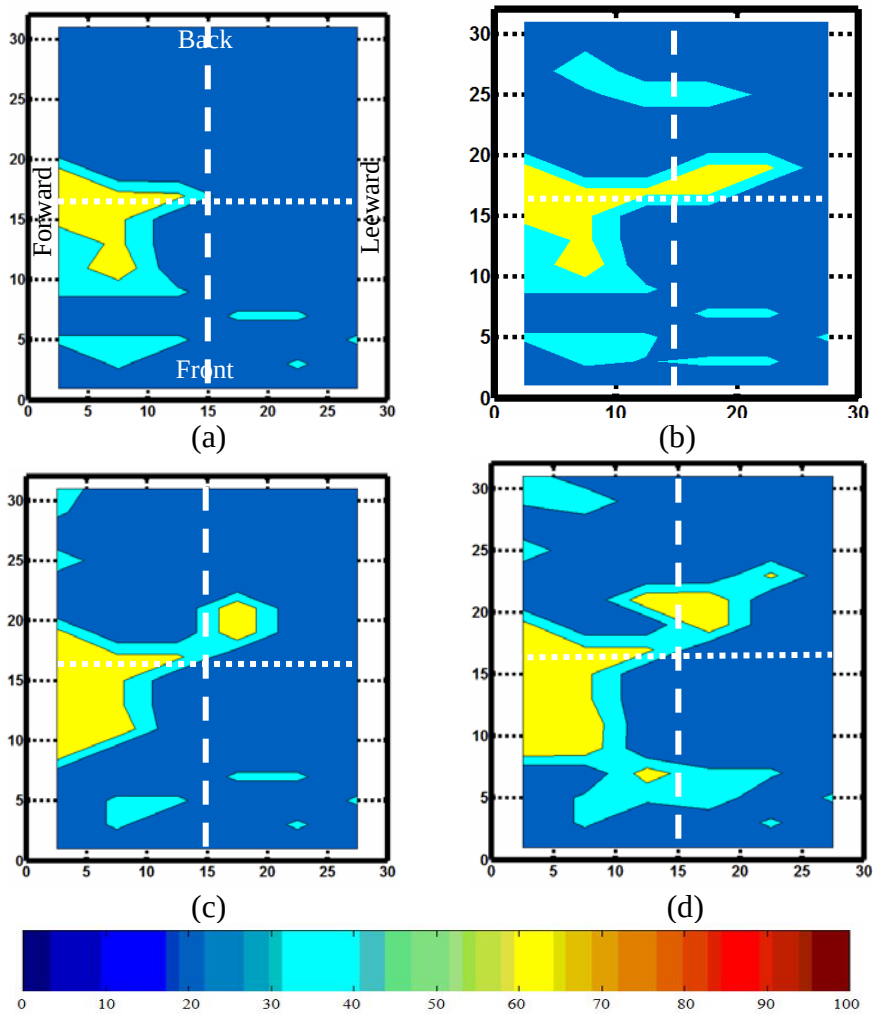

Figure **8.5**: Contour plots of the final pressure distribution in a rectangular die as an equivalent height in dm with Avicel (a) 26 g/min (b) 132 g/min, and BPM (c) 26 g/min, and (d) 132 g/min (scale in dm).

Front and back analysis: For Avicel powder, the front and back regions at a filling rate of 26 g/min, had 88% and 96% uniformity (Figure **8.6a**), respectively, while at 132 g/min had 65% and 89% (Figure **8.6b**), uniformity, respectively. The symmetry index values for the front-back at 26 and 132 g/min were 91% and 73%, respectively. BPM powder in front and back regions at a filling rate of 26 g/min, regions had 82% and

91% uniformity (Figure **8.6c**), respectively, while at 132 g/min had 57% and 77%, uniformity (Figure **8.6d**), respectively. The symmetry index values for the front-back at 26 and 132 g/min for BPM powder were 90% and 74%, respectively.

Forward and leeward analysis: For Avicel powder, the forward and leeward regions at a filling rate of 26 g/min had uniformity of 68% and 98% (Figure **8.6a**), respectively, while at 132 g/min the forward and leeward regions had 58% and 88% uniformity (Figure **8.6b**), respectively. The symmetry index values for the forward-leeward regions at a filling rate of 26 and 132 g/min were 69% and 34%, respectively. For BPM, in the forward and leeward regions at 26 g/min, the uniformity values were 66% and 91% (Figure **8.6c**), respectively, while at 132 g/min the values were 46% and 77% uniformity (Figure **8.6d**), respectively. The symmetry index values for forward-leeward region at 26 and 132 g/min were 72% and 59%, respectively (Table **8.2**).

Table **8.2**: Symmetry analysis values for a rectangular die for Avicel and BPM at 26 and 132 g/min filling rates

Filling method and die	Test materials	Filling rate (g/min)	Locations	% Uniformity	Symmetry index %
Point feed-Rectangular die	Avicel	26	Front	88	91
			Back	96	
			Leeward	98	69
			Forward	68	
		132	Front	65	73
			Back	89	
			Leeward	58	34
			Forward	88	
	BPM	26	Front	82	90
			Back	91	
			Leeward	91	72
			Forward	66	
		132	Front	57	74
			Back	77	
			Leeward	77	59
			Forward	46	

The results showed that: (1) the back and leeward regions generated more uniformity than the front and forward regions; (2) the symmetry index values for front-back region was higher than the leeward-forward region; (3) Avicel at 26 g/min in the leeward region generated the highest uniformity (98%); (4) BPM at 132 g/min filling rate in the forward region generated the lowest uniformity (46%); (5) the symmetry index values decreased with increasing filling rates.

Point feed for circular die: The contour plots of a circular shallow die for Avicel and BPM for 26 and 132 g/min filling rates are shown in Figure **8.6**. The contour plots were analyzed in front-back and forward-leeward regions and are summarized in the following sections.

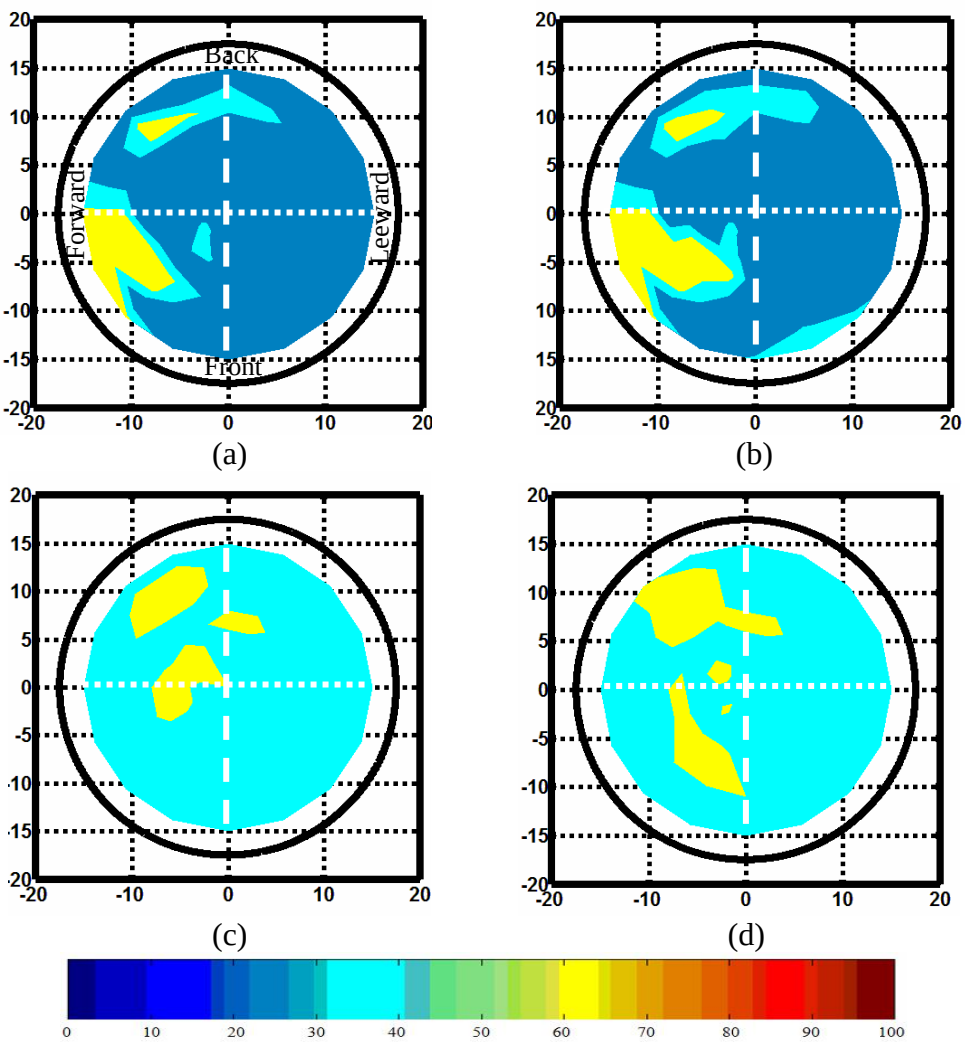

Figure **8.6**: Contour plots of the final pressure distribution in a circular die as equivalent height in dm with Avicel (a) 26 g/min (b) 132 g/min, and BPM (c) 26 g/min, and (d) 132 g/min (scale in dm).

Front and back analysis: Avicel at a filling rate of 26 g/min in the front and back regions had 77% and 86% uniformity (Figure **8.7a**), while at 132 g/min the front and back regions had 57% and 78% uniformity (Figure **8.7b**), respectively. The symmetry index values at 26 and 132 g/min were 89% and 73%, respectively. For BPM powder at a 26 g/min filling rate, the uniformity values were 96% and 82% (Figure **8.7c**), while at

132 g/min the values were 74% and 68% (Figure **8.7d**), for the front and back regions, respectively. The symmetry index values for BPM in the front and back regions at 26 and 132 g/min were 85% and 91%, respectively.

Forward and leeward analysis: The results showed that Avicel in the forward and leeward regions at filling rate of 26 g/min had 63% and 96% uniformity (Figure **8.7a**), respectively, while at 132 g/min had 44% and 91% uniformity (Figure **8.7b**), respectively. The symmetry index values for forward-leeward region at 26 and 132 g/min were 65% and 48%, respectively. For BPM at 26 g/min filling rate, the forward and leeward regions showed 74% and 97% uniformity (Figure **8.7c**), respectively, while at 132 g/min had 41% and 95% uniformity (Figure **8.7d**), respectively. The symmetry index values for the 26 and 132 g/min filling rates in the forward-leeward region were 76% and 43%, respectively (Table **8.3)**.

Table **8.3**: The results for symmetry analysis for a circular die for Avicel and BPM at 26 and 132 g/min filling rates

Filling method and die	Test materials	Filling rate (g/min)	Locations	% Uniformity	Symmetry index %
Point feed-Circular die	Avicel	26	Front	77	89
			Back	86	
			Leeward	96	65
			Forward	63	
		132	Front	57	73
			Back	78	
			Leeward	91	48
			Forward	44	
	BPM	26	Front	96	85
			Back	82	
			Leeward	97	76
			Forward	74	
		132	Front	74	91
			Back	68	
			Leeward	95	43
			Forward	41	

The results showed that: (1) the front-back regions had higher symmetry index values vs. the forward-leeward region; (2) BPM at 26 g/min filling rate, for the leeward region, generated the highest uniformity (97%); (3) the lowest symmetry index value of 43% was observed was in the leeward-forward region for BPM at 132 g/min filling rate; (4) symmetry index values decreased with increase in filling rates.

8.5.3 Variance metrics analysis

The statistical parameters, i.e., Max, Min, Mean, Max/Min, (Max-Min)/Mean, standard deviation (StDev), and coefficient of variation (COV) were used as variance metrics in this study. The statistical parameters for a rectangular and a circular die for Avicel and BPM powders for point feed filling are summarized in Table **8.4**.

Table **8.4**: Variance metrics parameters for Avicel and BPM at 26 and 132 g/min filling rates for the rectangular and circular dies using the point feed filling method

Filling method	Die	Test material	Filling rate g/min	Max (dm)	Min (dm)	Mean (dm)	Max /Min	(Max-Min)/ Mean	Standard Deviation	COV %
Point feed	Rec.	Avicel	26	1.11	0.19	0.36	5.84	2.5	0.06	16
			132	1.27	0.33	0.33	3.84	2.84	0.06	17
		BPM	26	1.10	0.18	0.36	6.11	2.56	0.06	18
			132	1.18	0.33	0.42	2.80	2.02	0.08	19
	Cir.	Avicel	26	1.10	0.20	0.34	5.50	2.64	0.05	15
			132	1.36	0.24	0.44	5.67	2.54	0.07	17
		BPM	26	1.66	0.66	0.35	2.51	2.85	0.04	13
			132	1.43	0.36	0.53	3.40	2.01	0.09	17

The results showed that: 1) BPM for a circular die at 26 g/min generated the lowest Max/Min, standard deviation, and COV, which implied the highest uniformity distribution; 2) a circular die generated a lower (Max-Min)/Mean than a rectangular die.

8.5.4 Uniformity analysis

Point feed for a rectangular die: The same color distribution was measured using AutoCAD (Autodesk Inc. San Rafael, CA, USA). For this analysis, the entire area of a rectangular and a circular die were measured.

The results showed that Avicel at a filling rate of 26 and 132 g/min had 71% (Figure **8.6a**) and 64% (Figure **8.6b**), uniformity, respectively, while BPM at 26 and 132 g/min had 69% (Figure **8.6c**) and 54% (Figure **8.6d**) uniformity, respectively. The accumulations were mostly located in the forward region of the die, due to the method of removing surcharge powder from die (from leeward to forward region). Avicel powder generated a higher uniformity compared to BPM. The reason is probably due to ratio of particle size to the die depth, for BPM the ratio is larger (0.1) than Avicel (0.01). This caused an increase in shear stress and resulted in non-uniformity during the leveling process.

Point feed using a circular die: The results showed that Avicel at filling rates of 26 and 132 g/min had 71% (Figure **8.7a**) and 65% (Figure **8.7b**) uniformity, while BPM at the same filling rates had 78% (Figure **8.7c**) and 69% (Figure **8.7d**) uniformity, respectively. As already discussed, Avicel had higher uniformity compared to BPM at both filling rates. The accumulation or high stress zones were mostly located in the forward region due to the path of removed of the surcharge powders. Table **8.5** summarizes the uniformity analysis for a rectangular die and a circular dies for Avicel and BPM for point feed filling method.

Table **8.5**: Uniformity analysis for a rectangular and a circular dies 26 and 132 g/min filling rates using point feed filling method

Filling method	Die	Test materials	Filling rate, g/min	% Uniformity
Point feed	Rectangular	Avicel	26	71
			132	64
		BPM	26	69
			132	54
	Circular	Avicel	26	71
			132	65
		BPM	26	78
			132	69

8.6 Conclusions

The point feed filling device was fabricated to evaluate the deposition characteristics of Avicel and BPM for the rectangular and circular dies. For the point feed method, two different deposition rates were used, 26 and 132 g/min. The following conclusions were determined based on the experimented data analysis:

1) The circular die generated higher uniformity than a rectangular die.
2) The leeward and front regions generated higher uniformity compared to the forward and back regions.
3) The ratio of particle size to the die depth highly influenced the uniformity distribution inside the die, i.e., uniformity of Avicel compared with BPM.
4) The center of the die generated the highest pressure during the filling process.
5) The die's corners and vicinity highly increased the stress inside the die.
6) The leveling process (from leeward to forward region) dramatically increased the non-uniformity inside the die, due to increase in the shear stress.

7) The front-back generated higher symmetry index values than the leeward-forward region for both dies.

8) The symmetry index values decreased with increasing filling rates for both die shapes.

9) The circular die generated a lower Max/Min, (Max-Min)/Mean, Standard deviation, and COV which implied a higher uniform filling compared to the rectangular die.

10) The point feed is a suitable device to use for deposition process.

8.7 References

1- Reed, J. S. 1995. *Principles of Ceramic Processing*. New York: John Wiley & Sons, Inc.

Chapter 9

Powder Deposition Characteristics in Circular Shallow Die Using Pneumatic Filling Method- Uniformity Comparison among Different Filling Methods

9.1 Pneumatic filling method

One of the most popular methods of moving particulate solids in the agricultural, construction, food, and chemical industries is by pneumatic conveying. Pneumatic conveying refers to the moving of bulk solids suspended in or forced by a gas stream through horizontal and/or vertical pipes (Pecora and Goldstein 1993). Pneumatic conveying can be used for particles ranging from fine powders to pellets with bulk densities ranging between 16 to 3200 kg/m^3. In this research, a pneumatic fill device was designed and fabricated to fill a circular die to investigate the filling characteristics. This device was limited to using only the BPM powder (coarse particle), since the Avicel powder (being much finer), generated substantial quantities of airborne dust during the test. A 200 mm long rectangular cross-section tube ($40 \times 20 \times 200$ mm), along with a circular air inlet (10 mm diameter) in front and a wide open outlet was used. In order to speed up the filling process, the rectangular tube was inclined at about 9^0 with respect to the horizontal surface. There was an aperture (2×4 cm) at center of the tube that discharged the particles into the die; the die was placed at the base of the aperture. The BPM powder was placed manually inside the tube at mid-way location between the air-inlet and aperture center. By trial-and-error, the optimal inlet gas pressure was

determined to be 69 kPa (10 psi) which generated a 26 g/min deposition rate inside the die. Friction of the gas inside the tube, friction between the solids and the inside of the tube, and particle velocity, were not considered in this design. A schematic of the pneumatic fill device and position of the circular die are shown in Figure **9.1**.

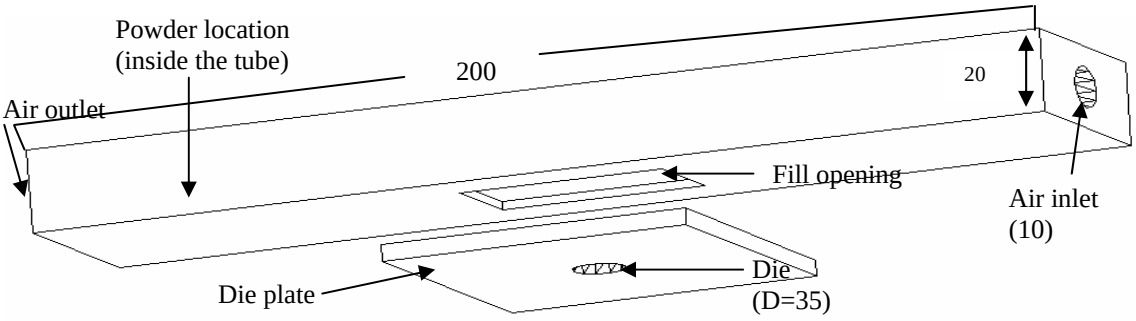

(a)

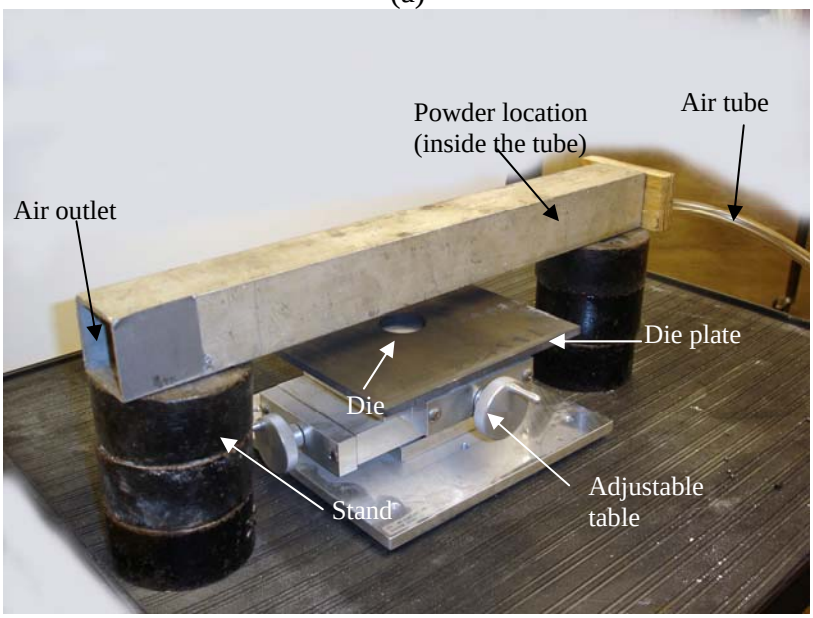

(b)

Figure **9.1**: (a) Schematic of the pneumatic fill device with a circular die (all dimensions in mm), (b) Photograph of pneumatic fill device.

9.1.1 Symmetry analysis

The pneumatic filling system was utilized to fill a circular die using BPM powder. Qualitative and quantitative evaluations were done using symmetry, variance metrics, and uniformity analyses. Figure **9.2** shows the contour plots for BPM powder for a circular shallow die.

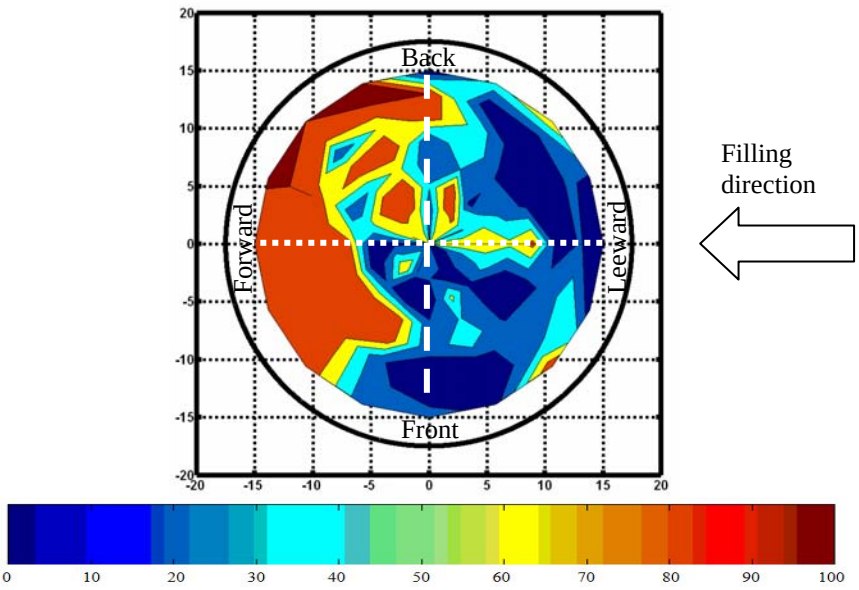

Figure **9.2**: Contour plots of the final pressure distribution in a circular die as an equivalent height for pneumatic filling. The scale of scrutiny for analysis is +/-20 dm (scale in dm)

The results showed that the front and back regions had 27% and 9% uniformity, while the forward and leeward regions had 44% and 11% uniformity, respectively. The symmetry index values for the front-back and the forward-leeward regions were 33% and 25%, respectively. The forward region generated high stress zones during the filling process. This was most likely caused by the particles entering the die with high kinetic energy during the filling process, which resulted in the particles accumulating in the

forward region of the die (i.e., this coincided with the pneumatic conveying direction of BPM). Table **9.1** summarizes the symmetry analysis results for the pneumatic filling method.

Table **9.1**: The results for symmetry analysis for a circular die for BPM at a 26 g/min filling rate using the pneumatic filling device

Filling method and die	Test materials	Deposition rate (g/min)	Locations	% Uniformity	Symmetry index %
Pneumatic-Circular die	BPM	26	Front	27	33
			Back	9	
			Leeward	44	25
			Forward	11	

9.1.2 Variance metrics analysis

The statistical parameters (Table **9.2)**, i.e., Max, Min, Mean, Max/Min, (Max-Min)/Mean, Standard deviation (StDev), and Coefficient of variation (COV) were used as variance metrics in this study.

Table **9.2**: Variance metrics parameters for BPM at a 26 g/min filling rate for the circular dies using the pneumatic filling method.

Filling method	Die	Test Material	Filling rate g/min	Max (dm)	Min (dm)	Mean (dm)	Max/Min	(Max-Min)/Mean	Standard Deviation	COV%
Pneumatic	Cir.	BPM	26	5.26	0.61	0.75	8.7	3.14	0.24	33

The results showed that: 1) the pneumatic filling method generated low uniformity (COV=33%) within the die; 2) the Max/Min, (Max-Min)/Mean values were very high (3.14) which implied low uniformity; and 3) the pneumatic filling method was deemed not to be an appropriate method to fill the die because of the low uniformity seen in the die.

9.1.3 Conclusions

The results showed that 807.78 mm^2 out of total area of 3846.5 mm^2 or 21% had the same color distribution, which represents a 21% uniformity inside the die. Pneumatic filling generated high stress zones inside the die, which caused low uniformity of the die. The following concluding remarks can be made based on this study:

1) The pneumatic filling method generated very low uniformity in a circular die (21%).
2) The pneumatic filling method had a high Max/Min, (Max-Min)/Mean, Standard deviation, and COV, which implied a low uniformity inside the die.
3) The pneumatic method generated low symmetry index values.
4) The leveling process (removal of the surcharge powder), which was from the leeward to forward regions, dramatically increased the non-uniformity inside the die resulting in asymmetrical increase in stress distribution.

9.2 Assessment

On the basis of this study, the feed shoe, rainy fill, and point feed filling methods were appreciate for filling shallow rectangular and circular dies. The filling period for the feed shoe was notably shorter than rotational rainy and point feed, i.e., the average filling time for low flow rate of 26 g/min for feed shoe, rotational rainy and point feed were 8 s, 70 s, and 120 s, respectively. The feed shoe also can be used for much higher filling speeds such as filling the die in about 3 s, 1 s, or less.

Depending on the specific requirements and economic consideration, an appropriate filling device may be chosen. Some guidelines for selection among the feed shoe, the rotational rainy fill, and the point feed are provided below.

Feed shoe (PDT-II)

Advantages:

1) The test is easy to perform and system simple to operate.
2) The device is fully automated.
3) The PDT-II has the capability to fill a single die or multiple dies.
4) The device is capable of filling the die at very high speed.
5) The average uniformity of pressure distribution was determined to be 55%.

Disadvantages:

1) No direct observation of the filling process.
2) The interactions with and influence of tube's wall on uniformity of pressure distribution is relatively high.
3) Filling profiles are too complex for mathematical analysis considerations.

When to use:

1) When time is a critical factor.
2) When multiple dies must be filled at the same time.
3) When the high uniformity of pressure distribution is not a determining factor.

Rotational rainy:

Advantages:

1) The average uniformity of pressure distribution was 77%.
2) Direct observation of the filling profile during the test is feasible.

3) A highly symmetrical pressure distribution inside the die can be generated.

Disadvantages:

1) Manual operation of the removal of surcharge powder (i.e., with time and resources this can be automated).
2) Long filling duration (70 s).
3) Time consuming to clean the device after each test.
4) RPM evaluation is necessary for different powders.

When to use:

1) When uniformity of pressure distribution is a critical factor.
2) When time is not a limiting factor.

Point Feed:

Advantages:

1) The average uniformity of pressure distribution was 64%.
2) The test is easy to perform.
3) Direct observation of the filling during the test is feasible

Disadvantages:

1) Manual operation of the removal of surcharge powder (i.e., with time and resources this can be automated).
2) Very high filling duration (120 s).

When to use:

1) When time is not a limiting factors.
2) When large granule sizes (>250 μm) are used to fill the die.

Finally, based upon the tests conducted during this study and the analysis carried out:

1) The rotational rainy fill appears to be the more appropriate method to generate the highest uniformity pressure distribution inside the die.
2) The point feed filling method appears to be the second best filling method in this study.
3) The feed shoe filling (PDT-II) with the lower uniformity was fully automated and determined to be the fastest filling method in this study.
4) The pneumatic filling is not a recommended method to fill shallow dies.

The significance of this study was to make a comparative assessment of the four filling methods and to help provide some rational basis for filling device selection. The results of this study, therefore, should have a significant impact on numerous applications involving production of tablets, compacts, and briquettes. A major application of uniformity of measurement is to understand the influence of filling characteristics on uniformity of pressure distribution inside the die. It is not possible to generate high quality tablet or compact without having an understanding of powders' deposition characteristics.

9.3 Uniformity comparison among different filling methods

The pressure distribution analysis for a rectangular and a circular die filled with a battery powder mixture (BPM) and the Avicel powder were accomplished. Four deposition methods: feed shoe, rotational rainy, point feed, and pneumatic were tested.

For the feed shoe filling method, a PDT-II with either a circular or a square cross-section tube moving at 20 or 100 mm/s speeds was used. For the rotational rainy fill and point feed methods, filling rates of 26 and 132 g/min, which corresponded to 20 and 100 mm/s feed shoe speeds, respectively, were tested. The quantitative and qualitative evaluations were conducted using symmetry, variance metric, and uniformity analyses. Based on this study, the following concluding remarks can be made:

1) A circular die generated a higher uniformity pressure distribution inside the die than a rectangular die.
2) The rainy fill method with either the rectangular or circular die generated the highest uniformity among all the different filling methods tested (average of 77% and 78.5% uniformity for the circular and rectangular dies, respectively).
3) The point feed and feed shoe methods resulted in intermediate uniformity values, 64% and 55%, respectively.
4) The feed shoe cross-section shape did not influence the uniformity of pressure distribution (the average uniformity for circular and square feed shoe were 56.0% and 55.8%, respectively).
5) The filling process using the feed shoe method was faster than rotational rainy and point feed methods. The average filling period for feed shoe, rotational rainy, and point feed were 8 s, 70 s, and 120 s, respectively.
6) The filling rate did not influence uniformity of pressure distribution when using rainy and point feed methods. i.e., no major differences in uniformity between 26 and 132 g/min filling rates were measured.

7) The feed shoe speed highly influenced the uniformity of pressure distribution (uniformity increased with increasing feed shoe speed).
8) The rectangular die generated higher stress zones than the circular die due to the prescence of corners.
9) BPM generated higher stresses inside the die (97 dm) than Avicel (60 dm) due to the larger particle density.
10) The leveling process highly influenced the uniformity of pressure distribution; the pressure distribution uniformity decreased by 20% after the leveling process.
11) The pneumatic filling method generated the lowest uniformity among all filling methods (21%) tested.
12) Using the feed shoe filling method, BPM generated a higher uniformity than Avicel powder, while Avicel had a higher uniformity when using the rotational rainy or point feed.
13) For all filling methods tested, the leeward region had a higher uniformity than the forward region due to the direction of leveling process, which removed the surcharge powders from the leeward to forward region.
14) During the feed shoe filling process, the forward and back regions accumulated more particles.

9.4 References

1- Pecora Aria A. B, and Leonardo Goldstein. 1993. New particulate solids pneumatic feeding device with mass flowrate control. *Powder Technology 79: 265-268*.

Chapter 10

Mathematical Models of Powder Deposition into Shallow Dies for Three Filling Methods

10.1 Abstract

In order to further the understanding of deposition process, models were developed and verified to simulate the filling characteristics for the entire deposition process. Three different filling methods were modeled: the feed shoe, rotational rainy, and point feed. The battery powder mixture (BPM) filled into a circular shallow die at 20 mm/s feed shoe speed equivalent to 26 g/min filling rate was used. A physics based explanation of the filling process is included that provides a rational basis for the use of Chapman-Richards model. In addition, the linear fill profile for point feed is explained as a special case of the Chapman-Richards model. The powder deposition profile of each filling method was divided into various phases. The average root mean square error (RMSE) and the mean value of average relative difference (ARD) of the models were calculated. The results showed that 1) the overall rate equation for all three filling methods was: $dh/dt = \alpha h F(t) + \beta$; 2) the RMSE for feed shoe, rotational rainy, and point feed were 0.16 dm, 0.44 dm, and 0.32 dm, respectively, whereas, the ARD for feed shoe, rotational rainy, and point feed were 7%, 16%, and 11%, respectively; 3) the deposition profile (Phase I) for feed shoe and rainy fill were sigmoidal in shape, while for the point feed it was linear.

10.2 Introduction

Any industry that deals with particulate materials must have a clear understanding of particle behavior during the handling and processing operations. Generally, materials in particulate form are easier and more economical to handle than finished products. Hereafter, the terms particulate materials, powders, and bulk solids will be used interchangeably. Given the widespread use of powders, it would be impossible to improve the handling and processing techniques without a precise knowledge of how particulate materials behave under various conditions.

A mathematical model is a theoretical physics based model that is used to explain the behavior of the system. Developing a mathematical model is the ultimate goal for engineers to simulate the cause and effect in a surrogate device which is used to represent a real world system to understand the response under various conditions (inputs) (Kessler and Greenkorn, 1999).

Some engineering mathematical models are built based on purely experimental observations, which treat variables in a physically most intuitive manner. The objective is to determine simple correlations of the behavior of the dependent and independent variables. At a more fundamental level, physical, chemical, and/or biological laws, are used to form the basis for mathematical model. In this context, the parameters that are embedded in the model have well defined physical meaning. In this research, the latter approach is attempted to formulate a mathematical model for powder deposition in dies.

No continuum models and methods have been published to simulate the deposition characteristics in shallow dies. Xie (2006) developed an overall rate equation

for feed shoe filling process for cylindrical dies using a battery powder mixture (BPM). The overall rate equation was $dP_p / d\tau = \alpha P_p F(\tau) + \beta$, where P_p is prorated pressure, τ is normalized time, α and β are coefficients, and F(τ) is a stage-specific deposition rate function. Although, the model successfully described the feed shoe deposition method, no clear and complete physical interpretation of α and β, and origin of $F(\tau)$ were presented.

10.3 Objectives

The objective of this research was to develop and verify a time-dependent model for the deposition process for feed shoe, rotational rainy fill, and point feed filling methods based on process physics. As mentioned in Chapter 9, the pneumatic filling methods is not a suitable approach to deposit powder in shallow dies, therefore, it was not considered for mathematical formulation.

10.4 Mathematical formulation

The two cornerstones of the deposition model are the overall force balance and mass balance equations. Although the static force balance provides insight to the pressure evaluation during deposition, it is used as the basis for simulating the prevailing dynamic conditions. Herein, it is assumed that the equations are point-specific located at die bottom. In order to better describe and analyze the die filling process, it was divided into two stages: 1) powder deposition process into a die that is only partially filled, and 2)

powder deposition process during surcharge build up, the analysis and mathematical formulations are described in the following sections.

10.4.1 Analysis of powder within die

Force Balance in powder mass: The most widely used equation for predicting vertical and lateral pressure in dies, bins, and containers is the Janssen's equation (Manbeck and Puri, 1995). Janssen's solution assumes the bulk density of material (ρ_b),angle of internal friction (φ), and the coefficient of friction between the die wall and powders (μ) are constant throughout the particle bed. The system is assumed to have axisymmetric load distribution, thus pressure distributions vary with depth but not with location around the circumference. A schematic of the free body diagram of the cylindrical die and force balance on powder mass at depth y is shown in Figure **10.1**.

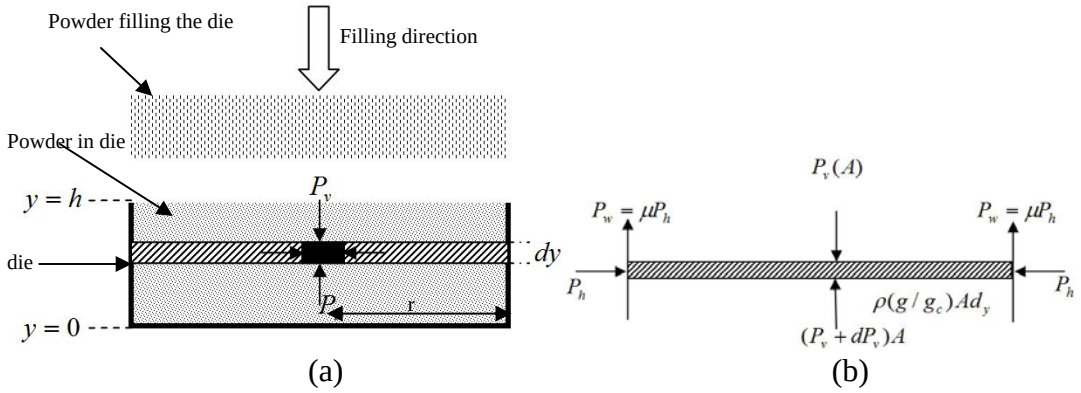

Figure **10.1**: Free body diagram of (a) cylindrical die during filling process, and (b) force balance on powder mass inside the die (Manbeck and Puri, 1995)

Summing forces acting on the differential elements in the vertical direction yields Equation 10.1 (Figure **10.1b**):

$$(P_v + dP_v)A + P_w C dy - P_v A - \rho_b g A dy = 0 \qquad \text{(Equation } \mathbf{10.1}\text{)}$$

where: A= cross-section;

C=die circumference;

P_w=vertical friction on the wall;

P_v=vertical pressure in the mass;

P_h=lateral pressure;

g= gravitational constant;

μ =coefficient of friction;

ρ_b = bulk density;

y= distance below surface of powder.

Equation 10.1 can be rewritten as:

$$P_y A + dP_v A + P_w c dy - P_y A - \rho_b A dy = 0 \qquad \text{(Equation } \mathbf{10.2}\text{)}$$

which is simplified to:

$$dP_v A + P_w c dy - \rho_b A dy = 0 \qquad \text{(Equation } \mathbf{10.3}\text{)}$$

Defining the ratio of lateral to vertical pressure within the powder mass (*k*) as:

$$k = \frac{P_h}{P_v} \qquad \text{(Equation } \mathbf{10.4}\text{)}$$

and defining the hydraulic radius (R) as:

$$R = \frac{A}{C} \qquad \text{(Equation } \mathbf{10.5}\text{)}$$

and solving Equation 10.3 yields the differential equation for the vertical pressure distribution in the powder mass (Manbeck and Puri, 1995):

$$-\frac{dP_v}{dy} = \frac{1}{A}(P_w C - \rho_b g A) \qquad \text{(Equation } \mathbf{10.6}\text{)}$$

Upon integration, this lead to:

$$P_v = \frac{\rho_b g R}{k\mu}(1 - e^{\frac{-k\mu y}{R}}),\ 0 \le y \le h \qquad \text{(Equation } \mathbf{10.7}\text{)}$$

where *h* is the die height as shown in Figure **10.1**.

Mass balance in powder mass: Beginning with this section the author has integrated the mass balance with the force balance equations to develop dynamic pressure equations during die filling. The physical principle of mass balance is given in Equation 10.8:

$$\dot{m}_2 - \dot{m}_1 + \frac{dm}{dt} = 0 \qquad \text{(Equation } \mathbf{10.8}\text{)}$$

where $\dot{m}_2$ = rate of outflow, $\dot{m}_1$ = rate of inflow, $\frac{dm}{dt}$ = accumulation rate. In the case of filling a container with no outflow, Equation 10.8 can be rewritten as:

$$\frac{dm}{dt} = \dot{m}_1, \text{ but } m_1 = \rho v = Q \text{ and } \dot{m}_1 = \dot{Q} \qquad \text{(Equation } \mathbf{10.9}\text{)}$$

Also $\rho\frac{dv}{dt} = \rho\dot{Q}$, $v=A\,.\,y$, where, v=volume, A= die cross section area, and y= fill height of powder in the die, then:

$$A\frac{dy}{dt} = \dot{Q} \qquad \text{(Equation } \mathbf{10.10}\text{)}$$

Next, Equation 10.7 can be rewritten in terms of general parameters α, and β, and for $y=h$, this reduces to:

$$P_v = \alpha(1 - e^{-\beta h}) \qquad \text{(Equation } \mathbf{10.11}\text{)}$$

where, $\alpha = \rho_b g R / \mu m$ and $\beta = k\mu / R$

Rearranging:

$$h = \ln \frac{(1 - \frac{P_v}{\alpha})}{\beta} \qquad \text{(Equation } \mathbf{10.12}\text{)}$$

Substitute equation 12 in equation 10, which leads to:

$$\frac{A}{\beta} \cdot \frac{d \ln\left(1 - \frac{P_v}{\alpha}\right)}{dt} = \dot{Q} \qquad \text{(Equation } \mathbf{10.13}\text{)}$$

$$\frac{-\frac{1}{\alpha} dP_v}{1 - \frac{P_v}{\alpha}} = \frac{\beta}{A} \dot{Q}.dt \qquad \text{(Equation } \mathbf{10.14}\text{)}$$

$$\frac{dP_v}{dt} = \left(1 - \frac{P_v}{\alpha}\right)^{\frac{-\beta\alpha}{A}\dot{Q}} \qquad \text{(Equation } \mathbf{10.15}\text{)}$$

$$\int_0^{P_v} \frac{dP_v}{1 - \frac{P_v}{\alpha}} = \int_0^t \frac{-\beta}{A\alpha} \dot{Q} dt \qquad \text{(Equation } \mathbf{10.16}\text{)}$$

$$-\alpha \ln(1 - \alpha P_v) = \frac{-\beta}{A\alpha} \dot{Q} t \qquad \text{(Equation } \mathbf{10.17}\text{)}$$

$$\ln(1 - \alpha P_v) = \frac{-\beta}{A\alpha^2} \dot{Q} t \qquad \text{(Equation } \mathbf{10.18}\text{)}$$

$$1 - \alpha P_v = e^{\frac{-\beta}{A\alpha^2}\dot{Q}t} \qquad \text{(Equation } \mathbf{10.19}\text{)}$$

$$P_v = \frac{1}{\alpha}\left(1 - e^{\frac{-\beta}{A\alpha^2}\dot{Q}t}\right) \qquad \text{(Equation } \mathbf{10.20}\text{)}$$

Substituting $K = \frac{1}{\alpha}$ and $b = \frac{\beta}{A\alpha^2}\dot{Q}$, yields:

$$P_v = K\left(1 - e^{-bt}\right) \qquad \text{(Equation } \mathbf{10.21}\text{)}$$

Rewrite pressure P_v as equivalent height $h = P_v /(\rho_p \times g)$:

$or \quad h = K(1 - e^{-bt})$ (Equation **10.22**)

where K and b are experimentally determined parameters and ρ_p is particle density.

10.4.2 Analysis of powder within surcharge mass

Equation 10.22 is a typical growth curve response; however, the most typical observed die filling pressure response was sigmoidal. For all three fill methods, there was always a powder surcharge that is a likely cause of the slowdown in pressure build-up. For the feed shoe, the pressure distribution is more complex and is believed to be caused by the cumulative effect of the feed shoe tube walls and powder head in the feed shoe tube. Since the surcharge of powders in a rainy fill provides a clearer explanation of the surcharge process physics, it is followed here. In addition, the point feed filling method's analysis is included.

As stated previously, the die was overfilled during the filling process. A simplified free body diagram of heap (mound) of the surcharge powder above the die is shown in Figure **10.2**.

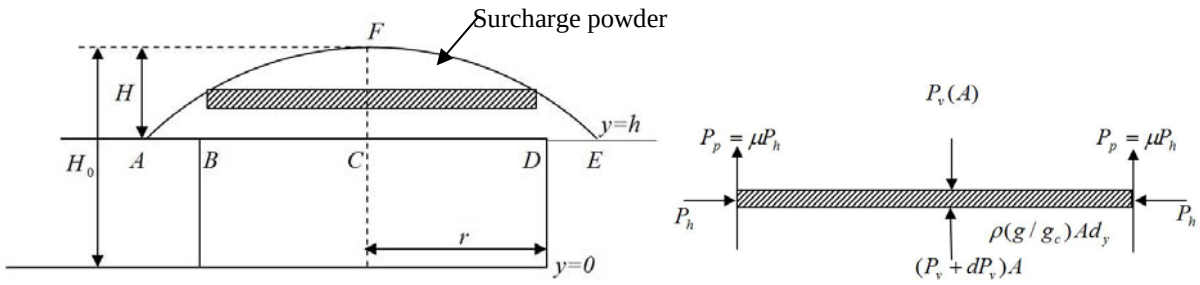

(a) (b)

Figure **10.2**: (a) Free body diagram of dimension of surcharge powder for rainy fill, (b) force balance diagram of powder mass inside the surcharge powder mass above the die cross-section (P_p= powder pressure)

Following the force balance analysis carried out for filled powder below the die height ($y<h$), the vertical pressure was obtained as:

$$P_v = A(1-e^{-b(H_0-h)}) \qquad \text{(Equation } \mathbf{10.23a}\text{)}$$

$$(H_0-h) = F_y^{'}(1-e^{-\beta^{'}(t-t_f)}) \qquad \text{(Equation } \mathbf{10.23b}\text{)}$$

where, t_f=time of filling the die completely, t= time at the end of filling process ($t>t_f$)

The above equations (10.23a) and (10.23b) are applicable as well during the powder surcharge build up. Based on visual observations during experiments with the rainy fill method, the surcharge powder profile can be approximated by a spherical cap (ABCDEFA) as shown in Figure **10.2 (a)**. The vertical pressure from the surcharge powder is:

$$P = \rho_b V g = \rho_b g(\frac{\pi H}{6}(3(AC)^2 + H^2) = \rho_b g\left(\frac{\pi H}{6}(3\theta r^2 + H^2)\right) \qquad \text{(Equation } \mathbf{10.24}\text{)}$$

where ρ_b = bulk density

V= volume of surcharge

g= gravitational constant,

θ = AC/r

or in terms of equivalent powder height:

$$h^* = \frac{P}{\rho_p g} = \frac{\pi}{6}\frac{\rho_b}{\rho_p} H(3\theta r^2 + H^2) \qquad \text{(Equation } \mathbf{10.25}\text{)}$$

Substituting equation 10.23b into 10.25 leads to:

$$h^* = \frac{\rho_b}{\rho_p}\frac{\pi\, r^2\theta}{2} F'\left(1 - e^{-\beta'(t-t_f)}\right) + \frac{\rho_b}{\rho_p}\frac{\pi}{6}\left(F'\right)^3\left(1 - e^{-\beta'(t-t_f)}\right)^3 \qquad \text{(Equation } \mathbf{10.26}\text{)}$$

The form of equation 10.26 is sigmoidal, which is comparable to Chapman-Richards equation shown below:

$$h^* = \alpha(1 - e^{-bt})^c \qquad \text{(Equation } \mathbf{10.27}\text{)}$$

where α , *b*, and *c* are parameters and their interpretations are given in a subsequent section.

For the point feed method, the shape of surcharge powder was conical. For this fill method, the surcharge pressure (based on volume of the cone) can be written as:

$$P = \rho_b V g = \rho_b \frac{1}{3}\pi(AC)^2 Hg = \pi\frac{\rho_b}{3} gH^3\theta^2 \tan\delta$$

where δ is half cone angle, θ is AC/r, AC is base radius of cone pile, and r is die radius. Or as equivalent height:

$$h^* = \frac{P}{\rho_p g} = \frac{\pi}{3}\frac{\rho_b}{\rho_p}\tan\delta\, H^3$$

From Equation (10.23b):

$$h^* = \frac{\pi}{3}\frac{\rho_b}{\rho_p}\tan\delta(F_y')^3\left(1 - e^{-\beta'(t-t_f)}\right)^3 \qquad \text{(Equation } \mathbf{10.28a}\text{)}$$

For the point feed fill method, the deposited powder's base expands until it reaches the walls of the die. During this time period, most of the die is unfilled, i.e., the walls of the shallow die do not directly influence the filling pressures. In this case, retaining the first non-zero term of the Taylor series for the equation 10.28a yields:

$$h^* = \beta \left(t - t_f\right)^c \qquad \text{(Equation } \mathbf{10.28b}\text{)}$$

where, β is a coefficient determined from experimental data.

equation (10.28b) is the generalized pressure build up profile for the point feed fill method. As will be shown later $c \approx 1$ for BPM at slow filling rates. Given the generality of equation 10.27, it was used for modeling the three filling methods. The point feed filling method is a special case of equation 10.27.

10.5 Feed shoe filling process

A typical pressure profile obtained by the pressure sensor element located at the center of the cylindrical die filled with the BPM at feed shoe speed of 20 mm/s is shown in Figure **10.3**. The plot represents the average of six runs. The same filling profile was observed for Avicel powder at 20 mm/s feed shoe speed. In order to compare the pressure profile of Avicel with BPM, each pressure value was divided by the particle density multiplied by gravity ($\frac{p}{\rho_p . g}$). This can be interpreted as equivalent height (h); in this study the particle density (ρ_p) of Avicel and BPM, used were 1.53 and 4.7 g/cc, respectively, and gravity constant (g) was 9.8 m/s^2. The height scale is in dm, dm is

decimeter, i.e., 1 dm=0.1 m. Throughout this study the data capture rate was 30 points per second.

.

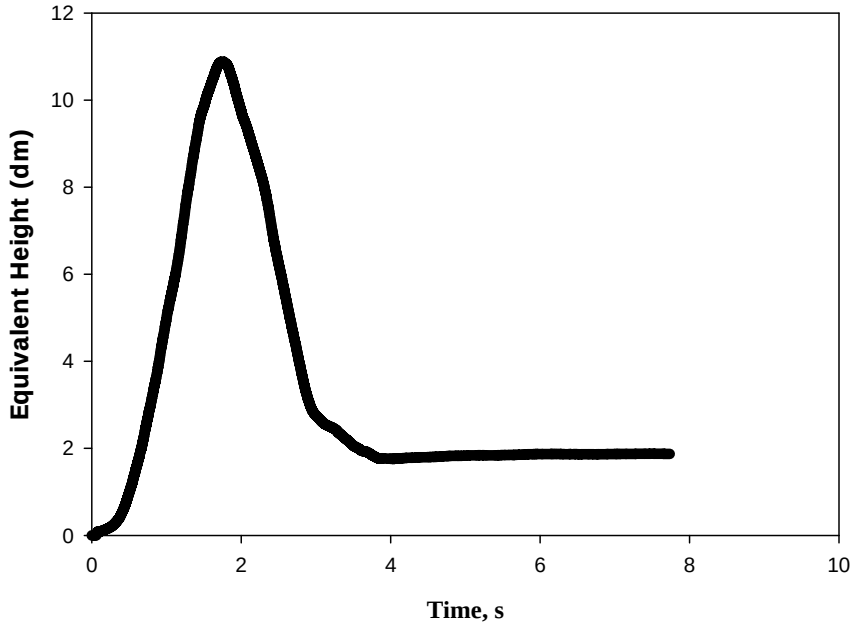

Figure **10.3**: Average equivalent height increase profile for the entire filling process at the center of cylindrical die filled with BPM at 20 mm/s feed shoe speed

Due to the complexity, the entire pressure profile could not be simulated by a single physics-based mathematical formulation. Therefore, the entire filling process was divided into various phases and Phase I was divided into two stages. Every phase was modeled using a simple rate equation. There were three reasons for the selection of a simple rate equation (Xie, 2006): 1) physics of deposition process of each stage, 2) similarity of measured data and modeled data, 3) simplicity of model. The positions of circular feed shoe tube during the filling process with reference to center of the die that

were used to show the start and end points of various phases are given in Figures **10.4** and **10.5**.

10.5.1 Feed shoe filling phases

The feed shoe filling profile shown in Figure **10.3** was divided into three distinctive phases, as shown in Figure **10.4**. Phase I was from time 0 to time T_1 which corresponded to forward stroke while the actual filling process occurred. Phase I was divided further into two stages which corresponded to feed shoe tube movement during the forward stroke. The two stages were, T_{1a} and T_{1b} where the first subscript denotes the phase and second subscripts represents the stage. During Phase II for time duration T_2, the feed shoe started to leave the die. The pressure applied by the powder inside the feed shoe tube started to be released. Phase III for time duration T_3 was post-filling process during which time the powder gradually approached an equilibrium value.

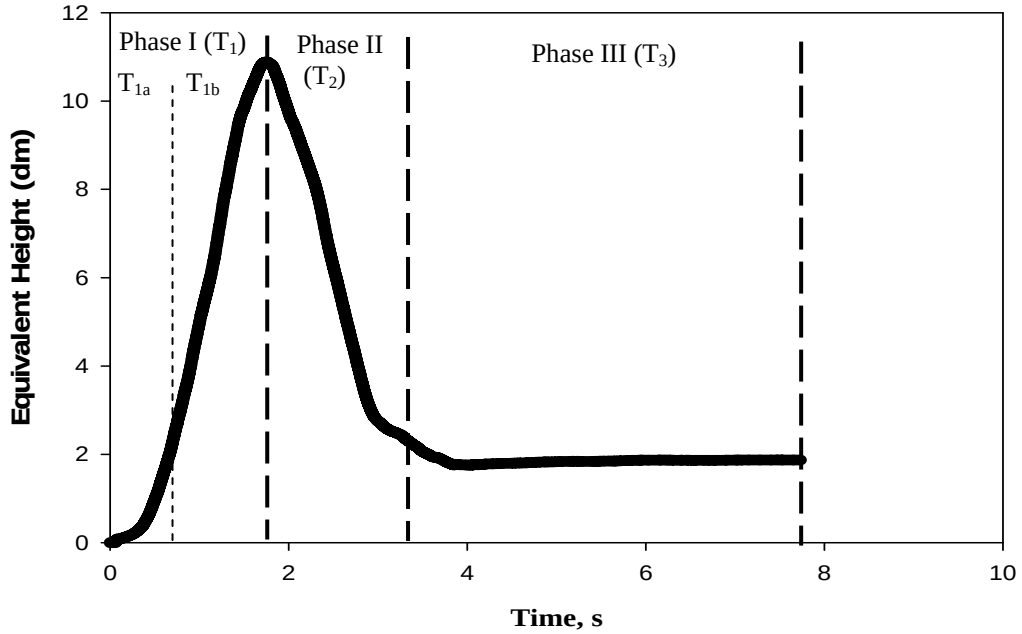

Figure **10.4**: Average equivalent height increase profile for the entire filling process at the center of sensor strip of 0^o-180^o orientation using BPM powder at 20 mm/s feed shoe speed

10.5.1.1 Phase I

In Phase I, actual filling of the die occured during the forward stroke of feed shoe tube. The relative positions of feed shoe tube at two stages marked the start and end points are shown in Figure **10.5**. These particular positions of feed shoe tube with circular cross-section were used to identify and discriminate filling stages in Phase I. Corresponding to these positions, the specific times for the feed shoe tube to reach these positions are listed below:

T_{1a}: when feed shoe tube nose reached middle of the die (0.57s).

T_{1b}: when the back wall of feed shoe tube reached the leeward direction of the die (1.11s).

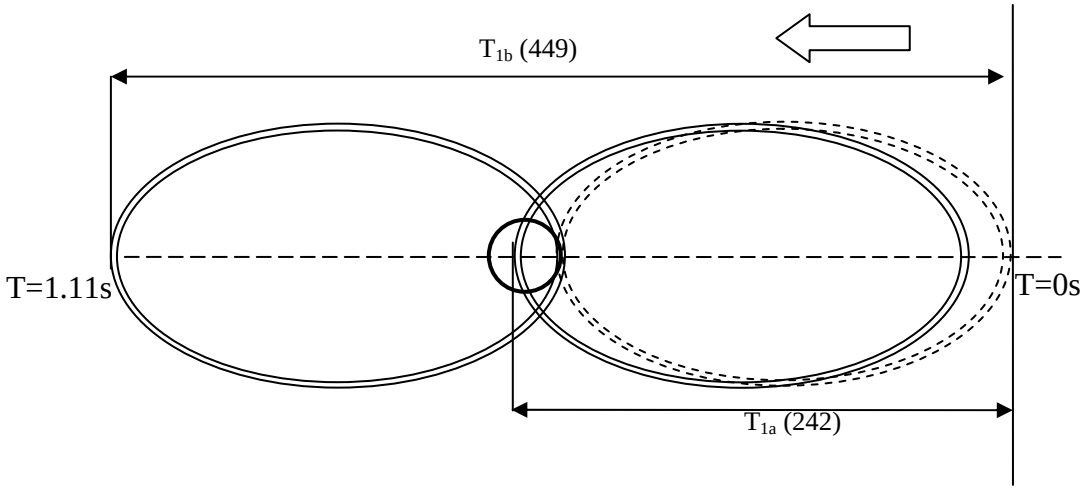

Figure **10.5**: Filling sequences in Phase I during the forward stroke showing feed shoe travel distance (in mm) and onset of stages described by T and its subscripts

Stage I (T_{1a}): The majority of filling was accomplished in this stage. The filling occurs rapidly showing an exponential deposition profile. The equation for this stage was formulated as gives in equations (22): $h = F(1 - e^{-bt})$, where h is pressure as equivalent height, and F, and b are coefficients.

Stage II(T_{1b}): In this stage, the die was overfilled and surcharge powder covered the top of the powder mass. The filling profile in this stage, as shown in the preceding section, followed the formulation $h = F(1 - e^{-bt})^c$, where c represents the fill characteristics during the deposition of surcharge layers.

Figure **10.6** shows the filling profile as equivalent height during the forward stroke for center of circular die (along 0^0-180^0 orientation) using a battery powder mixture (BPM) at 20 mm/s feed shoe speed.

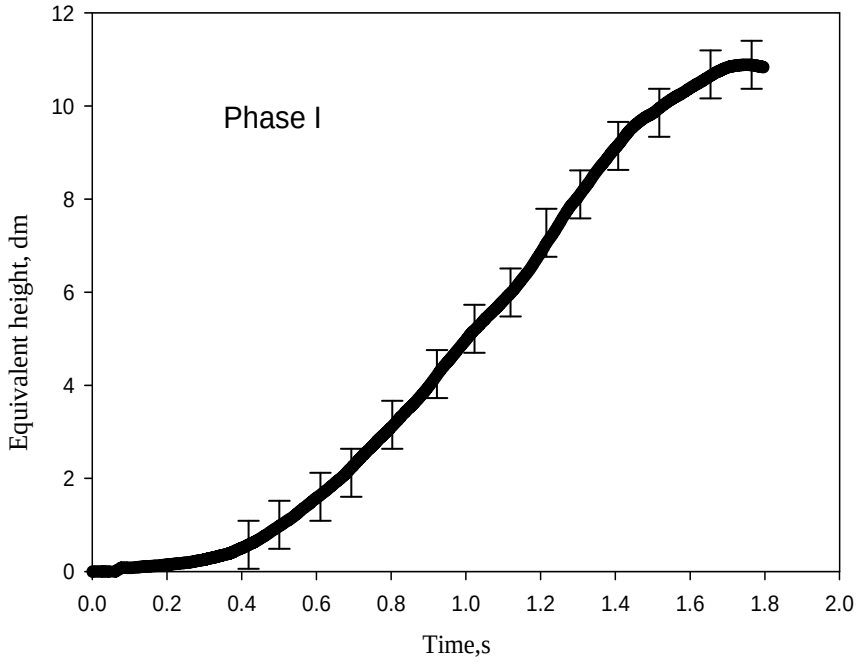

Figure **10.6**: The filling profile of Phase I at the center of 0^0-180^0 orientation of the pressure sensor strip die filled with BPM at 20 mm/s feed shoe speed and standard deviation of observations as error bars.

At time 0, the feed shoe tube front wall reached the leeward direction of the die (Figure **10.5**), while only a small fraction of the powder in the front of feed shoe was available to enter the die. The filling rate is very low at this time. With the feed shoe movement and increase of time, more powder in the front wall of feed shoe tube filled the die. With the increase in time, the die continued to fill and the distance between the top surface of the powder in the die and the bottom of the powder in the feed shoe gradually decreased; at this time, the die was filled, i.e., could not accommodate more powder.

Two stages of the Phase I could be mathematically represented by the following rate equation (equation 10.29):

$$h = \alpha(1 - e^{-bt})^c \qquad \text{(Equation } \mathbf{10.29}\text{)}$$

The curve is a sigmoidal shape as noted previously, where:

h = equivalent height

α , b, and c are three coefficient

In this model, coefficient a, is the asymptote, the maximum pressure ratio when time approaches ∞. Coefficient b represents the reciprocal of the characteristics time ($\frac{1}{b}$) of the deposition process, and the exponent c, as mentioned previously, represent the build up of pressure due to the surcharge powder. For the data for Figure **10.7**, α = 32.63, b=5.69, and c=3.00. The R-Square value of this regression was 0.97.

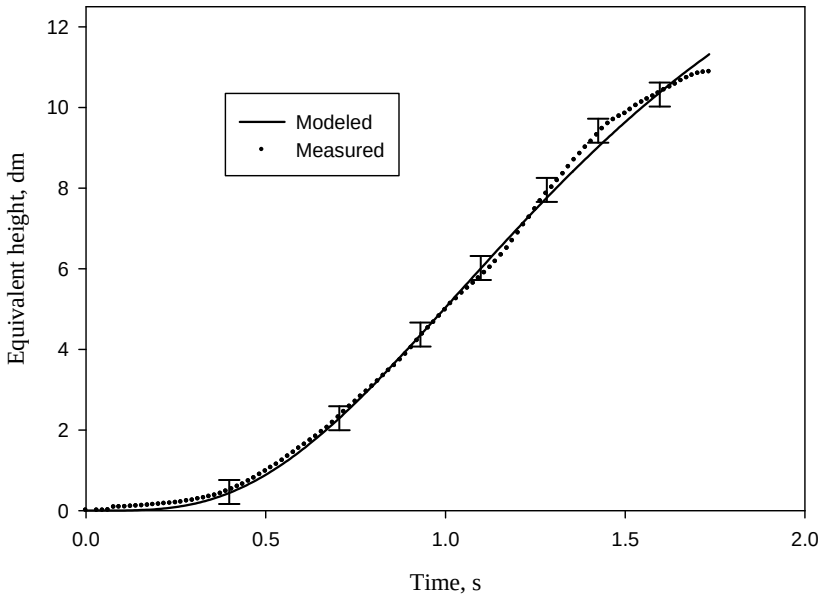

Figure **10.7**: Model of Phase I of the average equivalent height at the center of 0^0-180^0 orientation of pressure sensor strip filled with BPM at 20 mm/s feed shoe speed and standard deviation of observations as error bars.

Phase I is responsible for most of the powder filling during the deposition process. During the Phase I, the most pressure measured by the pressure sensor strip were exerted directly from the powder deposited into the circular die. No pressure was exerted or influenced by the feed shoe wall.

10.5.1.2 Phase II

The measured data points and the simulated straight line are shown in Figure **10.8**. The rate equation of this stage was:

$$\frac{dh}{dt} = m_2 \qquad \text{(Equation } \mathbf{10.30}\text{)}$$

where m_2= slope of the straight line. The slope m_2= - 6.785. The R-square value of this regression was 0.99.

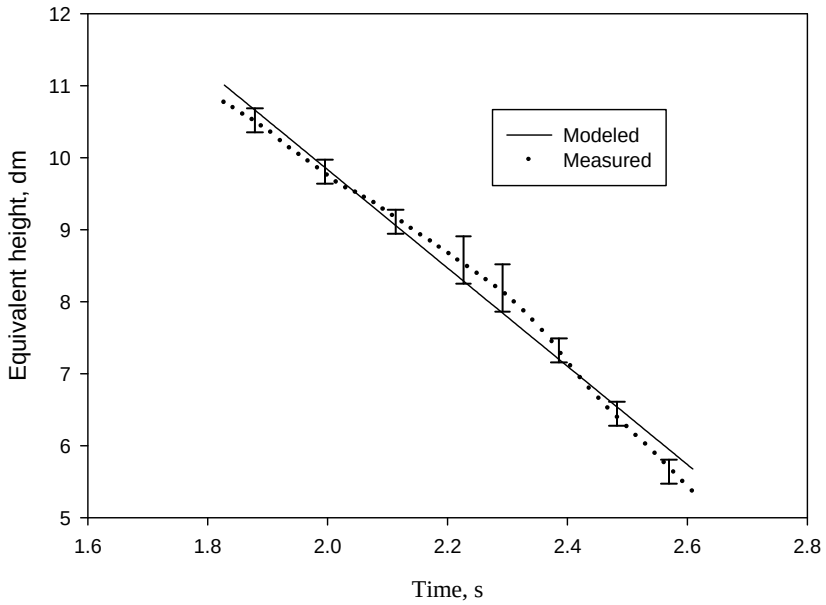

Figure **10.8**: Model of Phase II of the average pressure as equivalent height at the center of 0^0-180^0 orientation of pressure sensor strip filled with BPM at 20 mm/s feed shoe speed and standard deviation of observations as error bars.

10.5.1.3 Phase III

In this stage, the pressure reached an equilibrium state, and this state could best represent the pressure value of the end of filling process. Figure **10.9** compares the measured data points and modeled horizontal line of Phase III. The pressure profile decreased slowly in the beginning of this phase, followed by a close-to-horizontal profile. The reason for slow decline might be that some of the pressures at the end of forward stroke was gradually released. The rate of equivalent height in Phase III is simply $dh/dt = 0$.

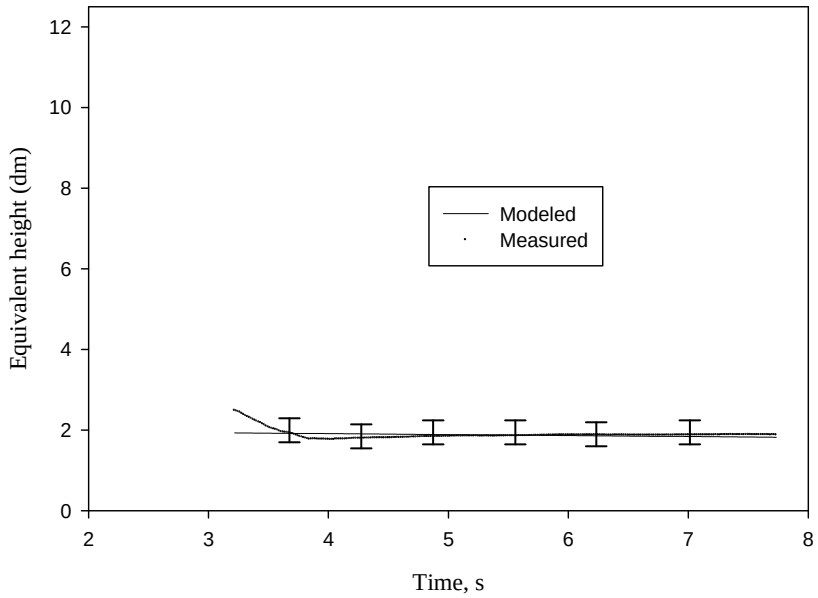

Figure **10.9**: Model of Phase III of the average pressure as equivalent height at the center of 0^0-180^0 orientation of pressure sensor strip filled with BPM at 20 mm/s feed shoe speed and standard deviation of observations as error bars.

10.5.2 Overall equation for all the three phases

Xie (2006) developed a mathematical rate equation for feed shoe filling method for multiple deep dies. This equation was used to develop the rate equation for a circular shallow die. The overall rate equation for shallow die was presented in equation 10.31:

$$\frac{dh}{dt} = \alpha h\ F(t) + \beta \qquad \text{(Equation } \mathbf{10.31}\text{)}$$

where α and β are coefficient, and *F(t)* is a function of time, locations, and powder characteristics. The coefficient and specific form of function *F(t),* and the range of time is

shown in Table **10.1**. The Phases I and II did not have the function *F(t)* (there α value was 0), since the changing rates of their pressure values were constant.

Table **10.1**: Model parameters for all the three phases of the center (r=0 mm) of the cylindrical die filled with the BPM powder at 20 mm/s feed shoe speeds

Phase #	*hF(t)*	α	β	Time (second)
I	$h/(e^{5.69t}-1)$	32.63	0	$0 \le 0 \le 1.8$
II	0	0	-6.785	$1.8 \le 0 \le 2.6$
III	0	0	0	$2.6 \le 0 \le 7.8$

Root mean square error (RMSE) and average relative difference (ARD) values were used to determine the quality of the model predictions. RMSE for data was 0.16 and ARD was 0.07 (or 7%). RMSE and ARD were calculated based on the following equations:

$$RMSE = \sqrt{\frac{\sum (h_{p,\mathrm{mod}el} - h_{p,measured})^2}{n}} \qquad \text{(Equation } \mathbf{10.32}\text{)}$$

$$ARD = \frac{\sum \frac{\left| h_{p,\mathrm{mod}el} - h_{p,measured} \right|}{h_{p,measureed}}}{n} \qquad \text{(Equation } \mathbf{10.33}\text{)}$$

where $h_{p,\,\mathrm{mod}el}$ = modeled equivalent height,

$h_{p,\,measured}$ = measured equivalent height,

n= the number of total data points.

10.5.3 Model validation

Tables **10.2** and **10.3** show the coefficients for r=4 mm obtained from data points, and r=2 mm which was obtained from interpolation of r=0 mm and r=4 mm, respectively. The RMSE and ARD were 0.12 dm and 0.05 (5%), respectively, which showed that the calculated values are in good agreement with measured values. The pressure profiles for measured and modeled data points at r=2 mm are shown in Figure **10.10**.

Table **10.2**: Model parameters for all the three phases of at r=4 mm of the cylindrical die filled with the BPM powder at 20 mm/s feed shoe speeds

Phase #	*hF(t)*	α	β	Time (second)
I	$h/(e^{5.43t}-1)$	29.87	0	$0 \leq 0 \leq 1.8$
II	0	0	-6.13	$1.8 \leq 0 \leq 2.6$
III	0	0	0	$2.6 \leq 0 \leq 7.8$

Table **10.3**: Model parameters for all the three phases for r=2 mm, which obtained from interpolation of r=0 mm and r=4 mm of the cylindrical die filled with the BPM powder at 20 mm/s feed shoe speed.

Phase #	*hF(t)*	α	β	Time (second)
I	$h/(e^{5.56t}-1)$	31.25	0	$0 \leq 0 \leq 1.8$
II	0	0	-6.46	$1.8 \leq 0 \leq 2.6$
III	0	0	0	$2.6 \leq 0 \leq 7.8$

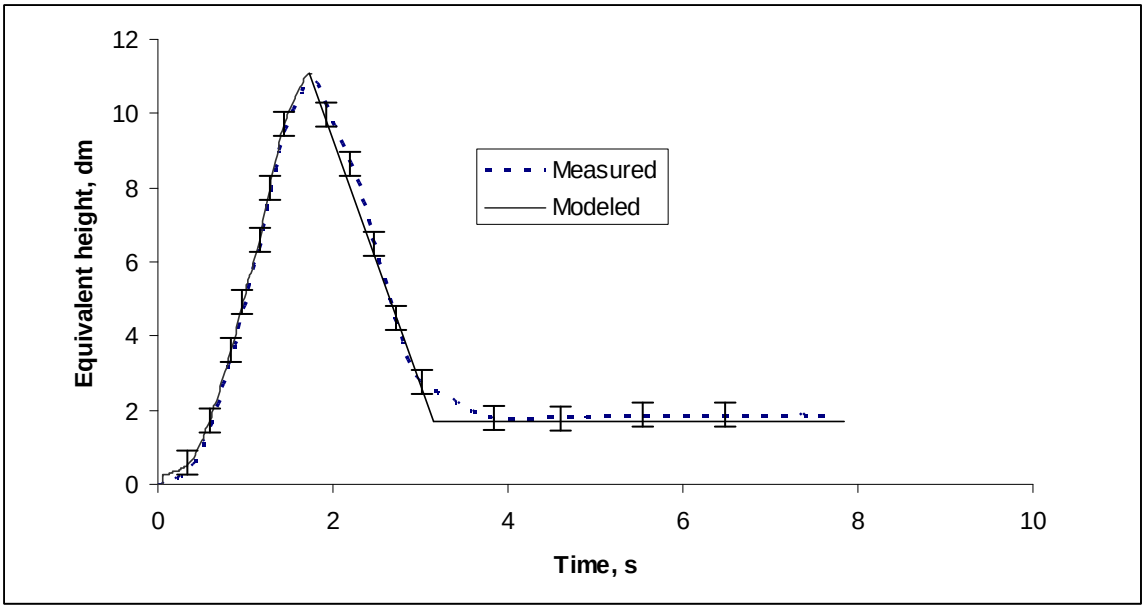

Figure **10.10**: Comparison of measured and modeled equivalent height of pressure sensor strip at r=2 mm for cylindrical die using feed shoe filling method at 20 mm/s feed shoe speed (RMSE=0.12 dm and ARD=5%) with standard deviation of observations as error bars.

10.6 Rotational rainy fill

Figure **10.11** shows a typical pressure profile for a cylindrical shallow die filled with BPM at 26 g/min filling rate. The plot represents the average of six runs with pressure sensor strip located at $0^0 - 180^0$ orientation. The entire filling profile was divided into four phases as follows:

Phase I (T_1)= filling process (the rotational rainy filled the die completely at this phase (42 s);

Phase II (T_2)= leveling process (removing surcharge powder manually)(50 s);

Phase III (T_3)= end of leveling process (57 s);

Phase IV (T_4)= equilibrium period (end of filling process) (70 s).

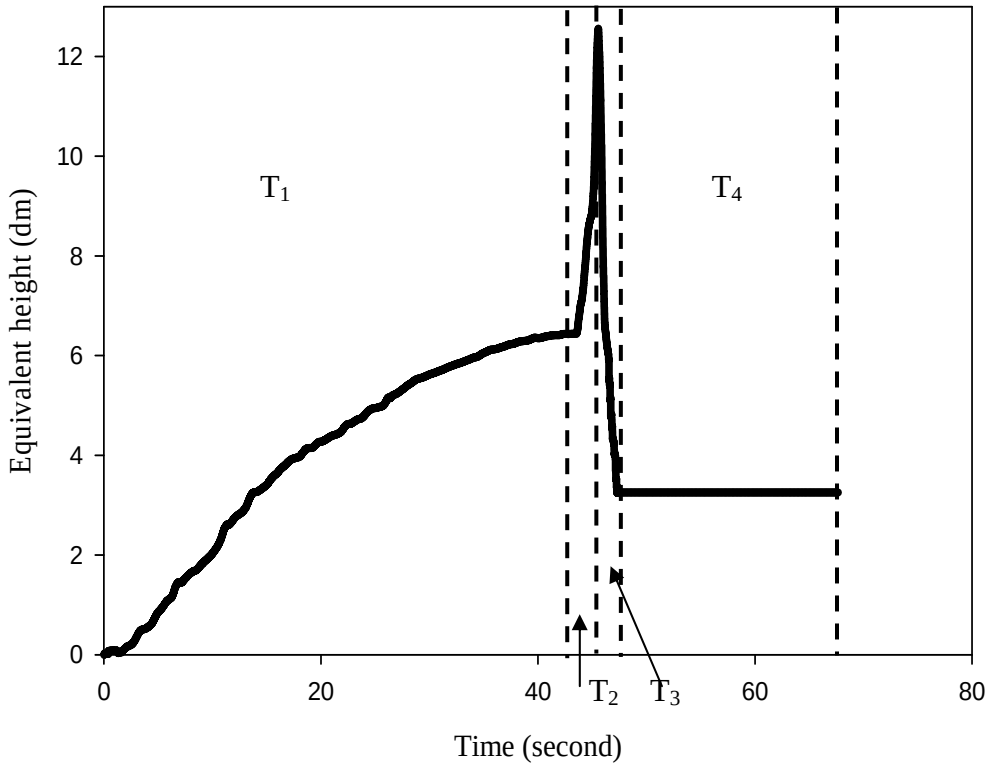

Figure **10.11** Filling profile at middle of circular die at 0^o-180^o orientation of pressure sensor strip filled with BPM powder at 26 g/min filling rate using rotational rainy fill method

10.6.1 Phase I

Phase I was the filling process during which the die was overfilled. In rotational rainy fill, the average time for this process was approximately 40 seconds. The powder filling rate (the slope of mass ratio curve) increased rapidly with time and gradually decreased after time 20 seconds. The die was over-filled after 20 seconds and surcharge powder started to accumulate after this time as discussed and shown in section 10.4.2.

Phase I had a sigmoidal shape curve which was represented by the Chapman-Richards model; $h = \alpha(1 - e^{-bt})^c$, where α = 19.32, b= 0.44, and c= 3.00. The R-square value of this regression was 0.94. The physics of the deposition process and interpretation of parameters during of Phase I, have already been discussed in section 10.4 and section 10.5.1.1. The measured data points and the calculated values for Phase I are shown in Figure **10.12**.

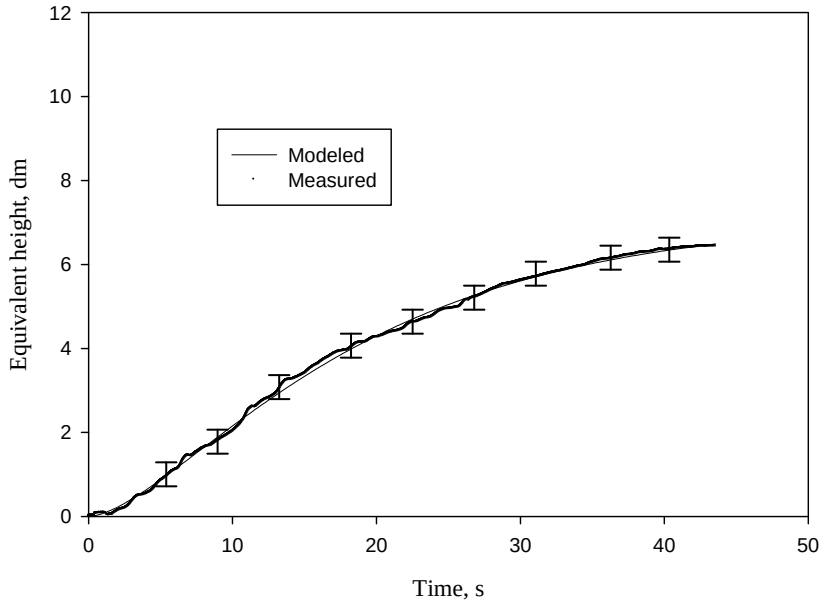

Figure **10.12**: Model of Phase I of the average pressure as equivalent height at the center of 0^0-180^0 orientation of pressure sensor strip filled with BPM at 26 g/min filling rate using rotational rainy fill and standard deviation of observations as error bars.

10.6.2 Phase II

During this phase, the surcharge powder was removed from the die. The leveling process generated high pressure inside the die due to increase in the shear stress among

particles. The leveling process was accomplished manually by using a fiberglass tube. The measured and modeled filling profile are shown in Figure **10.13**. The rate equation was:

$$\frac{dh_p}{dt} = m_2 \qquad \text{(Equation } \mathbf{10.34}\text{)}$$

where m_2= slope of the straight line. The slope m_2=0.158. The R-square value of this regression was 0.94.

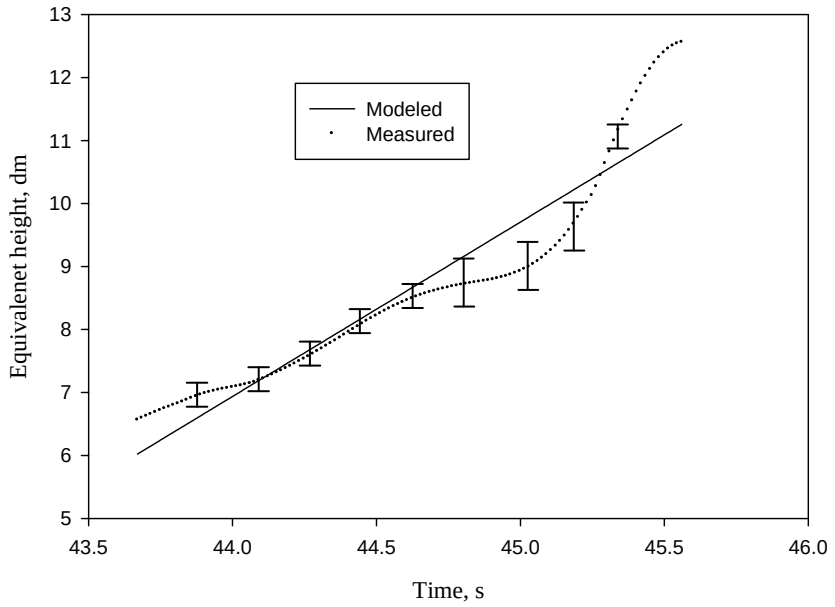

Figure **10.13**: Model of Phase II of the average pressure as equivalent height at the center of 0^0-180^0 orientation of pressure sensor strip filled with BPM at 26 g/min filling rate using rotational rainy fill and standard deviation of observations as error bars.

10.6.3 Phase III

Figure **10.14** compares the measured data and the modeled straight line of Phase III. The rate equation of straight line was:

$$\frac{dh_p}{dt} = m_3 \qquad \text{(Equation } \mathbf{10.35}\text{)}$$

where m_3= slope of the straight line. The slope m_3= - 5.08. The R-square value of this regression was 0.89. The main reason for Phase III not being a straight line might be due to the pressure release inside the die and rearrangement that occurred after completion of the leveling process.

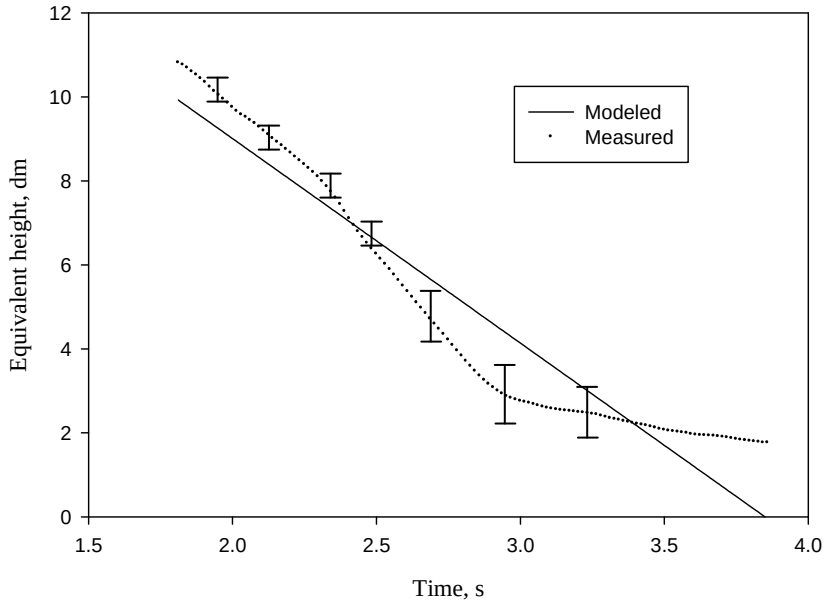

Figure **10.14**: Model of Phase III of the average pressure as equivalent height at the center of 0^0-180^0 orientation of pressure sensor strip filled with BPM at 26 g/min filling rate using rotational rainy fill and standard deviation of observations as error bars.

10.6.4 Phase IV

Phase IV was the last stage of rainy filling process, where the pressure became stable (Figure **10.15**). The rate equation for Phase IV was simplified as $dh_p / dt = 0$.

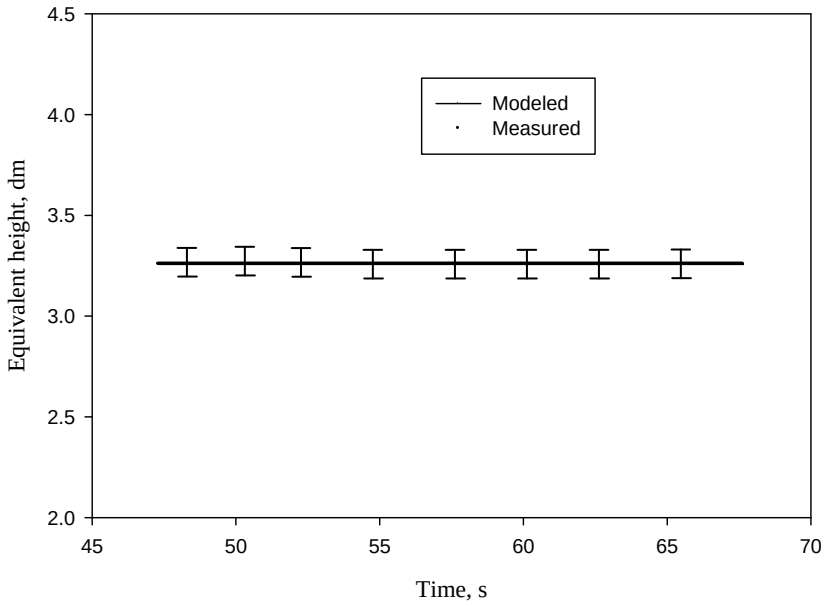

Figure **10.15**: Model of Phase IV of the average pressure as equivalent height at the center of 0^0-180^0 orientation of pressure sensor strip filled with BPM at 26 g/min filling rate using rotational rainy fill and standard deviation of observations as error bars.

For the entire deposition process, the root mean square error (RMSE) and average relative difference (ARD) for rotational rainy fill were 0.44 dm and 0.16 (16%), respectively. The differences between measured data and model calculated values were relatively higher vs. feed shoe filling. The coefficient and specific form of the function *F(t)*, and the range of times are shown in Table **10.4**

Table **10.4**: Model parameters for all the four phases of the center (r=0 mm) of the cylindrical die filled with the BPM powder at 26 g/min.

Phase #	*hF(t)*	α	β	Time (second)
I	$h/(e^{0.44t}-1)$	19.32	0	$0 \le 0 \le 42$
II	0	0	0.1583	$42 \le 0 \le 50$
III	0	0	-5.08	$50 \le 0 \le 57$
IV	0	0	0	$57 \le 0 \le 70$

10.6.5 Model validation

Tables **10.5** and **10.6** show the coefficients for r=4 mm obtained from data and r=2 mm obtained from interpolation of r=0 mm and r=4 mm, respectively. The RMSE and ARD for r=2 mm from interpolation values were 0.18 dm and 0.15 (15%), respectively, which are comparable with magnitudes to the r=0 and r=4 data sets; therefore, the model validation is acceptable. For the entire deposition process, the pressure profile for measured and modeled data points at r=2 mm are shown in Figure **10.16**.

Table **10.5**: Model parameters for all the four phases at r=4 mm of the cylindrical die filled with the BPM powder at 20 mm/s feed shoe speed.

Phase #	*hF(t)*	α	β	Time (second)
I	$h/(e^{0.55t}-1)$	17.18	0	$0 \le 0 \le 42$
II	0	0	0.144	$42 \le 0 \le 50$
III	0	0	-5. 443	$50 \le 0 \le 57$
IV	0	0	0	$57 \le 0 \le 70$

Table **10.6**: Model parameters for all four phases for r=2 mm, which obtained from interpolation of r=0 mm and r=4 mm of the cylindrical die filled with the BPM powder at 20 mm/s feed shoe speed.

Phase #	*hF(t)*	α	β	Time (second)
I	$h/(e^{0.49t}-1)$	18.25	0	$0 \le 0 \le 42$
II	0	0	0.151	$42 \le 0 \le 50$
III	0	0	-5. 261	$50 \le 0 \le 57$
IV	0	0	0	$57 \le 0 \le 70$

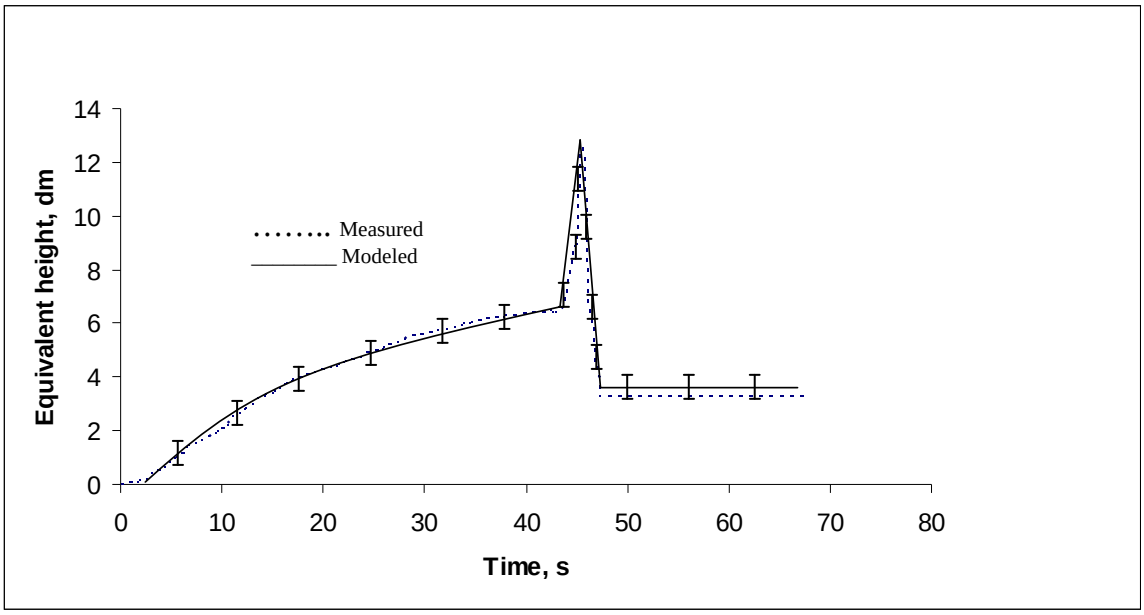

Figure **10.16**: Comparison of measured and modeled equivalent height of pressure sensor strip at r=2 mm for cylindrical die using rotational rainy fill at 26 g/min (RMSE=0.18 dm and ARD=15%) with standard deviation of observations as error bars.

10.7 Point Feed

Figure **10.17** shows the entire filling profile for the point feed filling method. The complete filling process can be divided into four phases. Corresponding to each phase, a specific time with each phase of the filling process is listed below:

Phase I (T_1)= filling process (the point feed filled the die completely at this phase) (100 s);

Phase II (T_2)= leveling process (removing surcharge powder manually) (105 s);

Phase III (T_3)= end of leveling process (110 s);

Phase IV (T_4)= end of filling process (120 s).

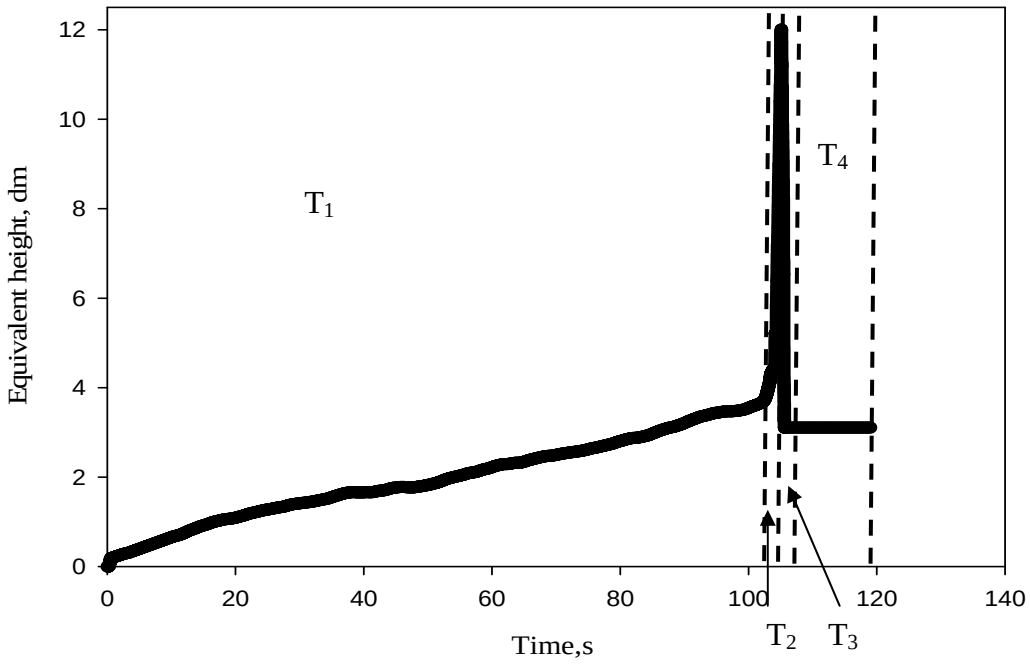

Figure **10.17** Filling profile at middle of circular die at 0^o-180^o orientation of pressure sensor strip filled with BPM powder at 26 g/min filling rate using point feed fill method

10.7.1 Phase I

Phase I had almost constant deposition rate as explained previously. The powder filling increased with time. The die was filled with constant deposition rate at 26 g/min. The measured data points and straight line model of Phase I are shown in Figure **10.18**. The rate equation of this state was:

$$\frac{dh_p}{dt} = m_1 \qquad \text{(Equation } \mathbf{10.36}\text{)}$$

where m_1=slope of the straight line (m_1=0.0311) and R-square was 0.99. The filling profile for point feed method is considerably different from feed shoe and rainy fill. This was explained in section 10.4, i.e., the powder deposited in the die with the point feed method is not directly influenced by the die walls; hence, a nearly linear profile. Furthermore, the particles' accumulation profile continuously failed along angle of internal friction during the filling process which generated a constant head increase rate.

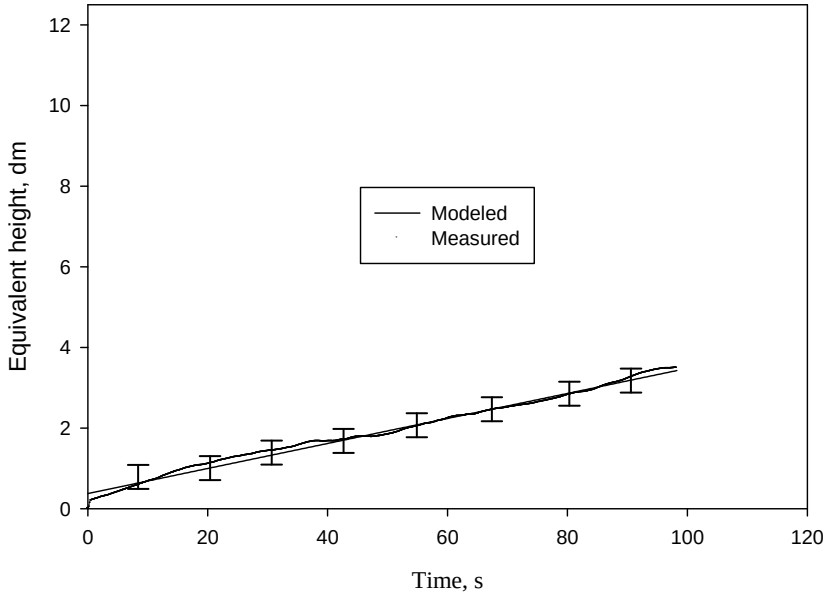

Figure **10.18**: Model of Phase I of the average pressure as equivalent height at the center of 0^0-180^0 orientation of pressure sensor strip filled with BPM at 26 g/min filling rate using point feed method and standard deviation of observations as error bars.

10.7.2 Phase II

Figure **10.19** shows the measured data and the calculated values for Phase II. During this phase, the leveling process occurred or the surcharge powder was removed manually from the die. The pressure rate rapidly increased due to increase in shear stress during the leveling process. The rate equation for this phase was $dh_p / dt = m_2$, where m_2=8.25 (slope of the line) and R-square was 0.99.

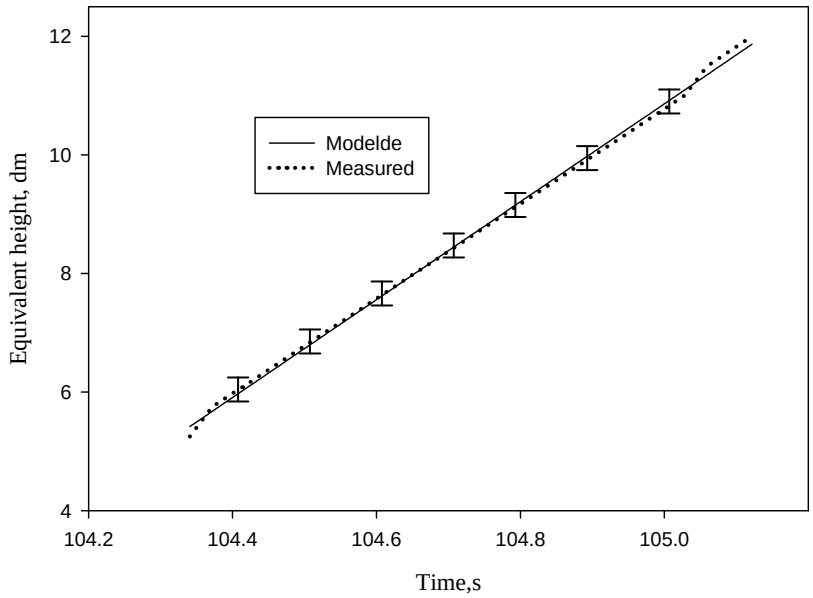

Figure **10.19**: Model of Phase II of the average pressure as equivalent height at the center of 0^0-180^0 orientation of pressure sensor strip filled with BPM at 26 g/min filling rate using point feed method and standard deviation of observations as error bars.

10.7.3 Phase III

Phase III was end of the leveling process. The pressure quickly decreased after the surcharge powder was completely removed from the die. Due to high shear stress during the manual leveling process, the pressure was slowly released that resulted in a non-linear declining pressure profile; this was approximated by a straight line (Figure **10.20**). Therefore, the rate equation for Phase III was:

$$\frac{dh_p}{dt} = m_3 \qquad \text{(Equation } \mathbf{10.37}\text{)}$$

where m_3= - 19.52 (slope of the line) and R-square was 0.94.

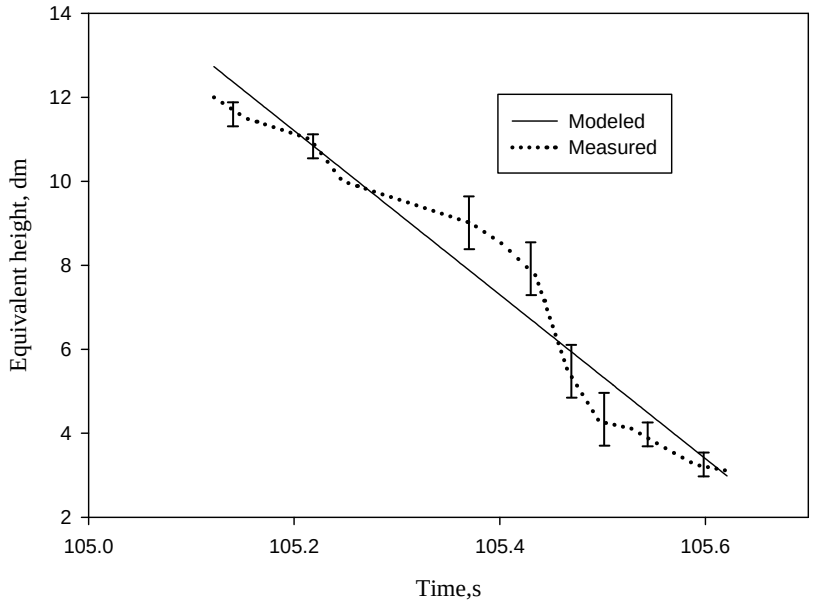

Figure **10.20**: Model of Phase III of the average pressure as equivalent height at the center of 0^0-180^0 orientation of pressure sensor strip filled with BPM at 26 g/min filling rate using point feed method and standard deviation of observations as error bars.

10.7.4 Phase IV

Phase IV was modeled as a horizontal line (Figure **10.21**). The modeled equivalent height was 3.11 dm, and it was obtained by taking the average of all the data points within this phase. The rate equation for this phase was $dh_p/dt=0$.

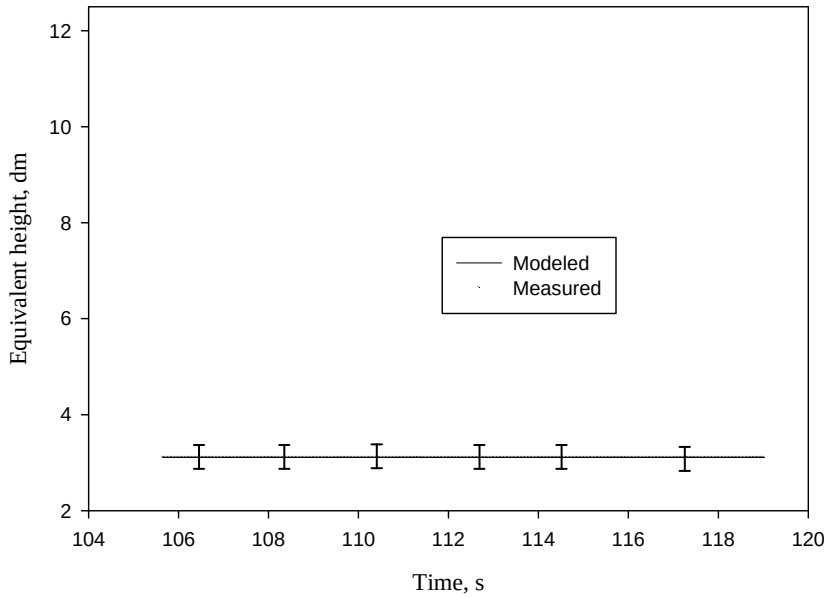

Figure **10.21**: Model of Phase IV of the average pressure as equivalent height at the center of 0^0-180^0 orientation of pressure sensor strip filled with BPM at 26 g/min filling rate using point feed method and standard deviation of observations as error bars.

For the entire deposition process, the root mean square error (RMSE) and average relative difference (ARD) for point feed filling method using a battey powder mixture at 26 g/min were 0.32 dm and 0.11 (11%), respectively. The coefficient and specific form of the function *F(t)* and the range of time are shown in Table **10.7**.

Table **10.7**: Model parameters for all the four phases of the center (r=0 mm) of the cylindrical die filled with the BPM powder at 26 g/min.

Phase #	*m*	Time (second)
I	0.0311	$0 \le 0 \le 100$
II	8.25	$100 \le 0 \le 105$
III	-19.52	$105 \le 0 \le 110$
IV	0	$110 \le 0 \le 120$

10.7.5 Model validation

The model coefficients for r=4 mm obtained from data and r=2 mm which was obtained from interpolation of r=0 mm and r=4 mm are shown in Tables **10.8** and **10.9**, respectively. The RMSE and ARD for r=2 mm for model calculated values were 0.14 dm and 0.08 (8%), respectively, which represents good validation for this study. The pressure profile for measured and model calculated values at r=2 mm are shown in Figure **10.22**.

Table **10.8**: Model parameters for all four phases at r=4 mm of the cylindrical die filled with the BPM powder at 20 mm/s feed shoe speed.

Phase #	*m*	Time (second)
I	0.055	$0 \leq 0 \leq 100$
II	8.87	$100 \leq 0 \leq 105$
III	-18.65	$105 \leq 0 \leq 110$
IV	0	$110 \leq 0 \leq 120$

Table **10.9**: Model parameters for all four phases for r=2 mm, which obtained from interpolation of r=0 mm and r=4 mm of the cylindrical die filled with the BPM powder at 20 mm/s feed shoe speed.

Phase #	*m*	Time (second)
I	0.043	$0 \leq 0 \leq 100$
II	8.56	$100 \leq 0 \leq 105$
III	-19.08	$105 \leq 0 \leq 110$
IV	0	$110 \leq 0 \leq 120$

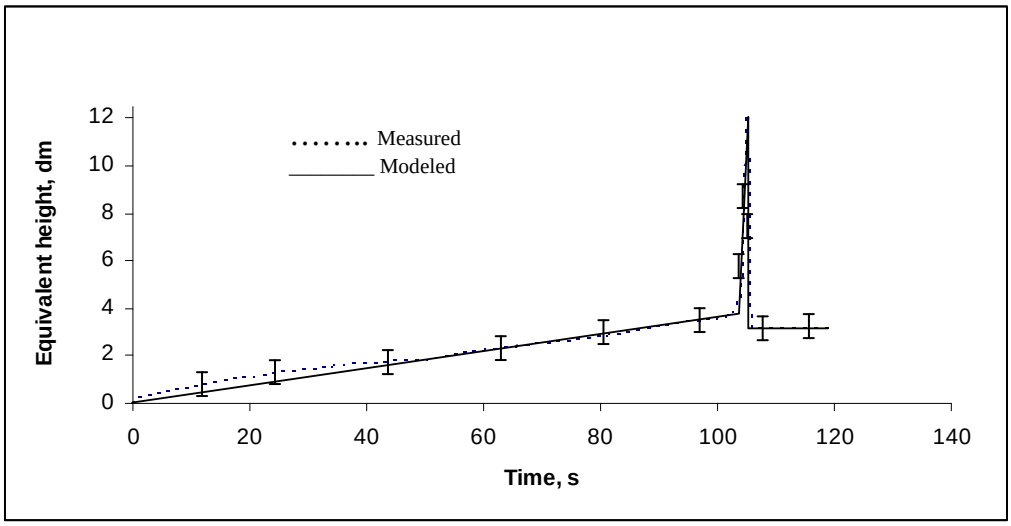

Figure **10.22**: Comparison of measured and modeled equivalent height of pressure sensor strip at r=2 mm for cylindrical die using point feed filling method 26 g/min (RMSE=0.14 and ARD=8%) with standard deviation of observations as error bars.

10.8 Conclusions

The following conclusions were arrived at from this study:

1) The deposition profile for feed shoe and rainy fill were the same shape (sigmoidal shape);
2) A physics based model was used to explain the sigmoidal slope of the pressure build up for the feed shoe and rainy filling methods.
3) The linear profile for the point feed was explained as a special case of the sigmoidal shape.
4) The overall rate equation for all three filling methods was: $dh/dt = \alpha h F(t) + \beta$;

5) The root mean square error (RMSE) for feed shoe, rotational rainy and point feed, were 0.16, 0.44, and 0.32, respectively.
6) The average relative differences (ARD) for feed shoe, rotational rainy and point feed were 7%, 16%, and 11%, respectively.
7) For model validation, RMSE for feed shoe, rotational rainy, and point feed were 0.15, 0.18, and 0.14, respectively.
8) For model validation, ARD for feed shoe, rotational rainy, and point feed were 5%, 15%, and 8%, respectively.

10.9 References

1- Manbeck B. Harvey and Virendra M. Puri. 1995. *Structure Loads in Grain Storage*.. pp 465- 525. Chapter in Stored Grain Ecosystems, edited by Digvir S. Jayas, Noel D. White, and William E. Muir. 1995. Marcel Dekker, Inc.
2- Kessler, P. David, and Robert A. Greenkorn. 1999. *Momentum, heat and mass transfer fundamentals*. Marcel Dekker, Inc.
3- Xie, X. 2006. Uniformity of Simultaneous Powder Deposition in Multiple Dies; Measurement and Modeling. Ph.D. diss., University Park. PA. Pennsylvania State Univ: Agricultural and Biological Engineering Dept.

Chapter 11

Conclusions and Recommendations for Future Work

Based on this study, the following concluding remarks can be made:

1) A circular die generated a higher uniformity pressure distribution inside the die than a rectangular die.
2) The rainy fill method with either the rectangular or circular die generated the highest uniformity among all the different filling methods tested (average of 77% and 78.5% uniformity for the circular and rectangular dies, respectively).
3) The point feed and feed shoe methods resulted in intermediate uniformity values, 64% and 55%, respectively.
4) The feed shoe cross-section shape did not influence the uniformity of pressure distribution (the average uniformity for circular and square feed shoe were 56.0% and 55.8%, respectively).
5) The filling process using the feed shoe method was faster than other the rotational rainy or point feed method. The average filling period for feed shoe, rotational rainy, and point feed were 8 s, 70 s, and 120 s, respectively.
6) The filling rate did not influence uniformity of pressure distribution when using rainy and point feed method, i.e., no major differences in uniformity between 26 and 132 g/min filling rates were measured.
7) The feed shoe speed highly influenced the uniformity of pressure distribution (uniformity increased with increasing feed shoe speed).

8) The rectangular die generated higher stress zones than the circular die due to the prescence of corners.
9) BPM generated higher stresses inside the die (97 dm) than Avicel (60 dm) due to the larger particle density.
10) The leveling process highly influenced the uniformity of pressure distribution; the pressure distribution uniformity decreased by 20% after the leveling process.
11) The pneumatic filling method generated the lowest uniformity among all filling methods (21%) tested.
12) Using the feed shoe filling method, BPM generated higher uniformity than Avicel powder, while Avicel had higher uniformity when using the rotational rainy or point feed.
13) For all filling methods tested, the leeward region had higher uniformity than the forward region due to the direction of leveling process, which removed the surcharge powders from the leeward to forward region.
14) During the feed shoe filling process, the forward and back regions accumulated more particles.
15) The deposition profile for feed shoe and rainy fill were the same shape (sigmoidal shape).
16) A physics based model was used to explain the sigmoidal slope of the pressure build up for the feed shoe and rainy filling methods.
17) The linear profile for the point feed was explained the special case of the sigmoidal shape.
18) The overall rate equation for all three filling methods was: $dh/dt = \alpha h F(t) + \beta$.

19) The root mean square error (RMSE) for feed shoe, rotational rainy, and point feed, were 0.16, 0.44, and 0.32, respectively.
20) The average relative differences (ARD) for feed shoe, rotational rainy, and point feed were 7%, 16%, and 11%, respectively.
21) For model validation, RMSE for feed shoe, rotational rainy, and point feed were 0.15, 0.18, and 0.14, respectively.
22) For model validation, ARD for feed shoe, rotational rainy, and point feed were 5%, 15%, and 8%, respectively.

Based on observations from this study, the following recommendations can be made for future study:

Feed shoe (PDT-II):

1) The particle accumulation causes a density/pressure gradient in particle packing which generates inhomogeneity in compacts. In order to minimize the non-uniformity, the particle trajectory and kinetic energy should be minimized by decreasing the filling rate/speed.
2) Using a die with round corners helps to increase the uniformity by decreasing the stress zones inside the die, which should be investigated further.
3) The ratio of particle size to die depth must be considered as an important filling factor.
4) Using smaller pressure sensors with a square or circular shape would increase data precision.
5) Using a smaller feed shoe tube will help to understand the influence of the feed shoe tube cross-section on uniformity of pressure distribution.

6) Testing more powders with different physical properties (such as particle size, size distribution, and bulk density) is necessary to strengthen and generalize the conclusion from this study.
7) Testing very low feed shoe speed (1-5 mm/s) is recommended so as to gain greater insights about the filling process.
8) Decreasing the amount of powder in the feed shoe tube is suggested.
9) If the upper parts of the tester are made of transparent materials, it will enable direct observation and recording of the filling process.

Rotational rainy:

10) Using a non-contact type automated leveling process is suggested.
11) Using additional powders with different physical properties (such as size, size distribution, and bulk density) should be tested.
12) Improving the rotational rainy fill in order to test higher RPMs is necessary.
13) Using small compartments for RPM evaluation is suggested.

Point feed:

14) Replacing the current leveling method (manual) will help to reduce the disturbance inside the powder mass. Some example of acceptable leveling method changes include: using automated leveling at a very low speed (1-5 mm/s), using soft materials (such as sponge), using air pressure (blower), and leveling from both sides.
15) Using more powder samples with different physical properties (such as, size, size distribution, and bulk density) are suggested.

16) Evaluation of powder deposition characteristics for different filling heights is recommended.

Pneumatic filling:

17) Pneumatic filling method is not suitable to fill the die using powders such as BPM.

18) Using granule sizes of larger than 1 mm is suggested for evaluation of the pneumatic filling method.

VITA

Saed Sayyar Roudsari

EDUCATION

- **Ph.D. in Agricultural and Biological Engineering, December 2007**
  Penn State University, University Park, Pennsylvania
- **M.Sc. Civil Engineering, May 2004**
  North Carolina A&T State University, Greensboro, North Carolina
- **B.Sc. Agricultural and Biological Engineering, May 1996**
  Iran (1996)

ACTIVITIES

- Served as judge for North Carolina A&T State University's Graduate Research Exhibition (GRE) for two consecutive years (2002-2003)
- Served as judge for Federal Aviation Administration (FAA)'s graduate poster presentation. Daytona Beach, FL, 2003
- President of Iranian Student Association at Penn State University (2004-2005)

PROFESSIONAL AFFILIATION

- Member of ISPE (International Society of Pharmaceutical Engineering)
- Member of ASABE- American Society of Agricultural, Food and Biological Engineering

HONORS/ AWARDS

- Recipient of young researcher award. Undergraduate year- 1995
- Member of Gamma Sigma Delta - Honor Society for Engineering
- Member of Alpha Epsilon - Honor Society for Biological Engineering